UNIVERSITY OF CALIFORNIA
RIVERSIDE

Discovery of Protease Inhibitory Antibodies Using High-Throughput Methods

A Dissertation submitted in partial satisfaction
of the requirements for the degree of

Doctor of Philosophy

in

Chemical and Environmental Engineering

by

Tyler Lopez

September 2018

Dissertation Committee:
Dr. Xin Ge, Chairperson
Dr. Ian Wheeldon
Dr. Ameae Walker

The Dissertation of Tyler Lopez is approved:

_____

_____

_____
Committee Chairperson

University of California, Riverside

Acknowledgments

First and foremost I would like to thank my advisor, Dr. Xin Ge, for his constant support and guidance throughout my Ph.D. research at UCR. In addition to improving my skills in the lab, he taught me the importance of developing an ideological flow in my writing. This improvement in writing led to several awards that allowed me to focus on research rather than working as a teaching assistant. Over the years, Dr. Ge has led by example and his hard work and dedication to our research serves as a model for me. During my Ph.D. the variety and complexity of my projects was often overwhelming. At certain points I was working on four different projects and Dr. Ge helped me to organize the projects into more manageable fragments and keep all of my projects advancing without delay. I am a very ambitious person, and Dr. Ge understood what my goals were and pushed me harder than I could push myself, not by a kick but with a helping hand, to ensure that I achieved them. One discreet example is his encouragement to attend a wide variety of conferences. At these conferences I was able to make connections and meet a wide variety of people which will help in my future endeavors. For all this and a thousand other ineffable reasons I would like to express my sincere gratitude and best wishes to Dr. Xin Ge.

I would also like to thank my committee members Dr. Ian Wheeldon, and Dr. Ameae Walker for their continuous support and advice throughout my years at UCR. Additionally, I would like to thank Dr. Walker for her labs collaborative research using my antibodies in mouse studies. Additionally, I would like to thank

Dr. Ru Rong Ji for his contribution to the MMP-9 portion of the genetic selection project by testing the IgG version of L13 in mice. The data they provided tremendously improved the quality of my research papers.

I would like to thank my lab partners Peter Nam, Cathy Li, Long Chen, Kibaek Lee, and Chuan Chen for their continued support and clever insights into unique problems I had throughout my research. The coffee and lunch breaks we took together served as a relaxed environment to discuss our research and the variety of projects we worked on gave me unique perspectives that allowed me to come up with creative solutions. In particular I would like to thank Dr. Nam for his expert training in my first years of research which set me on the path to succeed in a new field I had no previous experience in.

Throughout my Ph.D. I've had the privilege to train and work with a number of undergraduate researchers. I would like to thank Evan Kaihara, Zahid Mustafa, Ramon Sanchez, Aaron Ramirez, Chris Benitez, and Henry Pham for their long hours of work to advance my research. Without them my research would not have been able to be completed nearly as quickly.

I would like to thank my family for their continuous support throughout my Ph.D. The long hours and stress were made much more bearable knowing I had a meal waiting for me at home and someone always available for me to talk through my research with. My fiancé was also incredibly understanding of the time commitment required to acquire a Ph.D. and sacrificed many date nights to

the long hours I spent in lab. Even with everything going on she made sure that I took a little time to relax and rest.

Last but not least, I would like to thank the UCR graduate program and the NIH for their funding and support without which I could not have conducted my research.

ABSTRACT OF THE DISSERTATION

Discovery of Protease Inhibitory Antibodies Using High-Throughput Methods

by

Tyler Lopez

Doctor of Philosophy, Graduate Program in Chemical and Environmental Engineering
University of California, Riverside, September, 2018
Dr. Xin Ge, Chairperson

Dysregulation of proteases has been implicated in a variety of diseases such as cancer, inflammation, osteoporosis, neuropathic pain, and neurodegenerative diseases. Although several compound inhibitors of proteases have been approved by the FDA, many small molecule inhibitors of proteases failed in clinical trials due to severe side effects caused by non-specificity. Monoclonal antibodies thus hold a great promise as therapeutics able to inhibit pathogenic proteases with desired selectivity. However, proteases present a unique challenge for inhibitory antibodies discovery largely because of lack of a function based selection method.

This study has developed four inhibitory antibody functional high-throughput selection/screening methods: fast discovery by deep sequencing, epitope specific affinity maturation, conversion of inhibition selectivity by competitive FACS, and in vivo inhibition based genetic selection. Using these novel approaches, large

panels of antibodies were discovered / engineered inhibiting a variety of proteases including matrix-metalloprotease-14 (MMP-14), MMP-9, autophagic serine protease (Alp2), aspartic acid protease β-secretase 1 (BACE1), and cysteine protease cathepsin B (CTSB). Biochemical characterizations by biolayer interferometry and inhibition kinetics suggested that isolated antibodies exhibited high binding affinities and high inhibition potencies both in nM range with decent selectivity and proteolytic stability. The isolated antibodies blocked their protease targets from hydrolyzing the associated physiological substrates either competitively or non-competitively. Competitive ELISA with native inhibitors and epitope/paratope mutation studies indicated that most generated antibodies achieved their inhibitory functions by recognizing protease's catalytic clefts using their complementarity-determining region (CDR) H3. In a mouse model of drug induced neuropathic pain, intravenous application of IgG L13, a potent anti-MMP9 inhibitor, exhibited significant pain attenuation effects. And anti-Alp2 Fab 1 specifically stained Aspergillus fumigatus infected mouse lung tissues, demonstrating its potential in diagnosis and as a therapeutic. Collectively, these functional selection/screening methods developed in this study greatly facilitate the discovery and engineering of inhibitory antibodies, and can be applied for many proteases of clinical significance.

Table of Contents

List of Figures

List of Tables

Chapter 1: Introduction

1.1 Protease inhibition as a treatment

At least 569 proteases have been identified, which encode ~2.85% of human genome[1,2]. Based on their catalytic chemistry, proteases are classified into five main groups: serine, cysteine, threonine, aspartyl-, and metallo- proteases (Figure 1.1)[1]. Aspartyl proteases and metalloproteases utilize a water molecule to act as the nucleophile while serine, cysteine, and threonine proteases use the amino acids they are named for[3].

In the early stage of protease research it was believed that proteases were simple proteins responsible for protein catabolism and the generation of amino acids[1]. In more recent years it has been discovered that proteases are in fact a large family of enzymes responsible for influencing a huge number of biological processes[4,5,6,7]. Proteases exist in a delicate balance of networks with their endogenous inhibitors, to maintain homeostasis. However, their dysregulations are implicated in several diseases such as cancer, inflammation, osteoporosis, neuropathic pain, and neurodegenerative diseases[8,9,10,11,12,13]. Some well characterized examples include: cathepsin B, which promotes tumor growth, metastasis and angiogenesis through its proteolytic cascades[14]; cysteine protease falcipain 1, which is required for malaria to invade host cells[15,16]; matrix metalloproteinases (MMPs), which cause delayed wound healing due to excessive matrix degradation[17]; thrombin and factor XIa, whose unregulated activities are

responsible for blood coagulation[18]; and plasma kallikrein, whose upregulation due to serpin C1-inhibitor deficiency leads hereditary angioedema[19].

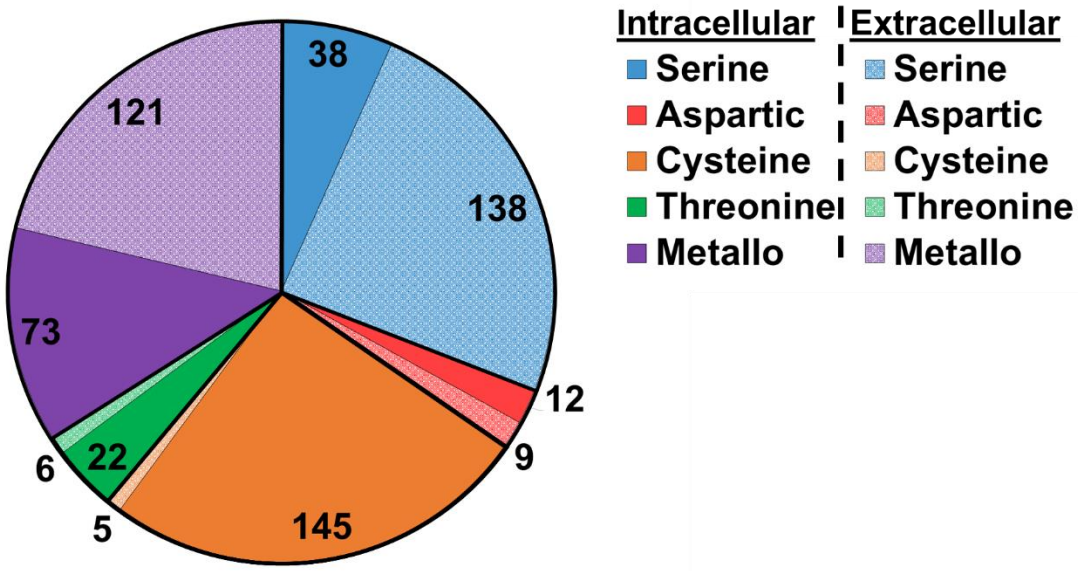

Figure 1.1: All identified human proteolytic enzymes are classified into five catalytic classes: metalloproteinases, serine, threonine, cysteine and aspartic proteases. The darker sections of each catalytic class correspond to intracellular or integral-membrane enzymes, whereas the lighter sections refer to extracellular or pericellular enzymes[1], which are potentially accessible for monoclonal antibodies.

Therefore, one apparent therapeutic strategy is to block abnormal or pathogenic proteolysis by inhibiting their catalytic reactions. In fact, it has been estimated that 5-10% of all pharmaceutical targets for drug developments are proteases[3]. However, each class of protease has specific requirements for activity and inhibition, therefore, techniques for selecting potential therapeutic protease inhibitors have to be robust under a plethora of conditions. Notably, vast majority of proteases contain concave catalytic domains, which inspire designs for structure-aided inhibitors (Figure 1.2).

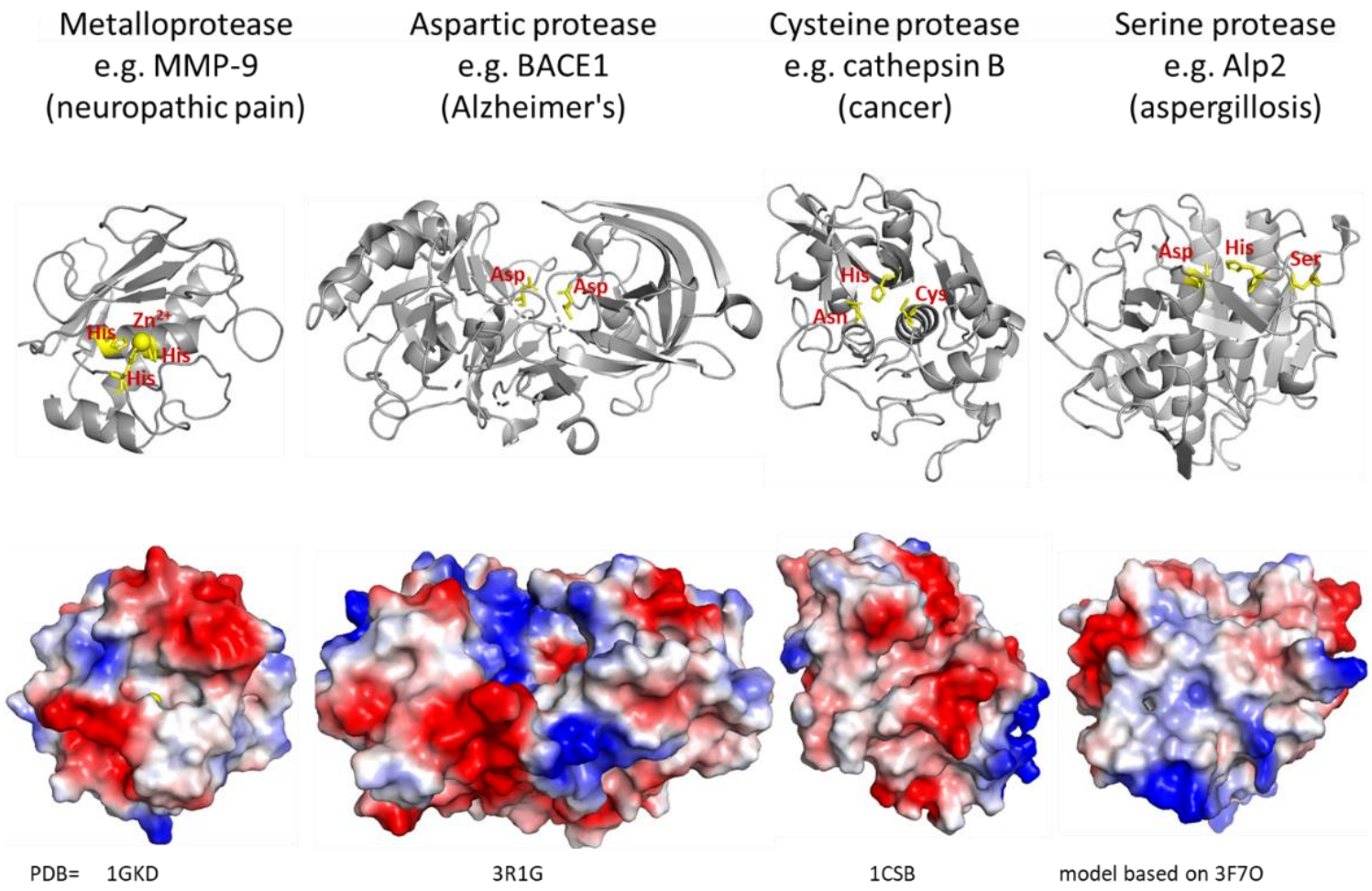

Figure 1.2: Surface generated images displaying the deep catalytic clefts of the four classes of protease targeted in this study. The catalytic motif is highlighted in yellow on the cartoon figures while the surface displays the vacuum electrostatic potential.

1.2 Examples of biomedically important proteases

1.2.1 Targeting matrix metalloproteinases (MMPs) for cancer treatment

MMPs are a class of zinc dependent endopeptidases responsible for tissue remodeling and extracellular matrix degradation. MMPs play important roles within various aspects of cancer pathology, including tumor growth, metastasis, and angiogenesis[8,20,21]. Two MMPs in particular stand out as therapeutic targets. Membrane type-1 matrix metalloproteinase also known as MMP-14 is a leading factor in cell migration due to its ability to cleave cell surface molecules such as CD44, pro-α_v integrin, and transglutaminase[8,22,23,24]. MMP-14 also processes proMMP-2 into active MMP-2, which promotes the migration of tumor cells[20,25]. MMP-9 is responsible for the activation of the angiogenic switch in pancreatic tumor cells[11]. In addition to involvement in the spread of cancer, MMP-9 cleaves pro-IL-1β into its active format which increases the sensitivity and excitability of sensory neurons resulting in neuropathic pain[26].

Mounting evidence has suggested that while many aspects of MMP proteolytic action are pro-tumorigenic, some MMP family members exhibit tumor-suppressing effects in certain circumstances[27,28]. For instance, MMP-8 favors host defense instead of stimulating tumor proliferation[29], and even MMP-9 can exhibit opposing functions depending on specific microenvironments[30]. For these reasons, selectively blocking individual tumorigenesis-promoting MMPs in an appropriate timeframe is highly desired for a successful therapy. However, achieving specific inhibition, i.e. inhibiting MMP-14 or MMP-9 while eliminating cross reactivity

towards other MMPs, is a major challenge for therapeutic development. This challenge is due to the highly conserved overall protein folding and identical reaction mechanism – all MMPs have a shared catalytic motif, VAAHExGHxxGxxH, which is located in the active center and has three histidines coordinating the catalytic zinc ion[31] (Figure 1.2: far left).

1.1.2 Targeting BACE1 for Alzheimer's treatment

Alzheimer's disease (AD) is the most common form of dementia worldwide and one of the leading causes of death in the US. According to the Alzheimer's Association, 5.7 million people are affected with AD in the US alone[32]. The center for disease control predicts that this number will increase to 14 million by 2050[32]. Current treatments such as cholinesterase inhibitors and memantine can alleviate the cognitive symptoms[33], but cannot cure or moderate the progression of AD. And antidepressants, anxiolytics, and antipsychotic medications only help to improve the mood of the patient as the disease progresses[34,35,36,37,38].

One of the major indicators of Alzheimer's disease is the presence of amyloid plaques formed by the aggregation of amyloid β (Aβ) peptides[39,40,41]. There are two pathways that amyloid precursor protein (APP) can take during degradation (Figure 1.3). In non-amyloidogenic degradation, APP is processed by α-secretase then γ-secretase leading to APP clearance. While in amyloidogenic degradation, β-secretase (BACE1) cleaves APP resulting in the intermediates which are then processed by γ-secretase to form amyloid β. Because Aβ is the

main component of amyloid plaques found in the brains of Alzheimer's patients, by specifically inhibiting BACE1 and sparing α-secretase and γ-secretase, it is possible to push the APP pathway towards the non-amyloidogenic product effectively and reduce the generation of amyloid plaques and thereby slow the development of AD[42,43,44,45]. In addition to the specific blocking of BACE1, delivery of the inhibitor across the blood-brain barrier (BBB) is another challenge facing the development of a therapeutic for the treatment of AD.

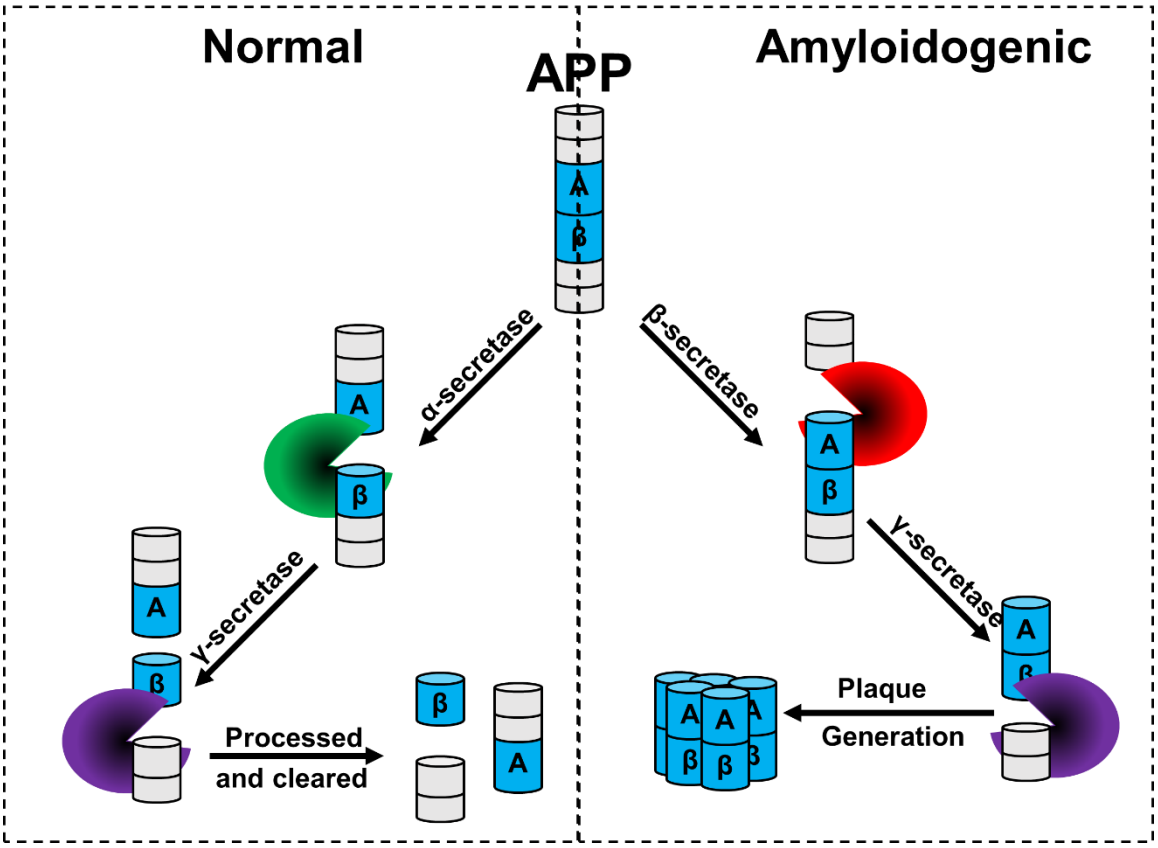

Figure 1.3: The APP degradation pathway showing the normal degradation by α-secretase (left) and the amyloidogenic pathway caused by β-secretase (right).

1.1.3 Targeting cathepsins for treatment of for neurodegenerative disorders, cancer, and Chagas' disease

Expression of cysteine proteases cathepsin B/E/K/S (CTSB, CTSE, CTEK, and CTSS respectively) is often increased in tumors relative to normal tissue[46]. As the key acid hydrolases within the lysosome, cathepsins are the principal effectors of protein catabolism and autophagy by which they support the increased metabolic needs of proliferating cancer cells[46]. Cathepsins also contribute to tissue invasion and metastasis due to their role in the degradation and turnover of the extracellular matrix. To elicit the effects of cathepsin inhibition, CTSB knockout mouse studies displayed a delay in tumor progression and a reduction in tumor burden[46]. However, CTSL knockout mice showed an increase in tumor progression and grade as well as a 180% increase in lymph node metastasis[46], demonstrating the need for a selective cathepsin B inhibitor. Currently CTSK inhibitors have proven effective in the treatment of arthritis, atherosclerosis, blood pressure regulation, obesity, and cancer, however during clinical trials several issues arose due to off-target effects[47]. Therefore, high specificity and potency are required for CTSB, CTSE, and CTSS based inhibitory therapeutics [48,49,50,51,52].

1.3 Small compound inhibitors as therapeutic treatments

Targeting particular proteases using small molecules has been extensively studied and Table 1 shows examples of effective compound-based protease inhibitors[6,53,54,55,56,57]. Nevertheless, small molecules have difficulty providing the required specificity in general due to the highly conserved catalytic mechanisms and structures of the reaction centers among related protease family members.[53]

For example, several small molecule protease inhibitors such as indinavir (Crixivan), nelfinavir (Viracept), ritonavir (Norvir), and saquinavir (Invirase and Fortovase) are used for the treatment of HIV. These molecules act by inhibiting the maturation of gag proteins responsible for infectivity, however they cause nephrolithiasis, diarrhea, circumoral paresthesias, and frequent systemic toxicity[54]. These side effects in addition to high costs of production due to the complex structure, as well as the development of drug resistance, make these small molecule inhibitors limited in their long-term effectiveness as a therapeutic[54].

Table 1.1. Small molecule protease inhibitors [6,54,55,56,57]

Indication	Compound	Target	Protease Class
Hypertension, myocardial infarction	Captopril	ACE	Metallo
	Enalapril		
	Lisinopril		
	Trandolapril		
	Zofenopril		
	Ramipril		
	Moexipril		
	Imidapril		
	Perindopril		
	Qinapril		
	Fosinopril		
	Benazepril		
	Cilazapril		
Periodontitis	Periostat	MMP1, MMP2	
AIDS	Ritonavir	HIV protease	Aspartic
	Amprenavir		
	Fosamprenavir		
	Atazanavir		
	Lopinavir		
	Indinavir		
	Saquinavir		
	Nelfinavir mesylate		
Alzheimer's Disease	GSK188909	BACE1	
	CTS-21166		
Thrombosis	Ximelagatran*	Thrombin	Serine
	Argatroban		
	Lepirudin		
	Desirudin		
	Fondaparinux sodium (indirect)	Factor X	
Thrombosis, unstable angina	Bivalirudin		
Respiratory disease	Sivelestat	Human neutrophil elastase	
Pancreatitis	Camostat mesilate	Trypsin-like	
Pancreatitis, inflammation	Nafamostat mesilate	Broadspectrum	
Chagas Disease	E64d	CTSB	Cysteine
Osteoporosis	Odanacatib	CTSK	
Cancer	Bortezomib	Proteasome	Threonine

Significant effort has also been made to discover BACE1 small molecule inhibitors capable of crossing the blood brain barrier (BBB) at therapeutic concentrations without significant side effects. The first small molecule inhibitor OM99-2 was an eight-residue peptide that inhibited BACE1, but its poor physicochemical characteristics resulted in inefficient cross of the BBB to be effective in vivo[55]. OM99-2 gave rise to several other peptide inhibitors: KMI-429, KMI-570, and KMI-684 all of which reduced the production of Aβ plaques when directly injected into the hippocampus of mice[55]. The peptide inhibitors led to the rise of small molecule inhibitors GSK188909 and CTS-21166[55]. While CTS-21166 has made it through Phase I clinical trials, no BACE1 inhibitor has been approved showing the need for a highly specific and potent therapeutic.

Cathepsin B is a well-studied protease that has several small molecule inhibitors such as E64, CA-047, LHVS, Z-FA-FMK, and CP-1ME[56]. These inhibitors were proven to inhibit CTSB, however all of them inhibited at least one other cathepsin. Some inhibitors are in preclinical stages[58] or even through Phase I clinical trials[59,60] for the inhibition of CTSB to treat Chagas disease or fatty liver disease respectively. Even with these advances in small molecule treatments there are still no CTSB inhibitors approved for drug use.

As another example, chemical compound inhibitors, e.g. hydroxamates, targeting broad-spectrum MMPs all failed in clinical trials due to severe side effects and a lack of efficacy overall[6]. The lack of specificity of small molecule inhibitors

targeting the catalytic domains of MMP family members is largely due to high amino acid similarity and active sites that are extensively conserved. Consequently, development of small molecule inhibitors to distinguish different MMPs is extraordinarily difficult[61].

In addition to small compounds, peptide-based protease inhibitors have also been developed[62,63]. Cyclic peptides specifically inhibiting MMP-2 and MMP-9 were isolated by phage display showing a recognition sequence of HWGF and a μM range potency[62]. These peptides were effective in mouse cancer models, but their rapid clearance in vivo required direct injection into the tumor site[63]. One strategy to both increase serum half-life and improve potency is by grafting the peptide inhibitor motif into CDR-H3 of antibody scaffolds[87,64].

1.4 Protease endogenous inhibitors and protease inhibitor-containing domains

Proteases are well regulated by their associated natural inhibitors to achieve the protease/antiprotease balance. For example, tissue inhibitors of metalloproteases (TIMPs) are a family of four similar proteins responsible for regulating metalloproteinases including MMPs[65], ADAMs (a disintegrin and metalloproteinase), and ADAMTSs (a disintegrin and metalloproteinase with thrombospondin motifs). Cystatin inhibits cysteine proteases such as ficin, papain, cathepsin B, and cathepsin C[66]. Alpha-1-antitrypsin, as a major serum serine protease inhibitor, inhibits the activity of many different endogenous serine proteases, such as neutrophil-derived elastase and proteinase-3[67]. Additionally,

kunitz domains[68], ecotin protein[69], and ankyrin[70] proteins inhibit serine proteases, trypsin-folding proteases, and caspases respectively.

Efforts have been made to engineer these protein-based inhibitors (e.g. TIMP-2) to be more specific inhibiting particular proteases (e.g. MMP-14). However, it is difficult to convert a broad-spectrum inhibitor to a completely specific one in general[71]. For example, engineering kunitz domains by phage affinity maturation toward plasma kallikrein resulted in several inhibitors with 75-300 pM potency, however these mutants also inhibited factor XIa and/or plasmin[68]. Similarly, a phage displayed library of TIMP2 mutants was panned for cdMMP-1 specific inhibitors by combining positive selection on cdMMP-1 with negative selection on cdMMP-3 to generate specific inhibitors[72]. Another moderately successful attempt to enhance the specificity of TIMP2 towards MMP-14 was performed by site directed mutagenesis based on computational design coupled with yeast surface display for evolution[73].

By applying negative depletion on five related proteases (FXa, FXIa, FXIIa, uPA and MT-SP1) and a focused library design, ecotin was engineered to inhibit plasma kallikrein at pM potency[69]. However, many isolated ecotin variants showed cross reactivity with MT-SP1 and FXIIa. In addition, the prokaryotic origin of ecotin may limit its use as a therapeutic due to issues with immunogenicity. Finally, when engineering DARPins (designed ankyrin repeat proteins) to inhibit tobacco etch virus (TEV) proteinase Nia^{pro}, an in vivo screening method based on proteolysis controlled transcription was demonstrated.[70] All of the above selection / screening

strategies developed by previous studies build the foundation for the engineering techniques discussed in this thesis.

1.5 Monoclonal antibodies as protease inhibitors

The demand for highly selective protease inhibitors and modest success of native inhibitor engineering makes monoclonal antibodies an attractive alternative to small molecules for protease inhibition[74,75,76,77,78,79]. Antibodies are characterized by high inherent specificity due to their large surface for protein-protein interactions[79]. IgG antibodies also have the added benefit of a long serum half-life averaging approximately 21 days[79]. Additionally, antibodies can penetrate tissue and tumors and bind to less accessible epitopes of the target proteins. Bispecific antibodies can also be made that bind to transferrin receptors for transport across the BBB allowing antibodies to function in the brain[80,81]. The list of FDA approved drugs continues to grow and the development of synthetic libraries expands the possibility of discovering a wide variety of new antibodies[82].

Because of the importance of antibodies in medicines and as research tools, numerous methodologies have been developed for the discovery of monoclonal antibodies. Three of the most popular methods of antibody discovery are hybridoma, phage panning, and fluorescence activated cells sorting (FACS). Using these methods several protease inhibiting antibodies have been isolated (Table 1.2).

Table 1.2: Monoclonal antibody based protease inhibitors and the methods used for their discovery.

Target	Method	Reference
BACE1	phage panning	83
BACE1	hybridoma	84
MMP-9	hybridoma	85
MMP-9	epitope synthetic mimicry	77
MMP-14	phage panning - competitive elution	86
MMP-14	rational design - motif grafting	87
CTSB	hybridoma	88
CTSS	hybridoma	89
bovine trypsin	rational design - motif grafting	90
human neutophil elastase	rational design - motif grafting	90
TNF-α converting enzyme	phage panning -including catalytic domain blocking	91
HtrA1	phage panning	92
HGFA	phage panning	93
MT-SP1	phage panning	76
HCV NS3 serine protease	genetic selection in cytoplasm	94

For example, an allosteric inhibitory antibody of BACE1 with 17 nM potency (after affinity enrichment) was discovered using standard phage panning[83]. Several inhibitory antibodies towards MMP-14 were isolated from a phage library by competitive elution using TIMP-2[86]. By hybridoma, an MMP-9 allosteric inhibitory antibody with ~ 200 pM potency was generated[85]. In another example, epitope synthetic mimicry was applied to design the immunogen for the generation of MMP-9 inhibitory mAbs from a murine immune response[77]. Ultra-long CDR-H3 designs derived from native or synthetic peptide inhibitors were grafted into bovine antibody scaffolding to generate inhibitors of bovine trypsin and human neutrophil elastase[90]. Similarly, a MMP-14 inhibitory antibody with low nM potency was isolated by inhibition motif grafting and CDR optimizations[87].

Despite above success, systematic discovery of protease inhibitory antibodies still presents a challenge in general, for the following two reasons. (1) The flat topography of native human antibodies is not compatible with the concave structures of protease catalytic clefts. (2) Binding based selection platforms have no control on inhibition function.

To address the first issue, our lab was inspired by camelid antibody repertories, and developed a synthetic human antibody library carrying convex paratopes encoded by long CDR-H3 regions with 23-27 amino acids[86]. Unlike human or murine antibodies that have CDR-H3s of 12 and 9 amino acids on average, a large portion of heavy chain antibodies produced by camels or llamas contain long CDR3s that penetrate concave structures of enzyme reaction pockets

and inhibit enzymatic functions[95,96,97,98,99]. Using this library combined with phage panning and competitive elution a panel of inhibitory Fabs targeting MMP-14 with nM potency and high selectivity was isolated. Particularly, Fabs 3A2 was a competitive inhibitor binding to the vicinity of reaction cleft, and exhibited therapeutic efficacy for melanoma and breast cancer treatment in animal models[100,101].

1.6 Research Objectives and Structure of Thesis

The overall goal of my thesis is to address the second challenge, by developing functional selection / screening high-throughput methods for the facile discovery of protease inhibitory antibodies. Using these methods, my research expands the protease targets from metalloproteases (MMP-9 and -14) to serine (Alp-2), cysteine (cathepsin B), and aspartyl proteases (BACE1). In addition, my research also addresses another important issue associated with standard mechanism inhibitors, i.e. proteolytic stability.

More specifically:

Chapter 2 focuses on applying next generation sequencing (NGS) to identify and recover inhibitory antibodies from phage panned libraries that cannot be found by conventional monoclonal ELISA. This development is based on the observation that during phage panning, ~30% antibody clones fail to enrich from the second to the third round, resulting in relatively low abundancy which can only be identified by deep sequencing.

Chapter 3 focuses on developing epitope specific dual color FACS (fluorescence activated cell sorting) for inhibitory antibody improvements. By displaying a scFv 3A2 error-prone library on yeast cell surface and conducting selection on MMP-14-GFP (green fluorescent protein) in the presence of a competing protein, TIMP-2 conjugated with Alexa-647, highly potent 3A2 variants with 6-11 fold stability enhancement were isolated.

Chapter 4 develops a novel approach for the generation of protease inhibitory antibodies. Applying dual color competitive FACS, we converted a MMP-14 specific inhibitor to a panel of MMP-9 specific inhibitory antibodies with dramatic selectivity shifts of 690-4500 folds.

Finally, Chapter 5 develops a genetic selection technique for discovering functional antibodies. By engineering protease cleavage sensors based on β-lactamase and achieving *E. coli* periplasmic co-expression of the protease target and an antibody library, we discovered panels of antibodies inhibiting a variety of proteases from four major classes with high selectivity and desired biological functions.

1.7 References

1. Lopez Otin, C., Matrisian, L. Emerging roles of proteases in tumour suppression. *Nature Reviews Cancer*. **7**, 800–808. (2007).

2. Ponomarenko, E., et al. The Size of the Human Proteome: The Width and Depth. *Int J Anal Chem*. 7436849. (2016).

3. Drag, M. & Salvesen G.S. Emerging principles in protease-based drug discovery. *Nat Rev Drug Discov*. **9**, 690–701. (2010).

4. Lopez-Otín, C. & Bond, J.S. Proteases: Multifunctional Enzymes in Life and Disease. *JBC*. **283**, 30433–30437. (2008).

5. Docherty, A.J., Crabbe, T., O'Connell, J.P., Groom, C.R. Proteases as drug targets. *Biochemical Society Symposia.* **70**, 147-161. (2003).

6. Turk, B. Targeting proteases: successes, failures and future prospects. *Nature Reviews Drug Discovery* **5**, 785-799. (2006).

7. Cudic, M., & Fields, G.B. Extracellular Proteases as Targets for Drug Development. *Current Protein & Peptide Science.* **10**: 297-307. (2009).

8. Zarrabi, K., et al. Inhibition of Matrix Metalloproteinase 14 (MMP-14)-mediated Cancer Cell Migration. *J. Biol. Chem*, **286**, 33167-33177. (2011).

9. Kajita, M., et al. Membrane-type 1 Matrix Metalloproteinase Cleaves CD44 and Promotes Cell Migration. *JCB*. **153**, 893–904. (2001).

10. Baciu, P.C., Suleiman, E.A., Deryugina, E.I., & Strongin, A.Y. Membrane type-1 matrix metalloproteinase (MT1-MMP) processing of pro-αv integrin regulates cross-talk between αvβ3 and α2β1 integrins in breast carcinoma cells. *Experimental Cell Research*. **291**, 167–175. (2003).

11. Bergers, G., et al. Matrix metalloproteinase-9 triggers the angiogenic switch during carcinogenesis. *Nature Cell Biology*. **2,** 737–744. (2000).

12. Reichard, U., Cole, G.T., Hill, T.W., Ruchel, R., & Monod, M. Molecular characterization and influence on fungal development of ALP2, a novel serine proteinase from Aspergillus fumigatus. *Int. J. Med. Microbiol*. **290**, 549-558. (2000).

13. Yamashima, T. et al. Inhibition of ischaemic hippocampal neuronal death in primates with cathepsin B inhibitor CA-074: a novel strategy for neuroprotection based on ‘calpain–cathepsin hypothesis. *European Journal of Neuroscience*. **10**, 1723–1733. (1998).

14. Koblinski, J.E., Ahram, M., Sloane, B.F. Unraveling the role of proteases in cancer. *Clin Chim Acta*. **291,** 113-35. (2000).

15. Greenbaum, D.C., et al. A role for the protease falcipain 1 in host cell invasion by the human malaria parasite. *Science.* **298**, 2002-2006. (2002).

16. Hopp, C.S., et al. Deletion of the rodent malaria ortholog for falcipain-1 highlights differences between hepatic and blood stage merozoites. *PLoS Pathog*. **1,** e1006586. (2017).

17. McCarty, S., & Percival, S. Proteases and Delayed Wound Healing. *Adv Wound Care*. **2**, 438–447. (2013).

18. Walker, C.P., & Royston, D. Thrombin generation and its inhibition: a review of the scientific basis and mechanism of action of anticoagulant therapies. *Br J Anaesth*. **88,** 848-863. (2002).

19. Kaplan, A.P. Enzymatic pathways in the pathogenesis of hereditary angioedema: The role of C1 inhibitor therapy. *J Allergy Clin Immunol*. **126**, 918-925. (2010).

20. Udi, Y., et al. Inhibition Mechanism of Membrane Metalloprotease by an Exosite-Swiveling Conformational Antibody. *Structure*, **23**, 104–115. (2015).

21. Golubkov, V.S., Chekanov, A.V., Doxsey, S.J., Strongin, A.Y. Centrosomal Pericentrin Is a Direct Cleavage Target of Membrane Type-1 Matrix Metalloproteinase in Humans but Not in Mice. *J. Biol. Chem*, **280**, 42237-42241. (2005).

22. Kajita, M., et al. Membrane-type 1 Matrix Metalloproteinase Cleaves CD44 and Promotes Cell Migration. *JCB*, **153**, 893–904. (2001).

23. Baciu, P.C., Suleiman, E.A., Deryugina, E.I., Strongin, A.Y. Membrane type-1 matrix metalloproteinase (MT1-MMP) processing of pro-αv integrin regulates cross-talk between αvβ3 and α2β1 integrins in breast carcinoma cells. *Experimental Cell Research*. **291,** 167–175. (2003).

24. Gingras, D., et al. Activation of the extracellular signal-regulated protein kinase (ERK) cascade by membrane-type-1 matrix metalloproteinase (MT1-MMP). *FEBS*. **507**, 231–236. (2001).

25. Deryugina, E.I., et al. MT1-MMP Initiates Activation of pro-MMP-2 and Integrin αvβ3 Promotes Maturation of MMP-2 in Breast Carcinoma Cells. *Experimental Cell Research*. **263**, 209–223. (2001).

26. Ji, R., Xu, Z., Wang, X., Lo, Eng. MMP regulation of neuropathic pain. *Trends Pharmacol Sci*. **30**, 336–340. (2009).

27. Overall, C.M., Kleifeld, O. Validating matrix metalloproteinases as drug targets and anti-targets for cancer therapy. *Nat. Rev. Cancer*. **6**, 227-239. (2006).

28. Kessenbrock, K., Plaks, V., Werb, Z. Matrix metalloproteinases: regulators of the tumor microenvironment. *Cell*. **141**, 52-67. (2010).

29. Decock, J., Thirkettle, S., Wagstaff, L., Edwards, D.R. Matrix metalloproteinases: protective roles in cancer. *J Cell Mol Med*. **15**, 1254. (2011).

30. Egeblad, M., Werb, Z. New functions for the matrix metalloproteinases in cancer progression. *Nat. Rev. Cancer*, **2,** 161. (2002).

31. Pavlaki, M. & Zucker, S. Matrix metalloproteinase inhibitors (MMPIs): The beginning of phase I or the termination of phase III clinical trials. *Cancer and Metastasis Reviews* **22**, 177–203. (2003).

32. Hebert, L.E., Weuve, J., Scherr, P.A., Evans, D.A. Alzheimer disease in the United States (2010-2050) estimated using the 2010 Census. *Neurology.* **80**, 1778-1783. (2013)

33. Raina, P., et al. Effectiveness of Cholinesterase Inhibitors and Memantine for Treating Dementia: Evidence Review for a Clinical Practice Guideline. *Ann Intern Med*. **148**, 379-397. (2008).

34. Aboukhatwa, M., Dosanjh, L., Luo, Y. Antidepressants are a rational complementary therapy for the treatment of Alzheimer's disease. *Molecular Neurodegeneration*, **5**:10. (2010).

35. Caballero, J., et al. The effects of commonly prescribed drugs in patients with Alzheimer's disease on the rate of deterioration. *J Neurol Neurosurg Psychiatry*. **78**, 233-239. (2007).

36. Schneider, L., et al. Effectiveness of Atypical Antipsychotic Drugs in Patients with Alzheimer's Disease. *N Engl J Med*. **355**,1525-1538. (2006).

37. Schneider, L., Dagerman, K., Insel, P. Risk of Death With Atypical Antipsychotic Drug Treatment for Dementia. *JAMA*. **294**,1934-1943. (2005).

38. Gill, S., et al. Antipsychotic Drug Use and Mortality in Older Adults with Dementia. *Ann Intern Med*. **146**, 775-786. (2007).

39. DeMattos, R., et al. A Plaque-Specific Antibody Clears Existing β-amyloid Plaques in Alzheimer's Disease Mice. *Neuron*. **76**, 908–920. (2012).

40. Schenk, D., et al. Immunization with amyloid-bold beta attenuates Alzheimer-disease-like pathology in the PDAPP mouse. *Nature.* **400**, 173-177. (1999).

41. Hardy, J. & Selkoe, D. The Amyloid Hypothesis of Alzheimer's Disease: Progress and Problems on the Road to Therapeutics. *Science*. **297**, 353-356. (2002).

42. Ledesma, M.D., et al. Brain plasmin enhances APP α-cleavage and Aβ degradation and is reduced in Alzheimer's disease brains. *EMBO reports*. **1**, 530-535. (2000).

43. Colombo, A., et al. JNK regulates APP cleavage and degradation in a model of Alzheimer's disease. *Neurobiology of Disease*; **33**, 518–525. (2009).

44. Rubinsztein, D. The roles of intracellular protein-degradation pathways in neurodegeneration. *Nature.* **443**, 780-786. (2006).

45. Haass, C., Kaether, C., Thinakaran, G., Sisodia, S. Trafficking and proteolytic processing of APP. *Cold Spring Harb. Perspect. Med.*, **2**, a006270. (2012).

46. Olson, O., & Joyce, J. Cysteine cathepsin proteases: regulators of cancer progression and therapeutic response. *Nature Reviews.* **15,** 713. (2015).

47. Brömme, D. & Lecaille, F. Cathepsin K inhibitors for osteoporosis and potential off-target effects. *Expert Opin Investig Drugs*. **18**, 585–600. (2009).

48. Yamashima, T., et al. Inhibition of ischaemic hippocampal neuronal death inprimates with cathepsin B inhibitor CA-074: a novelstrategy for neuroprotection based on 'calpain–cathepsinhypothesis. *European Journal of Neuroscience*. **10**, 1723–1733. (1998).

49. Leroy, V. & Thurairatnam, S. Cathepsin S inhibitors, *Expert Opinion on Therapeutic Patents*. **14**, 301-311. (2004).

50. Saegusa, K., et al. Cathepsin S inhibitor prevents autoantigen presentation and autoimmunity. *J. Clin. Invest*. **110**, 361–369. (2002).

51. Clark, A., et al. Inhibition of spinal microglial cathepsin S for the reversal of neuropathic pain. *PNAS.* **104**, 10655–10660. (2007).

52. Kwan, J., Eksioglu, E., Liu, C., Paul, V., Luesch, H. Grassystatins A-C from Marine Cyanobacteria, Potent Cathepsin E Inhibitors That Reduce Antigen Presentation. *J. Med. Chem*, **52**, 5732–5747. (2009).

53. Nagase, H.. Matrix Metalloproteinase Inhibitors in Cancer Therapy. *Springer*. 39-66. (2001).

54. Flexner, C. HIV Protease Inhibitors. *N Engl J Med*. **338**, 1281-1293. (1998).

55. Lu, Q., et al. L655,240, acting as a competitive BACE1 inhibitor, efficiently decreases β-amyloid peptide production in HEK293-APPswe cells. *Acta Pharmacologica Sinica.* **33**, 1459–1468. (2012).

56. Hook, G., Jacobsen, J.S., Grabstein, K., Kindy, M., Hook, V. Cathepsin B is a New Drug Target for Traumatic Brain injury Therapeutics: evidence for e64d as a Promising Lead Drug Candidate. *Frontiers in Neurology*, **6**, 10.3389/fneur.2015.00178. (2015).

57. Bone, H.G., et. al. Odanacatib for the treatment of postmenopausal osteoporosis: development history and design and participant characteristics of LOFT, the Long-Term Odanacatib Fracture Trial. *Osteoporos Int*. **26**, 699–712. (2015).

58. Doyle, P.S., Zhou, Y.M., Engel, J.C., Mckerrow, J.H. A cysteine protease inhibitor cures Chagas' disease in an immunodeficient-mouse model of infection. *Antimicrob Agents Chemother.* **51**, 3932–3939. (2007).

59. Alkhouri, N., Carter-Kent, C., Feldstein, A.E. Apoptosis in nonalcoholic fatty liver disease: diagnostic and therapeutic implications. *Expert Rev Gastroenterol Hepatol*. **5**, 201–212. (2011).

60. Holsinger, L.D.C., Dener, J., Green, M., Booth, R., Dalrymple, S. Efficacy of a reversible cathepsin B inhibitor in a rodent model of liver fibrosis and human pharmacokinetic profile. *Hepatology*. **52**, 1128A. (2010).

61. Zucker, S., Cao, J. Selective matrix metalloproteinase (MMP) inhibitors in cancer therapy: ready for prime time? *Cancer Biol Ther*. **8**, 2371-2373. (2009).

62. Koivunen, E., er al. Tumor targeting with a selective gelatinase inhibitor. *Nature Biotechnology*. **17,** 768-774. (1999).

63. Ndinguri, M., Bhowmick, M., Tokmina-Roszyk, D., Robichaud, T., Fields, G. Peptide-Based Selective Inhibitors of Matrix Metalloproteinase-Mediated Activities. *Molecules*. **17**, 14230–14248. (2013).

64. Liu, T. et al., Rational Design of Antibody Protease Inhibitors. *J. Am. Chem. Soc.* **137**, 4042–4045. (2015).

65. Brew, K., Dinakarpandian, D., Nagase, H. Tissue Inhibitors of Metalloproteinases: Evolution, Structure and Function. *Biochim Biophys Acta*. **1477**, 267-283. (2000).

66. Anastasi, A., et al. Cystatin, a protein inhibitor of cysteine proteinases. Improved purification from egg white, characterization, and detection in chicken serum. *Biochem J*. **211**, 129-138. (1983).

67. Maicas, N., et al. Human Alpha-1-Antitrypsin (hAAT) therapy reduces renal dysfunction and acute tubular necrosis in a murine model of bilateral kidney ischemia-reperfusion injury. *PLOS ONE*. 1 – 18 (2017).

68. Dennis, M.S., Herzka, A., Lazarus, R.A. Potent and selective Kunitz domain inhibitors of plasma kallikrein designed by phage display. *J. Biol. Chem*. **270**, 25411-25417. (1995).

69. Stoop, A.A., & Craik, C.S. Engineering of a macromolecular scaffold to develop specific protease inhibitors. *Nat. Biotechnol*. **21**, 1063-1068. (2003).

70. Kawe, M., Forrer, P., Amstutz, P., Plückthun, A. Isolation of intracellular proteinase inhibitors derived from designed ankyrin repeat proteins by genetic screening. *J. Biol. Chem*. **281**, 40252-40263. (2006).

71. Shirian, J., et al. Converting a broad matrix metalloproteinase family inhibitor into a specific inhibitor of MMP-9 and MMP-14. *FEBS Lett*. **592**, 1122-1134. (2018).

72. Bahudhanapati, H., Zhang, Y., Sidhu, S., Brew, K. Phage Display of Tissue Inhibitor of Metalloproteinases-2 (TIMP-2). *JBC*. **286**, 31761–31770. (2011).

73. Arkadash, V., et al. Development of High Affinity and High Specificity Inhibitors of Matrix Metalloproteinase 14 through Computational Design and Directed Evolution. *JBC*. **292**, 3481–3495. (2017).

74. Devy, L. Selective inhibition of matrix metalloproteinase-14 blocks tumor growth, invasion, and angiogenesis. *Cancer Res*. **69**, 1517-1526. (2009).

75. Ager, E.I. Blockade of MMP14 activity in murine breast carcinomas: implications for macrophages, vessels, and radiotherapy. *J Natl Cancer Inst*. **107**, djv017. (2015).

76. Schneider, E.L. A reverse binding motif that contributes to specific protease inhibition by antibodies. *J Mol Biol*. **415**, 699-715. (2012).

77. Sela-Passwell, N. Antibodies targeting the catalytic zinc complex of activated matrix metalloproteinases show therapeutic potential. *Nat Med*. **18**, 143-147. (2011).

78. Bonvin, P., Venet, S., Kosco-Vilbois, M., Fischer, N. Purpose-Oriented Antibody Libraries Incorporating Tailored CDR3 Sequences. *Antibodies*. **4**, 103-122. (2015).

79. Smith, A.J. New Horizons in Therapeutic Antibody Discovery: Opportunities and Challenges versus Small-Molecule Therapeutics. *Journal of Biomolecular Screening*. **20**, 437-453. (2015).

80. Yu, Y. et al. Boosting Brain Uptake of a Therapeutic Antibody by Reducing Its Affinity for a Transcytosis Target. *Science Translational Medicine*. **3**, 84ra44. (2011).

81. Chen, Y. & Liu, L. Modern methods for delivery of drugs across the blood–brain barrier. *Advanced Drug Delivery Reviews*. **64**, 640–665. (2012).

82. Hoogenboom, H. Selecting and screening recombinant antibody libraries. *Nature Biotechnology.* **23**, 1105–1116. (2005).

83. Atwal, J.K., et al. A therapeutic antibody targeting BACE1 inhibits amyloid-β production *in vivo*. *Science Translational Medicine*. **3**, 84ra43. (2011).

84. Zhou, L., et al. Inhibition of β-Secretase *in vivo* via Antibody Binding to Unique Loops (D and F) of BACE1. *J Biol Chem*. **286**, 8677–8687. (2011).

85. Marshall, D.C., et al. Selective Allosteric Inhibition of MMP9 Is Efficacious in Preclinical Models of Ulcerative Colitis and Colorectal Cancer. *PLoS One*. **10**, e0127063. (2015).

86. Nam, D.H., Rodriguez, C., Remacle, A.G., Strongin, A.Y., & Ge, X. Active-site MMP-selective antibody inhibitors discovered from convex paratope synthetic libraries. *Proc Natl Acad Sci U S A*. **113**, 14970–14975. (2016).

87. Nam, D.H., Fang, K., Rodriguez, C., Lopez, T., & Ge, X. Generation of inhibitory monoclonal antibodies targeting matrix metalloproteinase-14 by motif grafting and CDR optimization. *Protein Engineering, Design & Selection*. **30**, 113–118. (2017).

88. Fan, X. Molecular cloning and chimerisation of an inhibitory anti-cathepsin B antibody and its expression in Chinese hamster ovary cells. *Biol Chem*. **383**, 1817-1820. (2002).

89. Burden, R., et al. Antibody-Mediated Inhibition of Cathepsin S Blocks Colorectal Tumor Invasion and Angiogenesis. Clin Cancer Res. **15**, 6042-6051. (2009).

90. Liu, T., et al. Rational Design of Antibody Protease Inhibitors. *J. Am. Chem. Soc*. **137**, 4042−4045. (2015).

91. Tape, C., et al. Cross-domain inhibition of TACE ectodomain. *Proc Natl Acad Sci U S A*. **108**, 5578–5583. (2011).

92. Ciferri, C., et al. The trimeric serine protease HtrA1 forms a cage-like inhibition complex with an anti-HtrA1 antibody. *Biochem J*. **472**, 169-81. (2015).

93. Wu, Y., et al. Structural insight into distinct mechanisms of protease inhibition by antibodies. *PNAS*. **104**, 19784-19789. (2007).

94. Gal-Tanamy, M., et al. HCV NS3 serine protease-neutralizing single-chain antibodies isolated by a novel genetic screen. *JMB*. **347**, 991-1003. (2005).

95. Genst, E., at el. Molecular basis for the preferential cleft recognition by dromedary heavy-chain antibodies. *Proc Natl Acad Sci U S A*. **103**, 4586-4591. (2006).

96. Desmyter, A., et al. Crystal structure of a camel single-domain VH antibody fragment in complex with lysozyme. *Nat Struct Biol*. **3**, 803-811. (1996).

97. Lauwereys. M., et al. Potent enzyme inhibitors derived from dromedary heavy-chain antibodies. *EMBO J*. **17**, 3512-3520. (1998).

98. Forsman, A.M.M. Characterization of llama antibody fragments able to act as HIV-1 entry inhibitors. [PhD thesis][University College London]. (2008).

99. Spinelli S, et al. The crystal structure of a llama heavy chain variable domain. *Nat Struct Biol*. **3**:752-757. (1996).

100. Chen, K., et al. Use of a novel camelid-inspired human antibody demonstrates the importance of MMP-14 to cancer stem cell function in the metastatic process. *Oncotarget*. **9**, 29431-29444. (2018).

101. Remacle, A. Selective function-blocking monoclonal human antibody highlights the important role of membrane type-1 matrix metalloproteinase (MT1-MMP) in metastasis. *Oncotarget*. **8**, 2781-2799. (2017).

Chapter 2: Identification of inhibitory antibodies using Next Generation High-Throughput sequencing

This chapter is based on: Lopez, T., Nam, D.H., Kaihara, E., Mustafa, Z., Ge, X. Identification of highly selective mmp-14 inhibitory fabs by deep sequencing. *Biotechnology and Bioengineering*, **114**, 1140–1150. (2017).

Abstract (218 words)

Matrix metalloproteinase (MMP)-14 is an important target for cancer treatment due to its critical roles in tumor invasion and metastasis. Previous failures of all compound-based broad spectrum MMP inhibitors in clinical trials suggest that selectivity is the key for a successful therapy. With inherent high specificity, monoclonal antibodies (mAbs) therefore arise as attractive inhibitors able to target the particular MMP of interest. As a routine screening method, enzyme-linked immunosorbent assays (ELISA) have been applied to panned phage libraries for the isolation of mAbs inhibiting MMP-14. However, because of suboptimal growth conditions and insufficient antibody expression associated with monoclonal ELISA, a considerable number of potentially inhibitory clones might not be identified. Taking advantage of next-generation sequencing (NGS), we monitored enrichment profiles of millions of antibody clones along three rounds of phage panning, and identified 20 Fab inhibitors of MMP-14 with inhibition IC_{50} values of 10–4,000 nM. Among these inhibitory Fabs, 15 were not found by monoclonal phage ELISA. Particularly, Fab R2C7 exhibited an inhibition potency of 100 nM with an excellent selectivity to MMP-14 over MMP-9. Inhibition kinetics and epitope mapping suggested that as a competitive inhibitor, R2C7 directly bound to the

vicinity of the MMP-14catalytic site. This study demonstrates that deep sequencing is a powerful tool to facilitate the systematic discovery of mAbs with protease inhibition functions.

2.1 Introduction

Using phage panning and monoclonal ELISA screening, 14 Fabs inhibiting MMP-14 were isolated from the constructed human antibody libraries carrying long CDR-H3 regions. Particularly, Fabs 3A2 and 3D9 exhibited nM potency competitive inhibition toward MMP-14 with no reactivity to MMP-2 or -9[1]. However, it has been demonstrated that standard ELISA screenings are incapable of recovering all the antibodies enriched by phage panning or other screening/selection processes[2,3], for at least two reasons: (i) slow growth rates of certain enriched clones resulting in low cell density after propagation; (ii) low expression levels of certain antibody proteins resulting in weak ELISA signals.

Next-generation sequencing (NGS) technologies have revolutionized multiple aspects of biological researches[4,5,6,7], with profound impacts on discovery of specific and functional mAbs[8,9,10,11]. By high resolution profiling of an antibody library's diversity, with sequence and frequency information on virtually all clones during screening process, NGS followed by in-depth analysis has been employed to discover many valuable mAbs not found by ELISA screenings[2,3,12]. Encouraged by these studies, we aim to use in-depth analysis to systematically identify and characterize enriched long CDR-H3 clones from our previously panned libraries[1]. In current study, the DNA samples for Illumina sequencing were prepared without

PCR by direct ligation to custom-designed sequencing adapters, which avoid introducing amplification bias. After high-throughput sequencing and bioinformatics analysis, the genes of the 29 most abundant Fab clones in the second and the third rounds of panning (R2 and R3) were rescued. Associated Fabs were then produced and tested for affinity, inhibition, and selectivity (flowchart shown as Figure 2.1).

Using this technique, we identified 20 inhibitory Fabs, of which 15 were not found by previous ELISA screening. This study demonstrated that, as a supplement to ELISA, deep sequencing is a very powerful tool to facilitate the systematic discovery of antibodies with protease inhibitory functions.

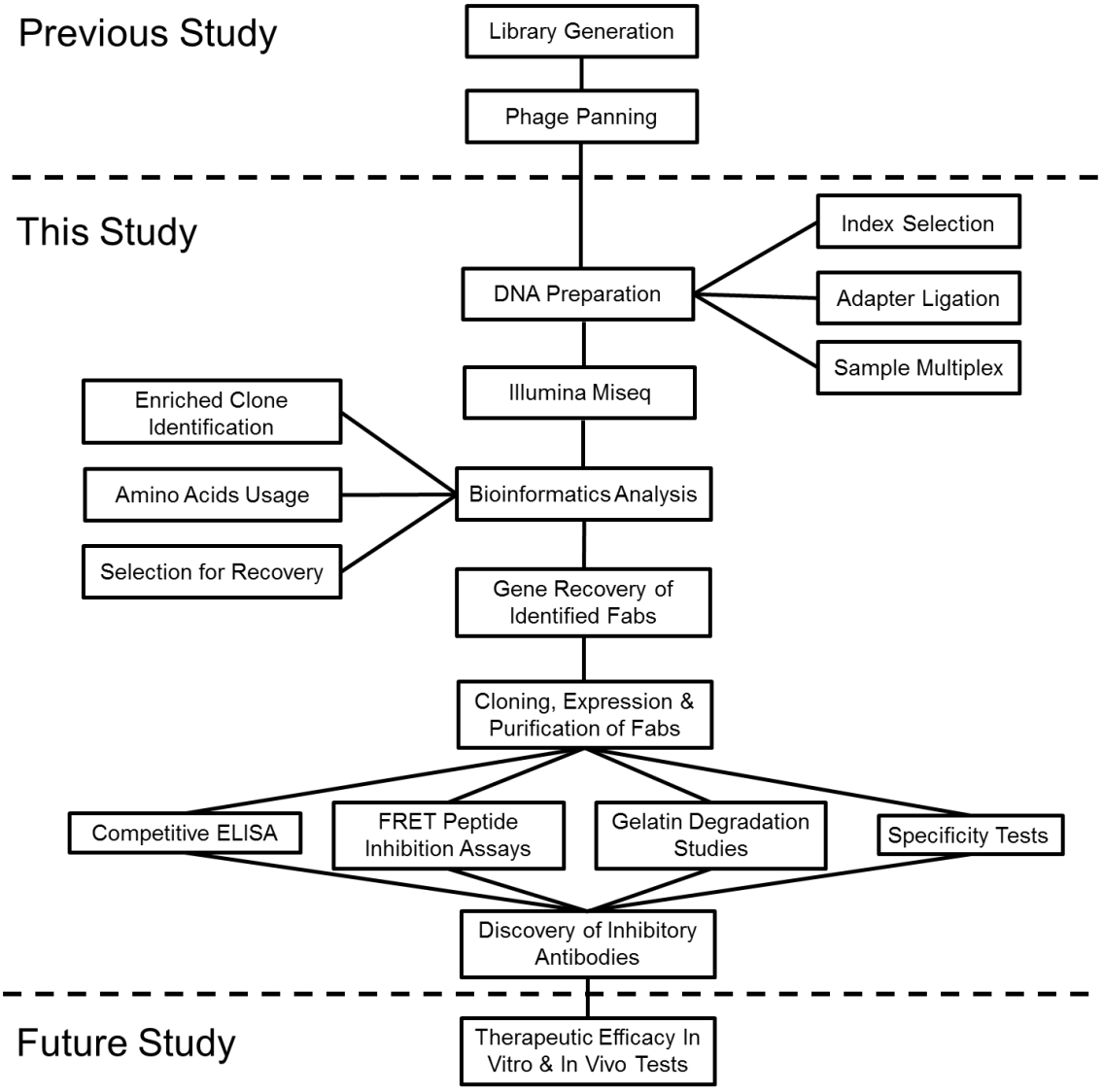

Figure 2.1: **Illumina sequencing and bioinformatics analysis for discovery of inhibitory antibodies.** Synthetic antibody libraries carrying long CDR-H3 were constructed and subjected to three rounds of phage panning against cdMMP-14 (previous study[1]). Panned phage libraries were analyzed by deep sequencing to identify Fab clones inhibiting cdMMP-14, and isolated antibodies were characterized biochemically.

2.2 Materials and Methods

2.2.1 Preparation of VH Library DNA for Deep Sequencing

Synthetic antibody Fab phage libraries (1.25×10^9 variants) carrying extended CDR-H3 (23–27 amino acids) were constructed and subjected to three rounds of panning[1] against the catalytic domain of MMP-14 (cdMMP-14), which was recombinantly expressed[13], purified, biotinylated, and immobilized on ELISA plates via streptavidin biotin interactions. During phage panning, the native competitive inhibitor of MMP-14, TIMP-2 was applied to elute bound phages. For each round of panning (R1, R2, and R3) as well as the original library (Og), Escherichia coli cells were infected with the eluted phages and cultured 6 h in 2×YT supplemented with 100 mg/ml ampicillin. The Fab library plasmids were miniprepped, and double digested with DraIII and BseRI, to isolate the fragments encoding VH FR2-CDR2-FR3-CDR3-FR4 (~280 bp) from gel electrophoresis (Zymo Research, Irvine, CA).

The Illumina sequencing adapters P5 and P7 were customized by introducing a DraIII overhang trinucleotide sequence TGG and a BseRI overhang binucleotide sequence TG at their 50 and 30 ends respectively (Figure 2.2A). To distinguish DNA samples from various panning rounds, sequencing indexes selected from Illumina's Nextera Kit were used as the barcodes. To maintain an A + C to G + T ratio of 1:1, I5 indexes [N/S/E] 501-504 and I7 indexes N703, N704, N709, and N710 were chosen for library samples Og, R1, R2, and R3, respectively (Figure 2.2B). Both strands of modified P5 and P7 adapters containing the selected

indexes were synthesized with 5’ phosphorylation (IDT,Coralville, IA), and annealed by gradient cooling from 95^{o}C to 25^{o}C over 45 min in a thermocycler (Bio-Rad, Hercules, CA) to generate double stranded adapters.

Prepared libraries of VH fragments were directly ligated with assembled P5 and P7 adapters via the sticky ends, a non-PCR approach without the introduction of biases caused by amplification. Specifically, 400 ng of DNA at a 10:1 molar ratio of adapters to VH fragments was mixed in a 50 mL reaction containing 1,000 U of T4 DNA ligase (NEB, Ipswich, MA). After incubation at 4^{o}C for 16 h, unreacted adapters were removed from the ligated products (DNA clean up kit, Zymo Research). The purity and concentrations of adapter ligated VH fragments were determined by spectrophotometry and by RT-qPCR. VH libraries before and after 1–3 rounds of panning were multiplexed based on their concentrations to generate a sequencing mixture with a 10:1:1:1 ratio. After multiplexing the quality of the library was checked using an Agilent 2100 Bioanalyzer

2.2.2 Bioinformatics Analysis

The multiplexed library was subjected to NGS using a MiSeq sequencer (Illumina, Riverside, CA). Deep sequencing data were analyzed using an automatic bioinformatics pipeline, which combines MATLAB, Perl, Excel, GSplit, and the Windows OS. Large raw FASTQ data files were first split into manageable pieces using GSplit. Each piece was then run through MATLAB to extract the DNA sequences and quality scores. The data were then passed to PERL to isolate high quality sequences containing in-frame CDR-H3 regions. The conserved

sequences flanking the CDR-H3 were utilized as the searching motifs for identification of CDR-H3[10]. Each clone was ranked and named according to its library and relative abundancy, for example, clone R2C3 represents the third most abundant clone after two rounds of panning.

A

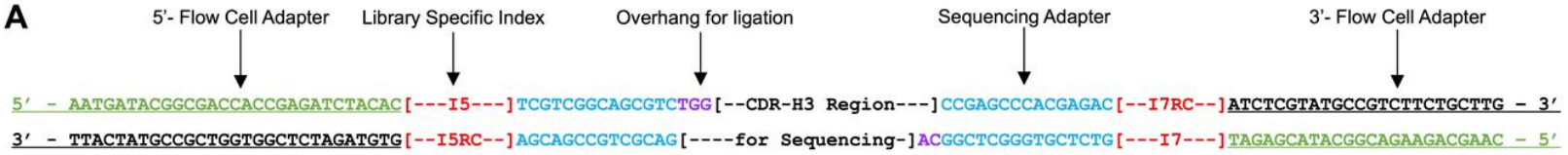

B

	I5 Index		I7 Index	
Library	Name	Sequence	Name	Sequence
Og	[N/S/E]501	TAGATCGC	N703	AGGCAGAA
R1	[N/S/E]502	CTCTCTAT	N704	TCCTGAGC
R2	[N/S/E]503	TATCCTCT	N709	GCTACGCT
R3	[N/S/E]504	AGAGTAGA	N710	CGAGGCTG

Figure 2.2: Custom-designed primers for Illumina sequencing. (A) Diagram of the full-length sequencing samples with four primers showing functions of each segment. Double-stranded upstream and downstream adapters were assembled by annealing primers via gradient cooling. The flow cell adapter is for binding to the surface of sequencing channels in flow cells. The index allows de-multiplexing of the libraries for accurate analysis and reduction of batch-to-batch variations. I5RC and I7RC represent the reverse compliments of the I5 and I7 index respectively. The sequencing adapters correspond to the sequencing primer used in MiSeq analysis. A high melting temperature is chosen to avoid de-associating the primers during the sequencing runs. The 3'-overhangs allow direct ligation of the digested double-stranded CDR-H3 DNA with adapters for sample preparation without PCR amplification. (B) Indexes used for each library. The I5 and I7 indexes are for the upstream and downstream adapters respectively, and chosen to maintain a 1:1 ratio of (A+C) : (G+T).

2.2.3 Cloning, Expression, and Purification of Fabs

Genes of identified highly abundant Fab clones were PCR amplified from their associated libraries using a universal forward primer recognizing the 50 of the VL fragment and clone-specific reverse primers matching the unique CDR-H3 sequences. All the primers were designed to have a Tm of 72^{o}C. After initial extraction an extension PCR was performed to amplify and introduce a PpuMI cutting site at the 30 of the CDR-H3. A Fab phagemid[1] was modified to introduce a PpuMI site via a silent mutation immediately downstream of the CDR-H3 region for direct cloning of amplified Fab genes using NsiI/PpuMI restriction sites. Ligated plasmids were cloned into E. coli Jude-I [(DH10B) F'::Tn10 (Tetr)] cells for sequence confirmation, then transformed into BL21 cells for expression.

Fabs containing a 6×His tag at C-terminal of CH1 were produced by culturing transformed BL21 cells in 2×YT at 30^{o}C for 15 h. After expression the periplasmic fractions were prepared by osmotic shock with 25% sucrose followed by treatments with lysozyme, EDTA, and $MgCl_2$. Samples were centrifuged at 15,000 g for 15 min at 4^{o}C to obtain the supernatants containing the Fabs. Periplasmic solutions were then passed through a 0.22 mm filter and purified by using Ni-NTA agarose (Qiagen, Valencia, CA).Purified Fab samples were buffer exchanged into 50 mM HEPES (pH 7.5) by dialysis at 4^{o}C using SnakeSkin tubing (ThermoScientific, Pittsburgh, PA), and concentrated by using ultrafiltration centrifugation tubes with MWCO of 10 kDa (Amicon, EMD Millipore, Temecula,

CA). The purity and concentration of produced Fabs were determined by SDS–PAGE and OD_{280} absorption measurements.

2.2.4 Antibody Characterizations:

2.2.4.1 Dose-Dependent ELISA and Specificity Tests

cdMMP-9, cdMMP-14, and cdMMP-14 mutants were cloned and produced in their active format in periplasmic space of E. coli without refolding or activation[13]. After labeling purified cdMMP-14 using EZ-Link Sulfo-NHS-LC biotinylation kit (ThermoFisher, Lafayette, CO), biotin-cdMMP-14 was incubated in a streptavidin coated ELISA plate (Thermo Scientific) blocked with biotin-BSA. After washing, 50 mL of 2mM Fabs were then added to the first well and serially diluted to ~1 nM and incubated for 30 min at 4^{o}C. After washing, the ELISA signals were developed by anti-Fab-HRP (Sigma, St. Louis, MO) and TMB (Thermo Scientific). The color development reaction was stopped by addition of H_2SO_4, and the absorptions at 450nm were measured. Binding selectivities of Fabs to cdMMP-14 over cdMMP-9 were studied by competitive ELISA. Fabs were incubated with a gradient concentration ofcdMMP-9 from 4 mM to 2 nM for 1.5 h at room temperature. After incubation, samples were transferred to an ELISA plate coated with 100 nM cdMMP-14 and processed as described above. Binding kinetics of isolated Fabs were measured by bio-layer interferometry. Using ForteBio BLItz system, biotinylated cdMMP-14 was loaded onto a streptavidin biosensor for 60 s to establish baselines. Fabs were introduced at a variety of concentrations and their association to immobilized cdMMP-14 was monitored for 3min then allowed to

dissociate into 50 mM HEPES (pH 6.8) for 10 min. Determined k_{on} and k_{off} parameters were used to calculate KD values.

2.2.4.2 FRET Inhibition Assays

The functionality of purified Fabs to inhibit cdMMP-14 activity was tested by FRET assays. Typically, 1 mM of purified Fab was serially twofold diluted into assay buffer (50 mM Tris-HCl pH 7.5, 150 mM NaCl, 5 mM $CaCl_2$, 0.5 mM $ZnCl_2$), and incubated with 10 nM cdMMP-14 for 30min at 4^{o}C. The kinetic measurements were started with the addition of 1mM M2350 peptide substrate (Bachem, Torrance, CA) and the fluorescence was monitored with excitation and emission wavelengths at 325 and 392 nm. To determine the type of inhibition Fabs were diluted to concentrations generating 70%, 50%, and 30% inhibition in HEPES assay buffer (50 mM HEPES pH 6.8, 150 mM NaCl, 5 mM $CaCl_2$, 0.5 mM $ZnCl_2$), and incubated with 10 nMcdMMP-14 at 4^{o}C for 30 min. For each Fab concentration, 50 mM to 2 mM FRET peptide substrates were added for kinetics measurements.

2.2.4.3 Gelatin Degradation Studies

A total of 10 nM cdMMP-14 was incubated with 1 mg/mL gelatin (porcine skin, Sigma) in the absence or presence of 1 mM Fabs for 24 h at room temperature, then samples were analyzed by 12 % SDS–PAGE. A synthetic inhibitor GM6001 and a non-inhibitory Fab R2C17 were used as the positive and negative controls.

2.3 Results

2.3.1 Illumina deep sequencing of long CDR-H3 Fab libraries

Human Fab phage display libraries carrying CDR-H3 regions with 23, 25, and 27 aa in length were synthesized and subjected to three rounds of panning (R1, R2 and R3) against catalytic domain of MMP-14 (cdMMP-14)[1]. For each round, the bound phages were eluted by incubation with n-terminal domain of tissue inhibitors of metalloproteinases (n-TIMP-2), which is a native inhibitor of MMP-14 behaving in a competitive mode[15]. In principle, only the Fab phages directly interacting with the catalytic portion of MMP-14 or allosterically interfering n-TIMP-2 binding can be eluted off. Therefore, the combination of convex paratope library design with epitope-specific elution presumably results in enrichment of specific inhibitory antibodies. This hypothesis was partially confirmed by the panel of inhibitory Fabs isolated by ELISA screening in our previous study[1]. Aiming to fully understand the sequence landscape changes during the panning process and to systematically identify and characterize a large number of the most enriched antibody clones, libraries R1, R2, R3 and the original library before panning (Og) were subjected to Illumina NGS (Figure 2.1). Briefly, Og, R1, R2, and R3 phagemids were purified, and their fragments encoding CDR-H3s with partial FR3 and FR4 regions were prepared by restriction digestion and direct ligation with custom-designed adapters for Illumina sequencing (Figure 2.2A). This PCR free procedure should minimize the introduction of amplification bias, which is critical for frequency based antibody discovery[2,3,9,10,11]. RT-qPCR analysis showed that

the assembled DNA samples had uniform melting temperatures, suggesting high quality and purity. The library DNA concentrations were quantified and the samples were multiplexed at a ratio of 10:1:1:1 (Og:R1:R2:R3) for sequencing. Analysis on an Agilent 2100 bioanalyzer further confirmed that the multiplexed DNA sample displayed sharp peaks associated with designed base pairs, indicating successful ligations with the flow cell adapters at both ends.

Sequencing raw data was de-multiplexed using unique indexes and processed in house to remove truncated and out of frame reads. Sequences either containing reading frame shifts due to sequencing errors or with low quality (quality scores less than 30) were excluded from further analysis. A total of 1.83×10^6, 1.09×10^7, 6.67×10^6, and 2.81×10^5 functional sequences were obtained for libraries Og, R1, R2, and R3 respectively, which accounted for 56-90% of the raw data (Table 2.1).

Table 2.1: Statistics of deep sequencing results.

	Raw Data	In-Frame Full-Length CDR-H3s	In-Frame Full-Length/raw data (%)	Unique CDR-H3s	Unique / In-Frame Full-length (%)	Frequency (copy numbers) of the most abundant clone
Og	2,039,671	1,834,712	8995.00%	1,834,576	99.99	0.000 (2)
R1	19,488,812	10,941,297	5614.00%	10,791,087	98.63	0.009 (981)
R2	11,761,506	6,665,700	5667.00%	6,229,221	93.45	0.129 (8600)
R3	50,457	28,127	5574.00%	19,906	70.77	1.888 (531)

Given that the library diversity usually decreased to $<10^5$ after the first round of biopanning, the Illumina results provided a considerable coverage and well represented the majority of R1, R2, and R3 library clones. The large diversity of Og (1.25×10^9) was not covered by NGS, nevertheless $>10^6$ reads are adequate to probe the quality of constructed library.

2.3.2 Long CDR-H3s enriched with hydrophilic and positively charged residues after panning on cdMMP-14

As the most important region of antigen binding, CDR-H3s were focused for bioinformatics analysis (Table 2.1). Their sequences were recognized by using the signature motifs flanking N- and C-termini of CDR-H3s[3,10]. Analysis results indicated that the original library as expected, contained an even distribution of CDR-H3s with 23, 25, or 27 aa (30-37% each). Interestingly, after phage panning more than half of Fabs (58%) had 25 aa in their CDR-H3s, and the proportions of CDR-H3s with 23 or 27 aa decreased to 7 and 19% (Figure 2.3A).

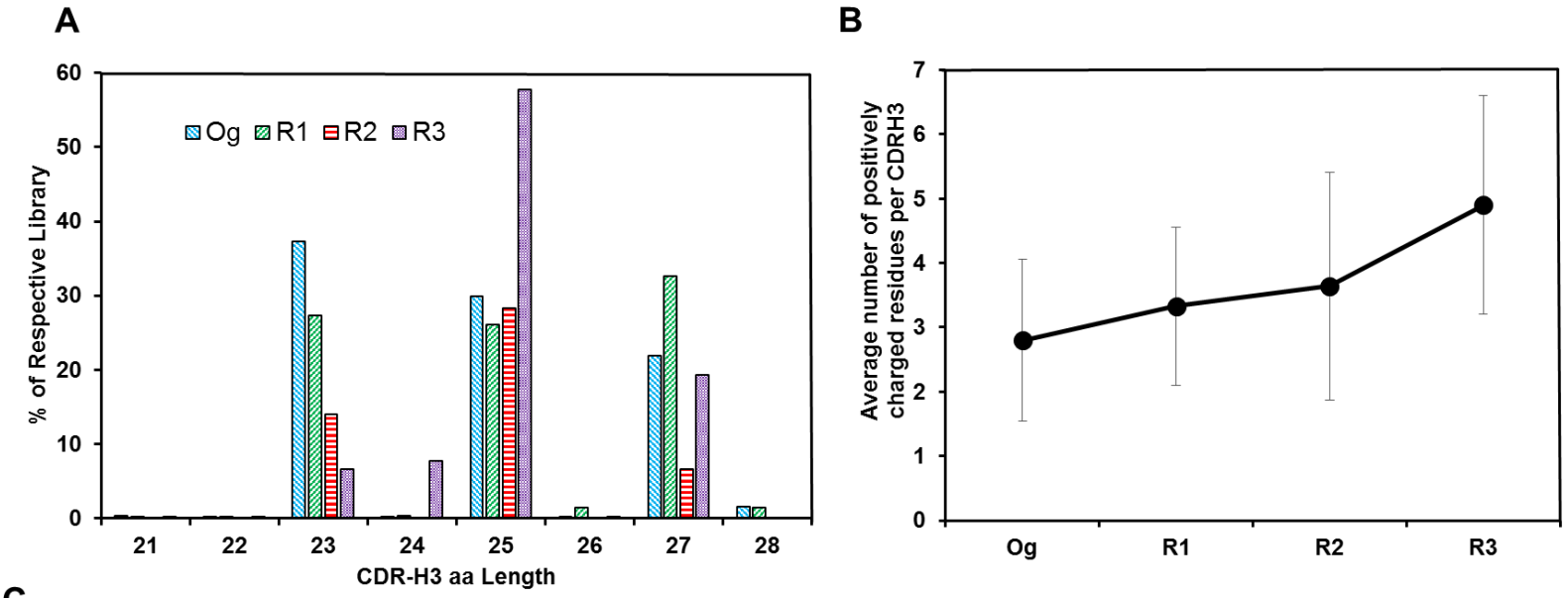

C

	92	93	94	95	96	97	98	99	100	100A	100B	100C	100D	100E	100F	100G	100H	100I	100J	100K	100L	100M
Positively Charged	-11	-14	**28**	-3	6	15	-7	**28**	**25**	-5	-7	**29**	17	-2	-2	1	2	-4	0	15	2	0
Negatively Charged	-11	2	-5	-4	4	0	-6	-6	-4	-6	-5	-5	-6	-4	-4	-2	-4	**22**	-5	-2	8	1
Polar	**24**	13	-4	-8	**30**	**22**	0	11	-12	-6	**33**	11	15	18	-10	5	-5	12	10	-5	6	0
Hydrophobic	-19	8	-5	2	**-31**	**-25**	**23**	**-27**	2	19	-18	**-26**	**-20**	-2	0	5	**20**	**-27**	-6	**-22**	-19	-12

Figure 2.3: Repertoire analysis of phage panned long CDR-H3 libraries. (A) CDR-H3 length distribution. (B) Enrichment of positively charged residues (R, H, K) at CDR-H3. (C) Amino acid composition changes at each position (92–100 M) of CDR-H3 with 25 aa. Residues were grouped according to biochemical properties: positively charged (R, H, K), negatively charged (D, E), polar (S, T, N, Q), and hydrophobic (A, I, L, M, F, W, Y, V). The percentage changes from the library Og to R3 are listed, positions with >20% change were highlighted in bold boxes.

Taking 25 aa CDR-H3s as an example, at each position of 92-100K, the Og library showed uniform usage of 20 amino acids (Figure 2.3), indicating constructed synthetic antibody libraries had high quality and well represented the diversity designs. During panning process, CDR-H3 amino acid usage distributions altered dramatically (Figure 2.3,Figure 2.4). Particularly, the average number of positively charged residues (Arg/His/Lys) steadily increased from 2.8 aa per CDR-H3 in Og to 3.3 in R1, 3.6 in R2, and finally 4.9 in R3 (Figure 2.3B). This suggests the panning process enriched positively charged paratopes, which probably enhances interactions with the negatively charged MMP-14 catalytic cleft vicinity[15]. The usages of amino acids grouped according to physicochemical properties were further analyzed at individual residue positions of CDR-H3s. Results for CDR-H3s with 25 aa are shown in Figure 2.3C, in which changes of 20% and more from Og to R3 are highlighted. Positively charged residues were enriched at positions 94, 99, 100, and 100C; proportions of negatively charged residues (Asp/Glu) increased at position 100I; polar residues (Ser/Thr/Asn/Gln) presented more at positions 92, 96, 97 and 100B; and hydrophobic residues (Ala/Ile/Leu/Met/Phe/Trp/Tyr/Val) presented less at position 96, 97, 99, 100C, 100D, 100I, and 100K. Overall, the increase of charged and hydrophilic residues with decrease of hydrophobic residues presumably improves Fab solubility, a phenomenon well documented in literatures[16,17,18].

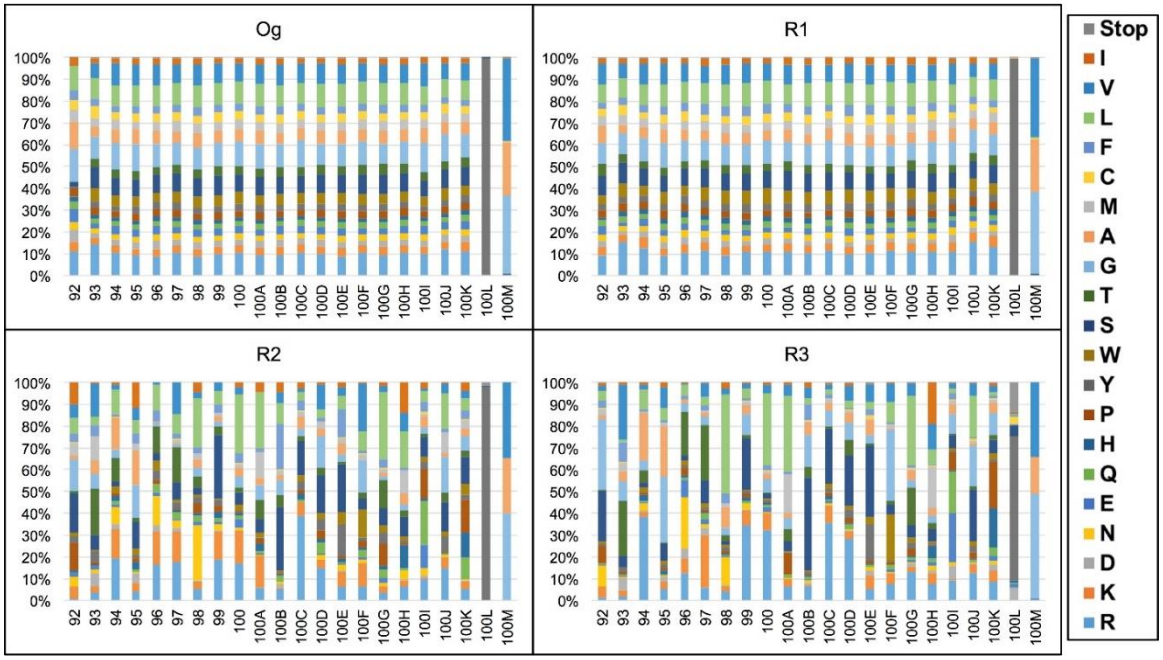

Figure 2.4: Analysis of amino acid usage at each position of CDR-H3s. The even distribution in the original library is indicative of high quality of the constructed library as designed. The usage distribution dramatically altered over the course of phage panning. CDR-H3s with 25 aa in length were used as an example for analysis.

2.3.3 Identification of highly abundant Fab clones and tracking their enrichment profiles

After bioinformatics analysis of the entire libraries in general, individual Fab clones with the highest abundancies were identified for further studies. Limited by Illumina reading length capacity, the most diverse regions, CDR-H3s were chosen as the signature sequences to represent the associated Fabs in analysis, and the full VH and VL sequences of particular clones of interest were later recovered by PCR using specific primers. For libraries Og, R1, R2 and R3, a total of 1.83×10^6, 1.08×10^7, 6.23×10^6, 1.99×10^4 different CDR-H3s were found (unique CDR-H3s, Table 2.1). The ratios between numbers of unique CDR-H3s over numbers of all in-frame full-length CDR-H3s in the associated library are 99.99% for Og, 96.63% for R1, 93.45% for R2 and 70.77% for R3. The copy numbers of each unique CDR-H3 sequences within R1, R2 and R3 were then counted, and their abundancies were calculated by dividing their copy numbers with the total number of functional CDR-H3s in that library (Table 2.1). Results demonstrated that the most abundant clones in R1, R2, and R3 had frequencies of 0.009%, 0.129%, and 1.889% respectively, reflecting the quick enrichment progress during panning as expected. Because R1 enrichment was pre-mature, only R2 and R3 were used for Fab identification in the following analysis.

Due to the synthetic nature and relatively small dataset (1.83×10^6) of Og library compared to constructed diversity (1.25×10^9), majority of clones in Og presumably should have a single copy number. Our results indeed indicated that

99.99% of Og CDR-H3s had a single copy, < 0.01% CDR-H3s have two copies and there are no clones with more than two copies (Table 2.1), suggesting each clone in Og has a low and even frequency. Consequently, the enrichment of a given clone in R1, R2 or R3 over Og can be directly reflected by their frequencies in the associated library, therefore, the clones with the highest abundancies are the most enriched clones. The 22 most abundant clones in R2 were identified with frequencies ranging from 0.13% to 0.02% (named as R2C1-R2C22 with their CDR-H3 sequences shown in Table 2.2). None of these 22 clones were detected in Og (zero copies). In R1, the majority of these 22 clones had zero copies and only R2C3 and R2C19 had one copy.

Notably, the ranks and abundancies of these 22 clones in R2 were not always correlated with these in R3. More specifically, 15 clones such as R2C3, R2C4, and R2C6 exhibited further enrichments, *i.e.* a higher abundancy in R3 than R2. Because of this enrichment pattern, 7 of the 22 most abundant clones were discovered using traditional ELISA screening (Table 2.2)[1]. Clones R2C9, R2C10, and R2C17 displayed increased frequencies from Og to R1 and to R2, however their frequencies in R3 were similar to R2. These plateaus can be attributed to the balance between enrichment driven by panning and the depletion caused by slow cell growth. Interestingly, several top ranked clones in R2 such as R2C7, R2C18, and R2C22 showed declined frequencies in R3. As a consequence, these particular clones were not identified in ELISA screenings of R3 library, because of their low frequencies in R3 (<0.01% with rankings >10,000, Table 2.3).

Table 2.2: In depth analysis of highly enriched clones from R2 and R3.

ID by NGS [a]	Sequence (CDR-H3 length)	% of R2	% of R3	Rank in R3	Binding Affinity [b]	Inhibition potency	Yield (mg/L)
R2C1*	STAATTLSRMSRSYWTIQLPYGMDY (25)	**0.13**	1.89	1	600 nM	Non-Inhibitory	1
R2C2*	GVRGNKLRLLSSRSGLMESHYVMDY (25)	**0.12**	1.66	2	> 1 μM	> 1 μM	2
R2C3*	PTTSRVNKKLFRVSVLHPGSYGMDY (25)	**0.11**	0.61	4	220 nM	> 1 μM	1
R2C4	GWRVYADRGHVRGYFRVWYGMDY (23)	**0.1**	0.53	3	> 1 μM	~1 μM	2
R2C5	IMKIKRNSLKFRGFVPLQMQYVMDY (25)	**0.09**	0.14	14	375 nM**	50 nM	3.5
R2C6	KDLLKTNRLTTRYKKSVSVGYGMDY (25)	**0.07**	0.53	5	> 1 μM	> 1 μM	1
R2C7	SCVWACCACRYWSGSDSHYAMDY (23)	**0.06**	0.01	~12500	153 nM	100 nM	1
R2C8	PGRHLQTTFKGYQFKYSRYIYAMDY (25)	**0.05**	0.16	12	> 1 μM	~1 μM	3.5
R2C9	VLNIFMDVGAARFPGLVRYGMDY (23)	**0.04**	0.05	~4200	657 nM**	80 nM	0.75
R2C10	MAKDFRILASVRMWVLASRLYVMDY (25)	**0.04**	0.03	~8400	360 nM	Non-Inhibitory	0.5
R2C11	RYGSDVFCVGCFFGVRLSYVMDY (23)	**0.03**	0.03	~9100	750 nM	600 nM	0.75
R2C12	SDSWVQGRDFCYYSAWVGYGMDY (23)	**0.03**	0.05	~2600	150 nM	150 nM	0.5
R2C13*	LYNGWLMVEGIGSAREGPTWYAMDY (25)	**0.03**	0.09	21	20 nM	150 nM	< 0.01
R2C14	VSNRYNRSSASIAGLQLFRPYGMDY (25)	**0.03**	0.05	~2600	> 1 μM**	10 nM	0.5
R2C15*	SVHMKLSNKILSGWSWNNSFYAMDY (25)	**0.03**	0.07	28	350 nM	> 1 μM	2
R2C16	FKNADFAAGGQWSKMLIARMYAMDY (25)	**0.03**	0.1	17	> 1 μM	> 1 μM	2.4
R2C17	VGAWRVPSERMFTYPSARTRYAMDY (25)	**0.03**	0.02	~11000	> 1 μM	Non-Inhibitory	0.4
R2C18	RDFGGFAGCLDGYVHVCWYAMDY (23)	**0.02**	<0.01	~13000	430 nM	Non-Inhibitory	0.5
R2C19*	LDRDRYIHVGRAGNTYSNYYYVMDY (25)	**0.03**	0.17	11	5 nM	Non-Inhibitory	0.5
R2C20*	NFRVESAGRPGKTVLRKDGKYAMDY (25)	**0.03**	0.47	6	> 1 μM	Non-Inhibitory	0.5
R2C21	LAWKSDNRGSFAKLQFTLKMYGMDY (25)	**0.02**	0.08	25	Non-Binding**	50 nM	0.25
R2C22	HSRDGWQHWFGNWAGLHSYGMDY (23)	**0.02**	<0.01	~13000	540 nM**	75 nM	0.15
R3C7*	EIHMLSRQARYLRDGRRPRGSMYVMDY (27)	0.01	**0.33**	7	30 nM	> 1 μM	2
R3C8	HCLLRSRRCEMSTKTRELNVYRYAMDY (27)	0.01	**0.3**	8	> 1 μM	> 1 μM	1
R3C9*	VKLQKDKSHQWIRNLVATPYGRYVMDY (27)	0.01	**0.29**	9	4 nM	10 nM	1
R3C10	GSLRRDFNLVVRSSWDIRSNYVMDY (25)	<0.01	**0.2**	10	> 1 μM	~1 μM	2
R3C13	WLRVSLKSGVYKVLARAVELDEYVMDY (27)	0.01	**0.14**	13	> 1 μM	> 1 μM	3
R3C15	GVRGNKLRLLSSRSGRMESHYVMDY (25)	<0.01	**0.14**	15	57.5 nM	170 nM	4
R3C16	MASIDLRMLSRMLAGPQFKVYGMDY (25)	0.01	**0.11**	16	Non-Binding**	~1 μM	1

Note:

[a]Clones were identified and ranked by their abundancies in their respective libraries (bold numbers). Previously discovered Fabs by monoclonal phage ELISA are labeled as *.

[b]Fab genes were rescued by PCR and sub-cloned for expression. Purified Fabs were tested for binding affinity (by ELISA EC_{50}) and inhibition potency (by FRET IC_{50}). Fabs with EC_{50} >2 × IC_{50} are labeled as **.

Table 2.3: Frequency analysis of the 20 MMP-14 binding clones identified by ELISA in previous study[1]).

ID by ELISA	ID by NGS	CDR-H3 Sequence (Length)	Og (%)	R1 (%)	R2 (%)	R3 (%)	Binding Affinity (nM)	Inhibition Potency (nM)
3A2	R3C9	VKLQKDKSHQWIRNLVATPYGRYVMDY(27)	0	0	0.01	**0.29**	3.8	9.7
3E2	-	GIKGLVFTGSQMKMLRRGNYNWYYVMDY(27)	0	0	0	0.03	47	42
3D9	-	RLMAYHGSCSSRLCQTAISPQRYAMDY(27)	0	0	0.01	0.04	6.4	61
2B5	-	IGVNAWAVKMSQRMLATRGSGWYYVMDY(27)	0	0	0	0.03	24	240
3G9	-	ATNEKFRRKSLQVRLLMRSWLAYAMDY(27)	0	0	0.01	0.04	160	390
33D2	-	SKYGPASRQLASRTSWSGPRGKYGMDY(27)	0	0	0	0	120	420
3F3	R2C13	LYNGWLMVEGIGSAREGPTWYAMDY(25)	0	0	**0.03**	0.09	34	970
33F3	R2C2	GVRGNKLRLLSSRSGLMESHYVMDY(25)	0	0	**0.12**	1.66	1000	2300
33D4	R2C15	SVHMKLSNKILSGWSWNNSFYAMDY(25)	0	0	**0.03**	0.07	460	3900
32D1	-	MSLHRNFNQQGRSRLLGRMPRTYGMDY(27)	0	0	0	0.04	350	4200
3A6	-	RPCKACRTRLELVRRGMDSGLRYGMDY(27)	0	0	0	0.05	980	4200
33C4	R2C3	PTTSRVNKKLFRVSVLHPGSYGMDY(25)	0	7.99E-03	**0.11**	0.61	220	4600
3E9	-	NGRYPGFLKRAHKRLLNFKAYVMDY(25)	0	0	0.01	0.01	51	6000
32C2	-	SQHAKKSTIIRMLEHQSRSGMQYVMDY(27)	0	0	0	0.01	150	8000
32E10	R2C19	LDRDRYIHVGRAGNTYSNYYYVMDY(25)	0	7.99E-03	**0.03**	0.17	9.7	-
32C11	R3C7	EIHMLSRQARYLRDGRRPRGSMYVMDY(27)	0	0	0.01	**0.33**	29	-
2H9	-	GTSFQVRCVLYRLLSPGRYVMDY(23)	0	0	0	0.02	120	-
3B2	R2C1	STAATTLSRMSRSYWTIQLPYGMDY(25)	0	0	**0.13**	1.89	590	-
2E4		SARLRLRGNHDRRRSKSVYYRPYVMDY(27)	0	0	0	0	840	-
33F5	R2C20	NFRVESAGRPGKTVLRKDGKYAMDY(25)	0	0	**0.03**	0.47	1600	-

Note:

1. Binding affinity and inhibition IC_{50} data were from previous study[13]. Clones are ranked by their inhibition potencies or binding affinities for non-inhibitory clones.

2. All these clones have zero copies in Og. In R1, except R2C3 and R2C19 have one copy, all other clones have zero copies.

Applying similar analysis, the 17 most abundant clones from R3 were also identified with frequencies ranging from 1.89% to 0.11%. For these 17 clones, 7 were not among the top 22 clones of R2. These 7 clones were named as R3Cx, in which x is the rank of that clone in R3. All R3Cx clones were undetected in Og or R1, had relatively low frequencies in R2 (<0.01%), and quickly enriched in R3 (0.33-0.11%).

2.3.4 Gene rescue and protein production for abundant Fabs

Fab genes of these 29 top ranked clones (22 from R2 and 7 from R3) were specifically amplified from their respective libraries by PCR using a universal forward primer recognizing N-terminal of the VL and a clone specific reverse primer recognizing unique CDR-H3s. After secondary extension PCR to introduce a restriction site at the C-terminal of VH, the VL-CL-VH fragments were sub-cloned into a Fab expression plasmid. Successful gene extraction and cloning were confirmed by Sanger sequencing. The Fabs were produced in the periplasmic space of *E. coli* with typical 0.5-2.0 mg purified proteins per litter of culture medium (Table 2.2), yields sufficient for initial biochemistry characterizations. Most top ranked clones exhibited relatively high expression levels compared to the lower ranked clones, suggesting expression level is an important factor affecting enrichment progress during phage panning. Purified Fabs remained stable and functional at room temperature for at least 24 hours.

2.3.5 Discovery of a panel of inhibitory Fabs with high selectivity

The binding affinities of purified Fabs were measured by ELISA and results indicated that majority of highly abundant clones (27/29) exhibited binding specificity to cdMMP-14 with EC_{50} values ranging from 4 nM to 3 µM (Figure 2.5). Among them, eight Fabs R2C1, R2C3, R2C12, R2C13, R2C19, R3C7, R3C9, R3C15 had relatively high affinities at 4-150 nM; five Fabs R2C5, R2C7, R2C10, R2C15, and R2C18 exhibited moderate affinities at 150-500 nM; and 14 other Fabs showed weak binding with EC_{50} values at 0.5-3 µM. Given these Fabs were isolated from synthetic phage libraries, a broad range of affinities was expected.

More importantly, inhibition functions of the purified Fabs on cdMMP-14 were examined using a FRET peptide substrate to derive IC_{50} curves (Figure 2.6).Of the 29 highly abundant Fab clones identified from R2 and R3, 20 exhibited inhibition with IC_{50} values ranging from 10 nM to 4 µM (Table 2.2). Particularly, R2C14 and R3C9 had an inhibition potency of 10 nM; eight Fabs R2C5, R2C7, R2C9, R2C12, R2C13, R2C21, R2C22 and R3C15 exhibited inhibition potencies at 50-200 nM; and 10 other Fabs had weak inhibition with IC_{50} 600 nM - 4 µM.

Three Fabs R2C5, R2C7, and R2C14 of high and moderate inhibition potencies (10-100 nM) but not found by ELISA screening in previous study were were further characterized for their binding selectivity to cdMMP-14 over highly homologous cdMMP-9. Tests were performed by incubating Fabs at their IC_{50} concentrations with varying concentrations of cdMMP-9 or cdMMP-14 then adding to an ELISA plate coated with streptavidin and biotinylated cdMMP-14. Fabs R2C5,

R2C7 and R2C14 bound to cdMMP-14 on the plate even with high concentrations of cdMMP-9 in solution, indicating no interactions with cdMMP-9 (Figure 2.7). While in control experiments, the amounts of Fabs binding to immobilized cdMMP-14 responded to concentrations of cdMMP-14 in solution as expected. Therefore, Fabs R2C5, R2C7 and R2C14 exhibited high selectivity to cdMMP-14. A further zymography test of Fab R2C7 demonstrated that it inhibited cdMMP-14 from degrading gelatin (Figure 2.8).

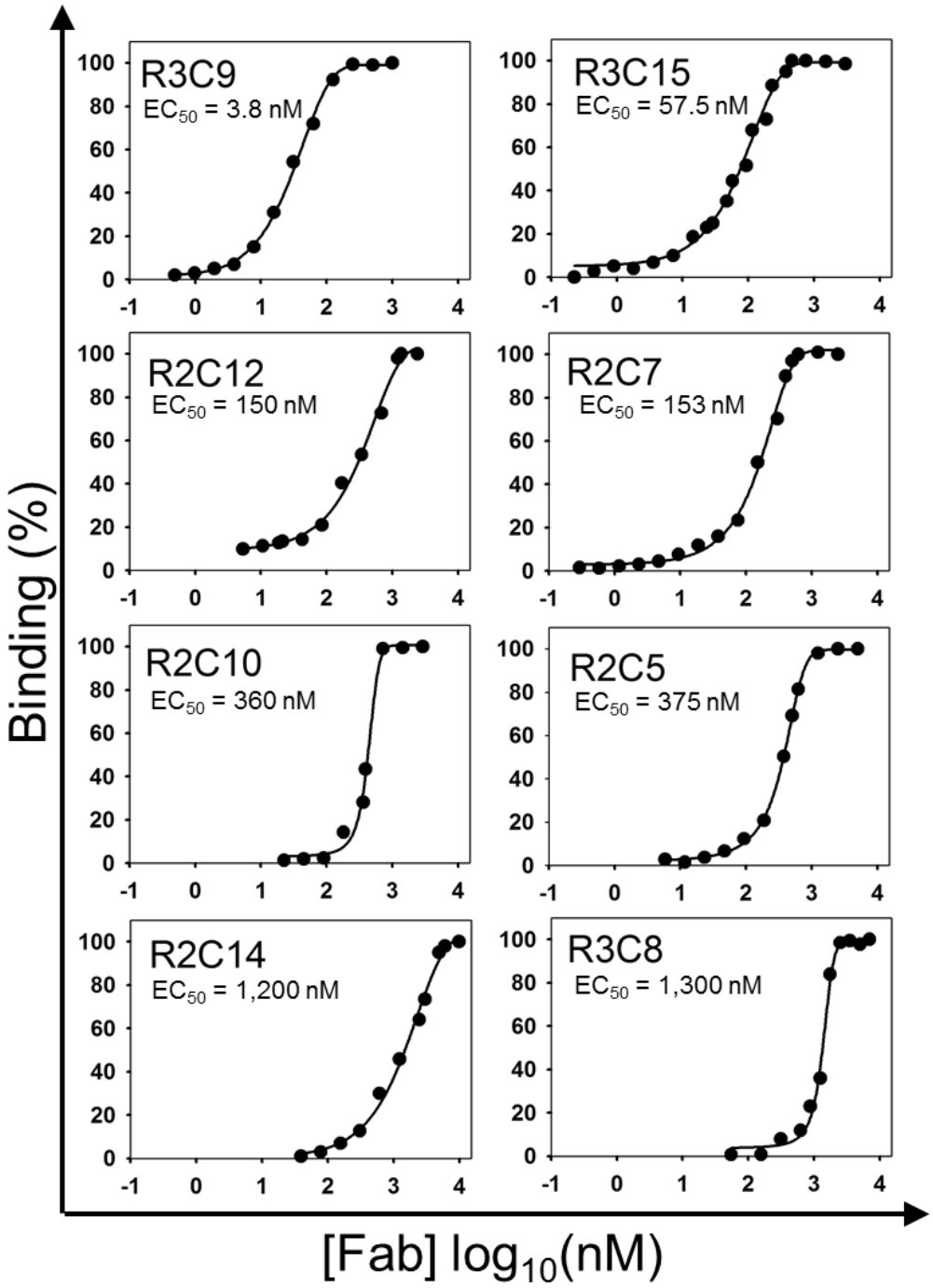

Figure 2.5: Fab binding affinities measured by ELISA. ELISA studies were performed by reacting purified Fabs with immobilized cdMMP-14 followed by tagging with anti-Fab-HRP. Color was then developed by the addition of TMB and read on a spectrophotometer. A range of binding strengths from 4 nM to 10 mM was found, which is expected from a synthetic antibody library.

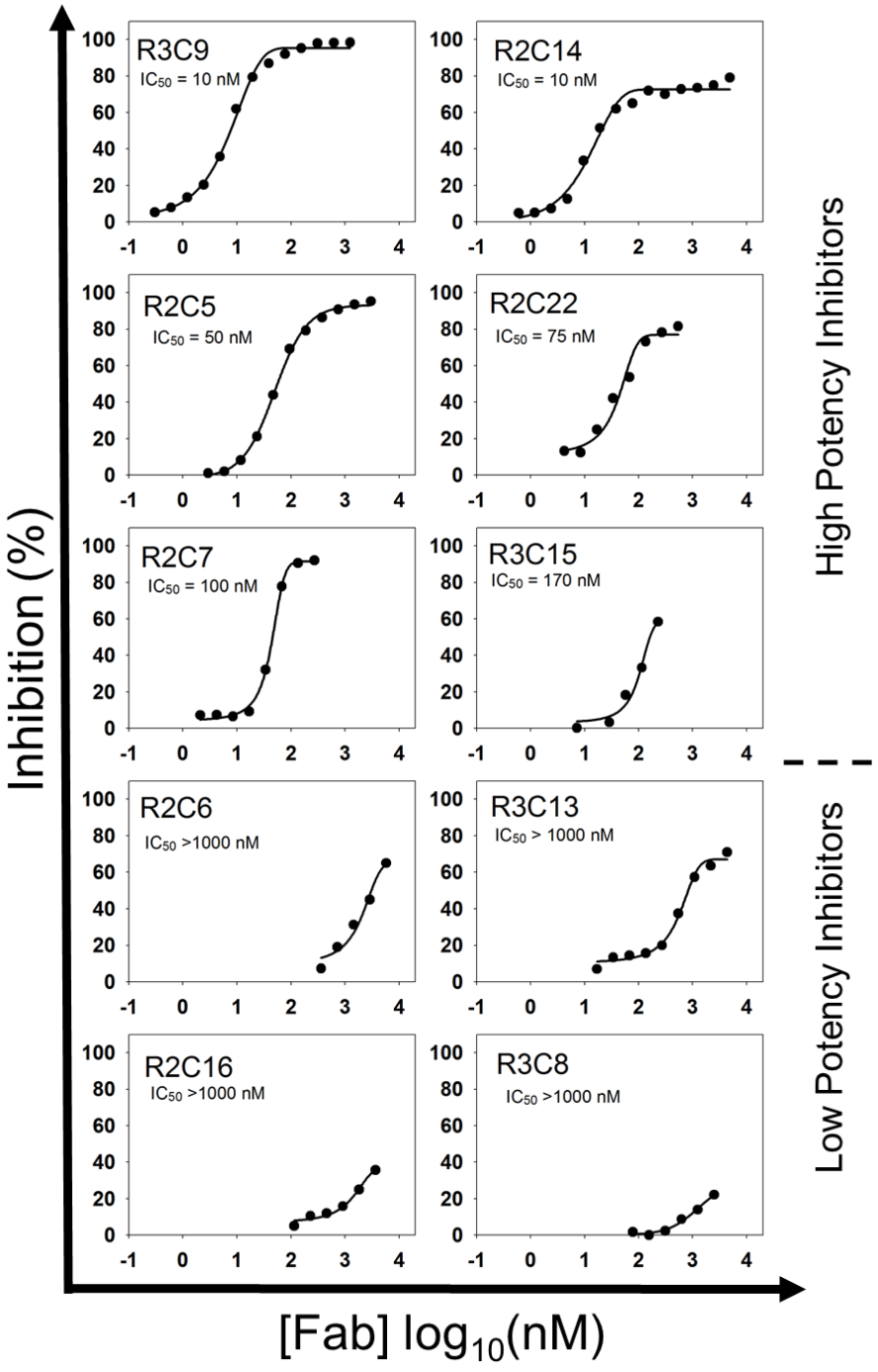

Figure 2.6: Potencies of inhibitory Fabs by FRET assays. FRET assays were performed by reacting the purified Fabs with cdMMP-14 for 30 min then adding FRET peptide substrate. The increase in fluorescence was monitored for 1 h to determine inhibitory function. A variety of inhibitory clones with potencies ranging from 10 nM to 8.0 mM was found.

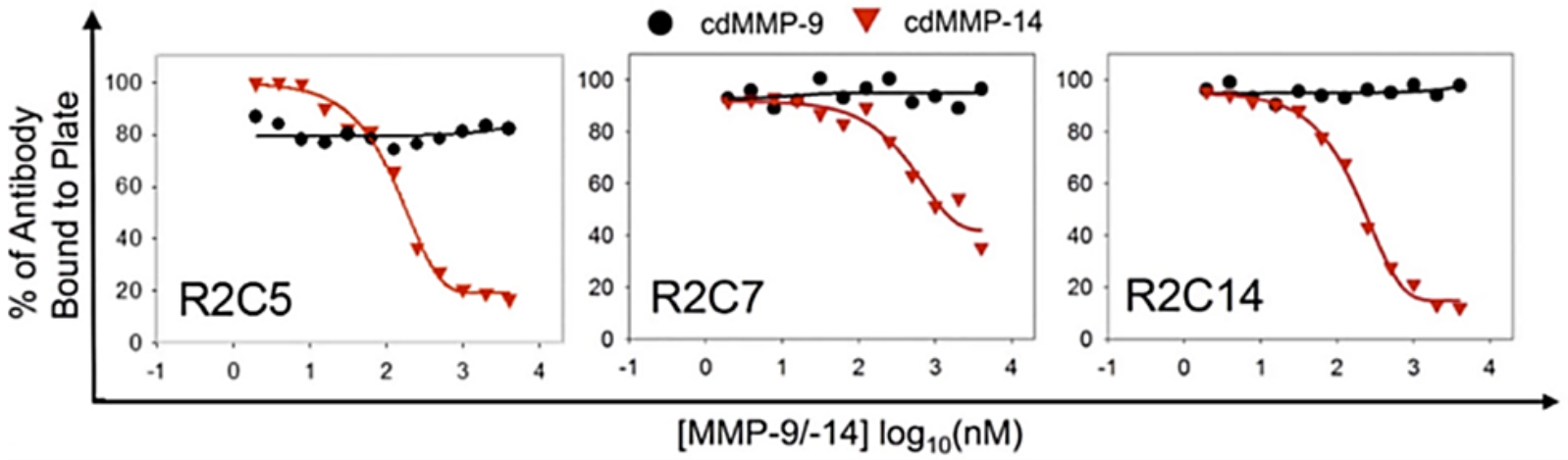

Figure 2.7: Specificity tests by competitive ELISA. Fabs at their respective IC50 concentrations were incubated with varying concentrations of cdMMP-9 or cdMMP-14 then added to ELISA plates coated with 100 nM cdMMP-14. Fabs bound to the cdMMP-14 on plates, even at high concentrations of cdMMP-9, indicating there are no interactions between Fabs and cdMMP-9. As the control experiments, when incubating with cdMMP-14 in solution, Fabs transferred from the plate to the solution as the concentration of cdMMP-14 in solution increased.

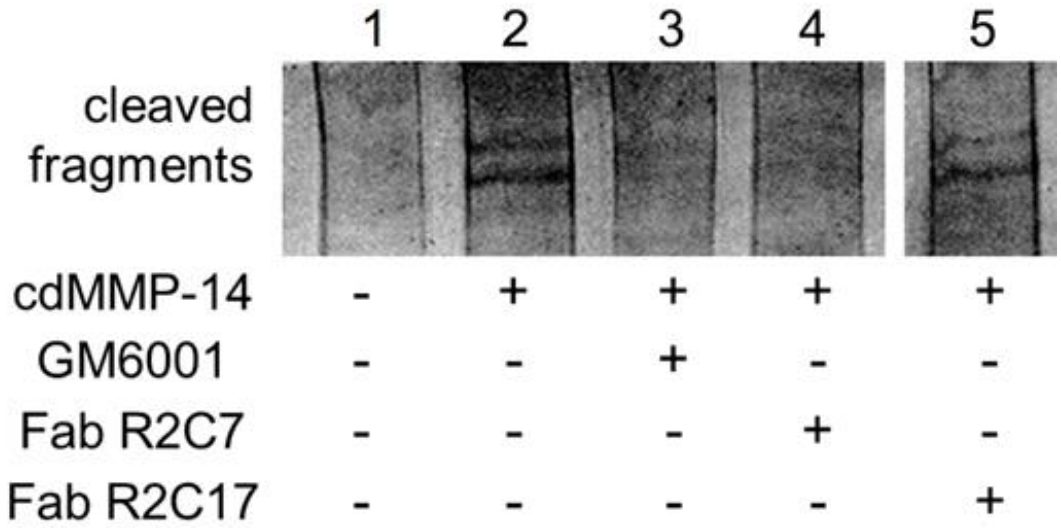

Figure 2.8: Zymography studies showing Fab R2C7 inhibits cdMMP-14 from degrading gelatin. 10 nM cdMMP-14 with 1 mg/mL gelatin was incubated in the presence or absence of the inhibitor of interest, and processed by 12% SDS-PAGE gel. Lane 1, no cleaved fragments without cdMMP-14; Lane 2, cleavage of gelatin by cdMMP-14; Lane 3, GM6001 inhibited cdMMP-14 from cleaving gelatin; Lane 4, Fab R2C7 inhibited cdMMP-14 from cleaving gelatin; Lane 5, non-inhibitory Fab R2C17 lacked function to block cdMMP-14. Relative intensities of the bands associated with cleaved fragments were shown in the last row (background intensity in Lane 1 was set as zero).

2.3.6 Inhibition Mechanism of R2C7

To determine the type of inhibition, a series of enzymatic activity assays in the presence of 0, 150, and 300 nM Fab R2C7 were performed. The obtained Lineweaver-Burk plots demonstrate an unchanged turnover rate (V_{max}) and an increased Michaelis constant (K_m) when Fab concentration was raised, indicating a competitive inhibition mode (Figure 2.9A). Competitive ELISA with increased concentrations of n-TIMP-2 resulted in decreased amounts of Fab R2C7 bound to immobilized cdMMP-14 (Figure 2.9B), suggesting that R2C7 and n-TIMP-2 directly competed on binding to cdMMP-14, and presumably their epitopes were at least

partially overlapping. As the control experiments, when incubating with cdMMP-14 in solution, Fabs transferred from the solution to the plate as the concentration of cdMMP-14 in solution decreased to ~10 nM.

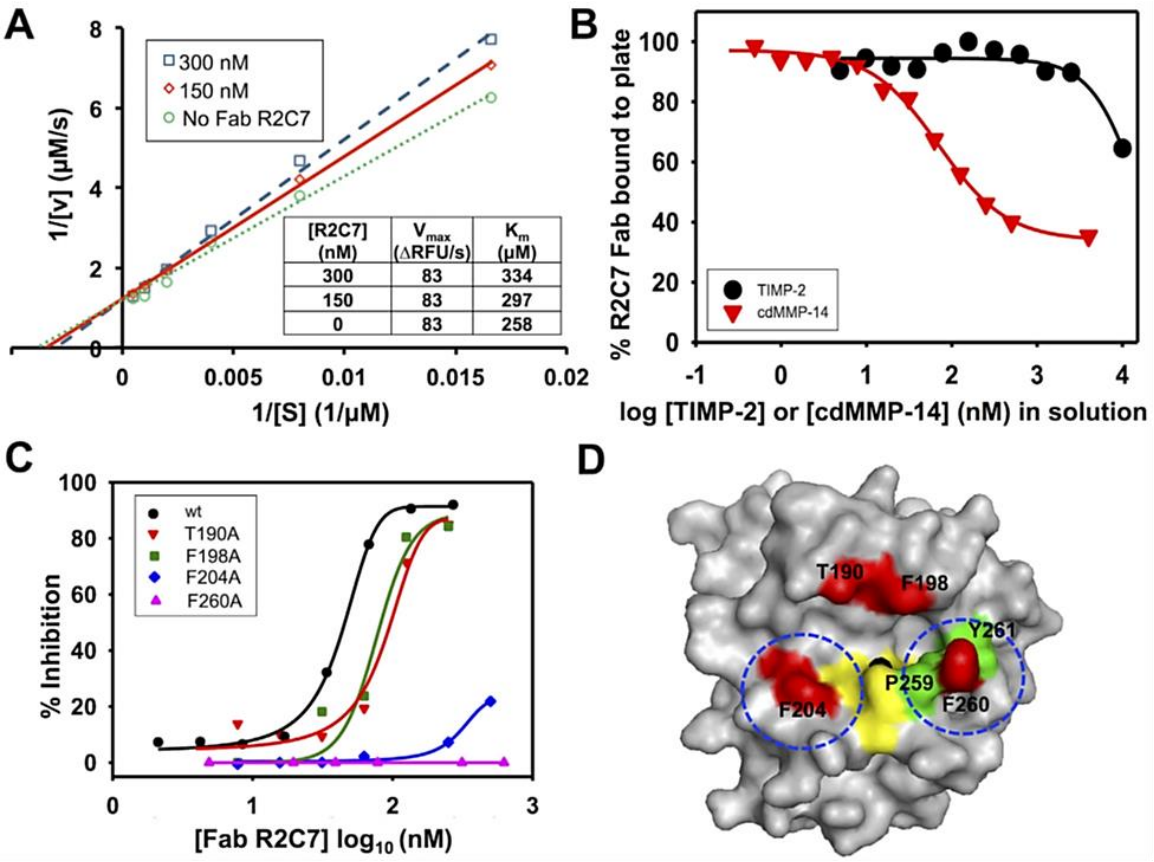

Figure 2.9: Inhibition mechanism of R2C7. (A) Lineweaver–Burke plots of cdMMP-14 at the presence of 0, 150, 300 nM Fab R2C7. Unaltered V_{max} and increased K_m with increasing Fab concentrations indicate a competitive inhibition mode. (B) Competitive ELISA with TIMP-2. Fab R2C7 was mixed with varying concentrations of TIMP-2 in solution before addition to an ELISA plate coated with 100 nM cdMMP-14, and the signals were developed by using anti-Fab-HRP and the associated substrate. (C) R2C7 epitope mapping by inhibition assays. Four positions T190, F198, F204, and F260 surrounding the catalytic cleft of cdMMP-14 were chosen for alanine mutagenesis. Compared to wt cdMMP-14, F260A, and F204A cannot be inhibited by Fab R2C7. (D) R2C7 epitope image generated using PyMOL based on MMP-14 crystal structure (PDB 1bqq), showing the catalytic zinc (solid black), site directed mutagenesis positions (red), the three histidine residues of the catalytic motif HEXXHXXGXXH (yellow), and the residues forming the wall of S1' cleft (green, except F260 which is also a mutation site thus in red). Determined locations of R2C7 binding are circled.

To further determine whether R2C7 is a direct or allosteric competitive inhibitor, binding site of Fab R2C7 was studied by alanine scanning mutagenesis of MMP-14. Four residue positions around reaction pocket of cdMMP-14 (T190A, F198A, F204A, and F260A) were selected for Ala substitution, and these cdMMP-14 mutants were prepared by periplasmic expression without refolding[13]. Inhibition assays with FRET peptide substrate indicated that R2C7 lost its inhibition ability toward cdMMP-14 mutants F204A and F260A, while keeping the same level of inhibition potency toward T190A and F198A as wild type cdMMP-14 (Figure 2.9C). Notably, F204 and F260 are responsible for the formation of a relatively deep S1' site of MMP-14 among MMP family[18,19], suggesting R2C7 binds to the reaction pocket vicinity of cdMMP-14 directly (Figure 2.9D).

2.4 Discussion and Conclusions

Next generation high-throughput sequencing is a powerful tool for analyzing rounds of selected libraries, which led to the identification of unique inhibitory antibodies in current study. In conjugation with convex paratope antibody library design, an n-TIMP-2 elution method was used during the phage panning process to enrich the libraries in competitive inhibitory clones. Traditional ELISA screenings were performed on the third round panned library by randomly picking individual colonies. This method resulted in the discovery of some of the most abundant clones in R3, as well as a few random clones that were not necessarily abundant but nonetheless picked (Table 2.3). However, some clones enriched in R2 but declined in R3 will likely be missed in ELISA screening. For example, the seventh

most abundant clone in R2, R2C7 is ranked ~12,500 in R3 with a frequency of 0.01%. Clones such as R2C7 (with an inhibition potency of 100 nM), are valuable candidates for further development but are depleted in continual rounds of panning. Applying ELISA on R2 is not realistic either, because even the most enriched clones in R2 had a frequency of ~1/1,000. By NGS, laborious ELISA screenings is avoided and all enriched clones with their abundancies above the background can be identified and tracked along rounds of the panning process. Using this approach, many valuable clones with high inhibition potencies, such as R2C7, R2C9, R2C12, and R2C22, were newly discovered. In fact, 15 of 20 identified inhibitory Fabs were not found by ELISA, demonstrating the power of NGS.

Because only a trace fraction of Og was sequenced, all of the 29 highly abundant clones identified from R2 and R3 have zero copies in Og. Therefore their frequencies in R2 and R3 can be directly used to reflect their enrichment over Og. By tracking their frequencies during phage panning process, we found three patterns—rise, plateau, and decline (Figure 2.10).

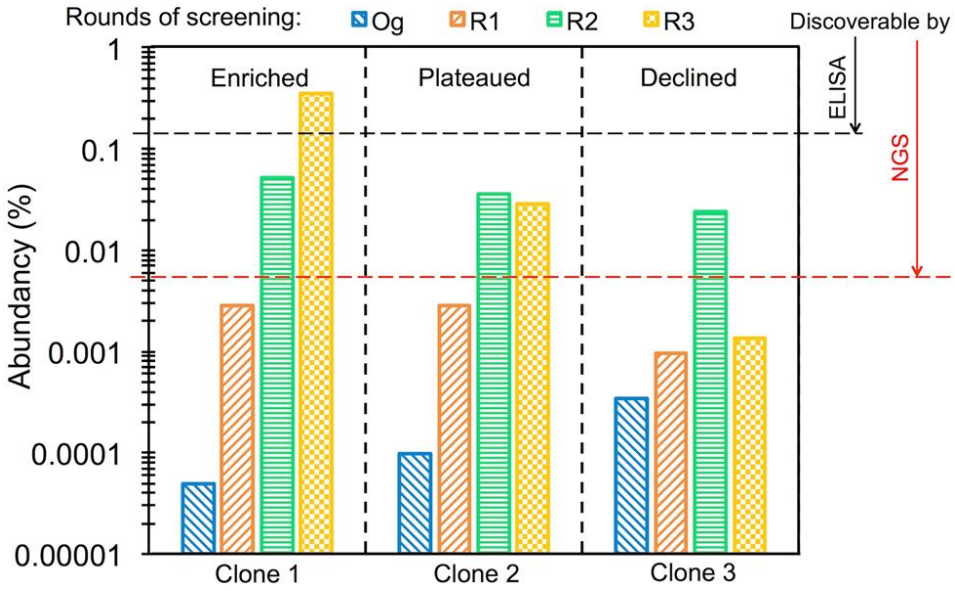

Figure 2.10: Three unique phenomena for individual clones were observed during the enrichment process clones which enriched in abundancy (left), clones that enriched to a point then plateaued (center), and clones that enriched the declined in abundancy (right).

The observed different enrichment and depletion patterns occur because phage panning is a multi-step process involving cell growth, Fab expression and display, and competitive binding. Suboptimal conditions at any of these steps can result in a decrease of abundancy. For example, an individual clone that grows slowly will be overtaken and gradually phased out by its faster growing competitors. This effect has nothing to do with the strength of the antibody, however, it will still result in the stagnation or depletion of the clone relative to the total library in subsequent rounds of panning. Another major concern during the phage ELISA selection process is low expression levels of antibody molecules. A clone that binds strongly, but does not express well may not have a high enough signal to be selected; this results in the loss of the clone. Finally, individual clones will compete for binding sites on the bound MMP-14. This results in the loss of weaker binding yet potentially inhibitory clones.

The 20 MMP-14 binding Fabs identified by ELISA in previous study were also tracked to monitor their enrichment profiles. As results shown in (Table 2.3), 9 of the 20 clones were among the most abundant 29 clones identified by NGS. The remaining 11 clones have frequencies less than 0.01% in R2 and less than 0.05% in R3, thus were not discovered by frequency-based NGS and bioinformatics, but randomly picked by monoclonal ELISA. To better understand the Fab populations isolated by ELISA, or NGS, or both methods, the correlations between binding affinity (ELISA EC_{50}) and inhibition potency (FRET assay IC_{50}) of each Fabs were plotted.

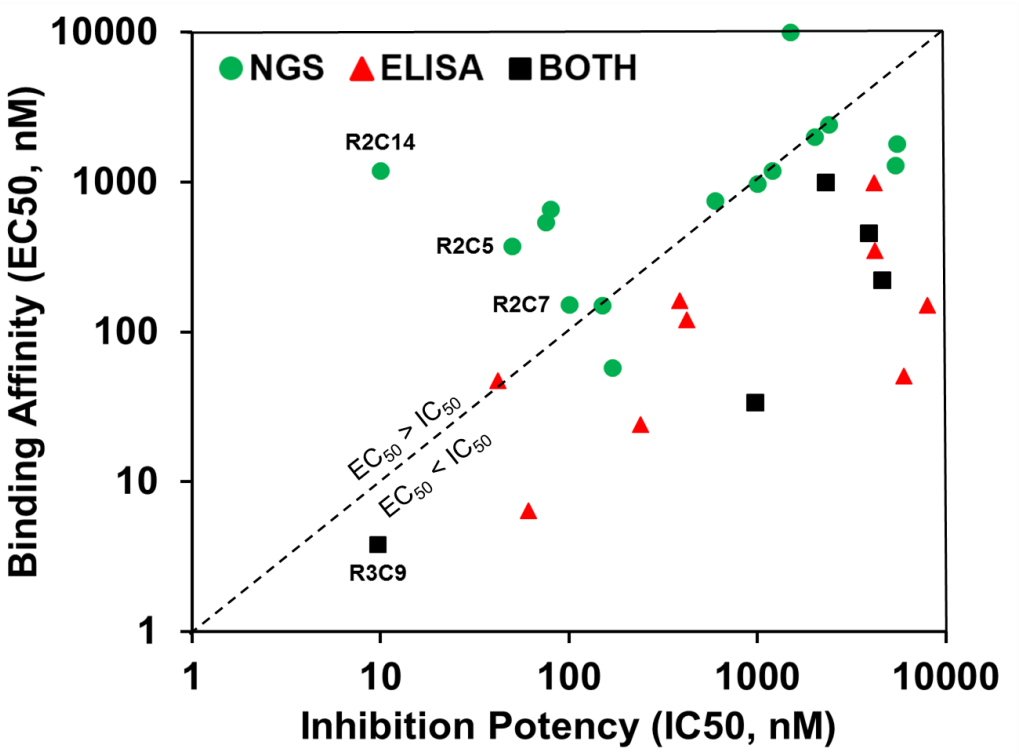

Figure 2.11: Relationship between binding affinity and inhibition potency. The clones found by NGS (green circles), phage ELISA (red triangles), or both methods (black squares) are compared. The diagonal dashed line represents equal EC_{50} and IC_{50} values.

As shown in Figure 2.11, most of the Fabs generated by ELISA screening have their EC_{50}s less than their IC_{50}s, whereas a few inhibitory Fabs identified by NGS, for example, R2C5 and R2C14, exhibited higher affinity EC_{50} values than inhibition IC_{50} values. A likely explanation of this phenomenon is that these Fabs are suicide inhibitors[14], which are slowly cleaved by high concentrations of cdMMP-14 after incubation for hours (Figure 2.12). To further characterize these selected Fabs, their binding kinetics k_{on} and k_{off} parameters were measured by bio-layer interferometry. Data indicated that Fabs R2C5, R2C7, and R2C14 had calculated K_D values of 15.3, 27.0, and 6.1 nM (Figure 2.13), which were less than their inhibition IC_{50}s (50, 100, and 10 nM, respectively).

Collectively these results suggest that the low apparent binding affinities measured by ELISA were attributed to slowcleavage of Fabs by immobilized cdMMP-14 on ELISA plates, while the quick and real-time analysis by bio-layer interferometry can measure the binding kinetics before significant cleavage takes place. Guided by the knowledge of theoretical cut sites of MMP-14, for example, usually containing a positively charged residue at the P4 position and a hydrophobic residue at the P1' position[19], studies on site-specific mutagenesis are currently being undertaken to engineer cleavage resistant Fabs.

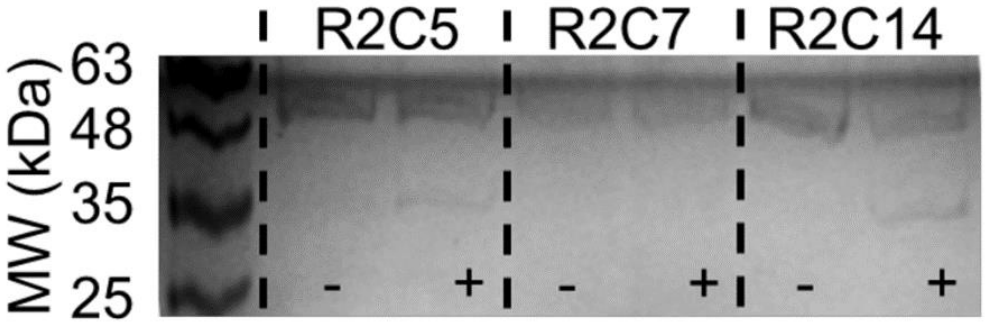

Figure 2.12: Identification of suicide inhibitors. 1 μM Fabs R2C5, R2C7 and R2C14 were incubated in the presence (+) or absence (-) of 200 nM cdMMP-14 for 2 hours at room temperature then analyzed by 12% SDS-PAGE. Truncated R2C5 and R2C14 fragments were observed while R2C7 was resistant to be cleaved by cdMMP-14.

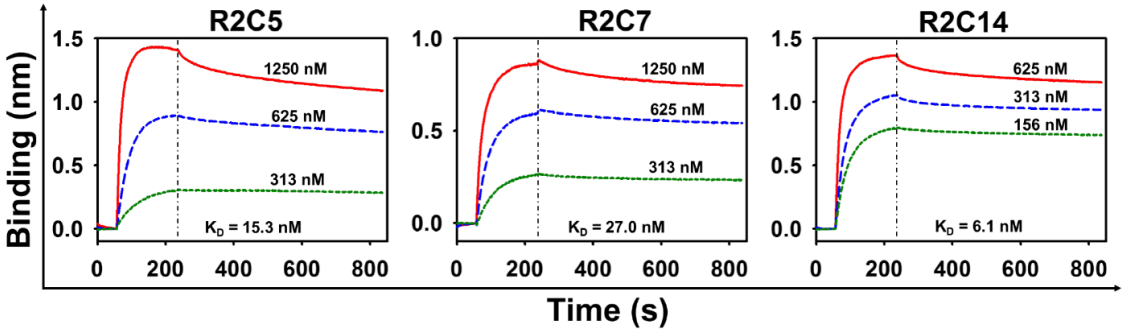

Figure 2.13: Binding kinetics measurements of Fabs R2C5, R2C7, and R2C14 by bio-layer interferometry. Using ForteBio BLItz system, biotinylated cdMMP-14 was loaded onto a streptavidin biosensor for 60 sec to establish baselines. Fabs were introduced at a variety of concentrations and their association to immobilized cdMMP-14 was monitored for 3 min then allowed to dissociate into 50 mM HEPES (pH 6.8) for 10 min (change to dissociation is indicated by the vertical black dashed line). Determined k_{on} and k_{off} parameters were used to calculate K_D values.

Avoiding sequencing artifacts is critical for the success of frequency based antibody discovery. PCR often introduces bias due to the differential amplification of some DNA templates over others. In this study, sequencing adapters were custom-designed for direct ligation with antibody CDR-H3 fragments prepared by phagemid extraction and restriction digestion. This procedure without amplification presumably minimized quantification biases caused by PCR.

In conclusion, combination of the convex paratope antibody library design with next-generation deep sequencing of panned libraries allowed us to identify a panel of highly potent and highly selective Fabs inhibiting cdMMP-14 not found by ELISA. Particularly, Fab R2C7 exhibited 100 nM inhibition potency by binding to the catalytic cleft vicinity of cdMMP-14. In addition to R2C7, several potent inhibitory Fabs for example, R2C5 and R2C14, with IC_{50} values at 10–50 nM with excellent selectivity were also isolated. And Fabs R2C5, R2C9, R2C12, R3C15 were found to be competitive inhibitors as well. This panel of inhibitory Fabs provides us a rich pool of lead candidates for further selection of suitable epitopes for therapeutics and optimization of pharmacological properties through affinity maturation and solubility/stability improvement. Besides MMP-14, several other MMP family members have been recognized playing important roles invariety of indications, therefore the methodology demonstrated in the current study can be readily applied for the generation of highly potent inhibitory mAbs targeting other MMPs or serine proteases[21,14] of physiological significance. These highly selective

inhibitors can also been used as research tools for better understanding of the not well-defined network of MMPs with their substrates.

2.5 References

1. Nam, D.H., Rodriguez, C., Remacle, A.G., Strongin, A.Y., & Ge, X. Active-site MMP-selective antibody inhibitors discovered from convex paratope synthetic libraries. *Proc Natl Acad Sci U S A*. **113**, 14970–14975. (2016).

2. Ravn, U., et al. Deep sequencing of phage display libraries to support antibody discovery. *Methods*. **60**, 99-110. (2013).

3. Ravn, U., et al. By-passing *in vitro* screening-next generation sequencing technologies applied to antibody display and in silico candidate selection. *Nucleic Acids Research*. **38**, e193. (2010).

4. Georgiou G, et al. The promise and challenge of high-throughput sequencing of the antibody repertoire. *Nat Biotechnol*. **32**, 158-168. (2014).

5. Margulies M, et al. Genome sequencing in microfabricated high-density picolitre reactors. *Nature*. **437**, 376-380. (2005).

6. Metzker, M.L. Applications of next-generation sequencing technologies - the next generation. *Nat Rev Genetics*. **11**, 31-46. (2010).

7. Pushkarev, D., Neff, N.F., Quake, S.R. Single-molecule sequencing of an individual human genome. *Nat Biotechnol*. **27**, 847-850. (2009).

8. Naqid, I.A. et al. Mapping polyclonal antibody responses to bacterial infection using next generation phage display. *Scientific Reports*. **6**, 24232. (2016).

9. Reddy ST, Ge X, Boutz D, Ellington AD, Marcotte EM, Georgiou G. Rapid Isolation of Monoclonal Antibodies from Animals. WO2011146514; US20110312505; EP2572203; CA2799746; CN201180035306. (2011).

10. Reddy, S.T., et al. Monoclonal Antibodies Isolated Without Screening by Analyzing the Variable-Gene Repertoire of Plasma Cells. *Nat Biotechnol*. **28**, 965-969. (2010).

11. Zhua, J., et al. Mining the antibodyome for HIV-1–neutralizing antibodies with next-generation sequencing and phylogenetic pairing of heavy/light chains. *Proc Natl Acad Sci U S A*. **110**, 6470-6475. (2013).

12. Turner, K.B., et al. Next-Generation Sequencing of a Single Domain Antibody Repertoire Reveals Quality of Phage Display Selected Candidates. *PLoS ONE*. **11**, e0149393. (2016).

13. Nam, D., Ge, X. Direct production of functional matrix metalloproteinase -14 without refolding or activation and its application for *in vitro* inhibition assays. *Biotechnol. Bioeng*. **113**, 717-723. (2015).

14. Farady, C.J., Sun, J., Darragh, M.R., Miller, S.M., Craik, C.S. The mechanism of inhibition of antibody-based inhibitors of membrane-type serine protease 1 (MT-SP1). *J Mol Biol*. **369**, 1041-1051. (2007).

15. Fernandez-Catalan, C. Crystal structure of the complex formed by the membrane type 1-matrix metalloproteinase with the tissue inhibitor of metalloproteinases-2, the soluble progelatinase A receptor. *EMBO J*. **17**, 5238-5248. (1998).

16. Nieba, L., Honegger, A., Krebber, C., Plückthun, A. Disrupting the hydrophobic patches at the antibody variable/constant domain interface: improved *in vivo* folding and physical characterization of an engineered scFv fragment. *Protein Eng*. **10**, 435-44. (1997).

17. Lawrence, M.S., Phillips, K.J., Liu, D.R. Supercharging Proteins Can Impart Unusual Resilience. *J Am Chem Soc.* **129**, 10110-10112. (2007).

18. Chiti, F., Stefani, M., Taddei, N., Ramponi, G., Dobson, C.M. Rationalization of the effects of mutations on peptide and protein aggregation rates. *Nature*. **424**, 805-808. (2003).

19. Nagase, H.. Matrix Metalloproteinase Inhibitors in Cancer Therapy. *Springer*. 39-66. (2001).

20. Kridel, S.J., et al. A unique substrate binding mode discriminates membrane type-1 matrix metalloproteinase from other matrix metalloproteinases. *J Biol Chem*. **26**, 23788–23793. (2002).

21. Schneider, E.L. A reverse binding motif that contributes to specific protease inhibition by antibodies. *J Mol Biol*. **415**, 699-715. (2012).

Chapter 3: Epitope Specific Affinity Maturation Improved Stability of Potent Protease Inhibitory Antibodies

This chapter is based on: Lopez, T., et al. Epitope Specific Affinity Maturation Improved Stability of Potent Protease Inhibitory Antibodies. *Biotechnology and Bioengineering*, Accepted (13 August 2018). DOI: 10.1002/bit.26814

Abstract

Targeting effectual epitopes is essential for therapeutic antibodies to accomplish their desired biological functions. This study developed a competitive dual color FACS to maturate a matrix-metalloprotease 14 (MMP-14) inhibitory antibody. Epitope specific screening was achieved by selection on MMP-14 during competition with nTIMP-2, a native inhibitor of MMP-14 binding strongly to its catalytic cleft. 3A2 variants with high potency, selectivity, and improved affinity and proteolytic stability were isolated from a random mutagenesis library. Binding kinetics indicated that the affinity improvements were mainly from slower dissociation rates. *In vitro* degradation tests suggested the isolated variants had half-lives 6-11 fold longer than the wild type. Inhibition kinetics suggested they were competitive inhibitors which showed excellent selectivity toward MMP-14 over highly homologous MMP-9. Alanine scanning revealed that they bound to vicinity of MMP-14 catalytic cleft especially residues F204 and F260, suggesting that the desired epitope was maintained during maturation. When converted to IgG, B3 showed 5.0 nM binding affinity and 6.5 nM inhibition potency with *in vivo* half-life of 4.5 days. In addition to protease inhibitory antibodies, the competitive FACS

described here can be applied for discovery and engineering biosimilars, and in general for other circumstances where epitope specific modulation is needed.

3.1 Introduction

As modulators of molecular interactions with high affinity and high specificity, monoclonal antibodies have emerged as important therapeutics targeting cancers, immune diseases and infections[1,2,3]. In addition to affinity and specificity, the therapeutic efficacy of a given monoclonal antibody often depends on the specific epitope recognized i.e. exactly where on the antigen binding occurs[4,5,6,7,8]. Since the establishment of hybridoma technique four decades ago, numerous antibody isolation and engineering methods have been developed[9,10]. The conventional approaches of antibody isolation usually start with binding-based library screening followed by monoclonal characterizations including epitope mapping and function evaluation. Because the later steps are low-throughput and time-consuming, it is desirable to incorporate epitope specificity controls into the initial screening procedures[11,12].

One excellent example of epitope specific interaction can be found between proteolytic enzymes and their macromolecular inhibitors[13,14,15]. Most protease inhibitory proteins achieve their functions by directly recognizing the protease active site in a substrate-like competitive manner[16]. Inspired by this orthosteric inhibition mechanism, we aim to develop a high-throughput epitope specific selection method to engineer protease inhibitory antibodies. More specifically, a

biomedically important protease, matrix metalloprotease-14 (MMP-14) was chosen as a model target for the development.

MMP-14 is a zinc-dependent endopepsidase associated with tumor growth, metastasis and angiogenesis[17,18,19,20]. MMP-14 also processes proMMP-2 into active MMP-2, a main contributor in degradation of the extracellular matrix and facilitation of tumor cell migration[21]. Previous failures of all broad spectrum MMP small molecule inhibitors in multiple clinical trials taught us that selectivity is the key for the success of any MMP inhibition therapy[22]. However, the high similarity of protein folding and catalytic chemistry among MMP family members presents a daunting challenge for the generation of highly selective compound inhibitors[23]. Our studies[24,25,26], among others[27,28,29,30], demonstrated the feasibility that antibody based inhibitors could exhibit the desired high selectivity. Particularly, Fab 3A2 with 4.8 nM affinity, 9.7 nM potency, and high selectivity toward MMP-14 was isolated from a library containing ultra-long CDR-H3s[24]. However, like many standard mechanism protease inhibitors or inhibitory mAbs[31,32], 3A2 can be cleaved by its own target, MMP-14, after incubation at low pH for an extended period (Figure 3.1). For therapeutic development, it is necessary to improve proteolytic stability of 3A2 while retaining its inhibition potency and selectivity.

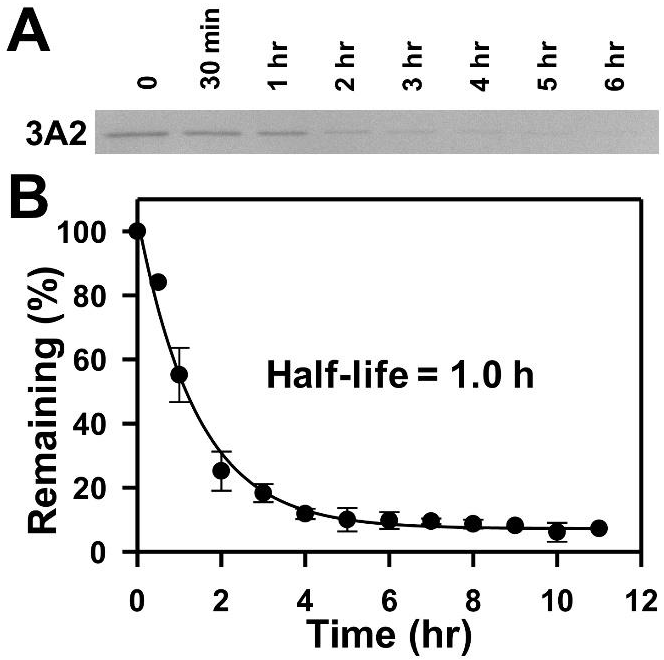

Figure 3.1: *In vitro* stability of scFv 3A2 wt. (A) SDS-PAGE analysis of 1 µM scFv 3A2 wt after incubation with 1 µM cdMMP-14 at 37ºC for indicated time. (B) Quantification of scFv bands by densitometry was plotted over time to determine half-life.

Cell surface display coupled with fluorescence activated cell sorting (FACS) is a powerful method to select antigen specific antibodies and improve their binding strength and pharmacokinetics[33,34,35]. During *in vitro* affinity maturation, an existing antibody clone is subjected to site-directed or random mutagenesis (e.g. by error-prone PCR), and generated libraries are displayed on cell surface (e.g. yeast display). After incubation with the fluorescently labelled antigen, cells are quantitatively analyzed for the selection of clones with improved affinity. Notably, affinity maturation can result in epitope drift[36]. For protease-inhibiting antibodies, isolated variants with higher affinities are not necessarily associated with improved inhibition potency. It is possible that through conventional affinity maturation, the

epitope can migrate to a region which interferes less with catalytic pocket resulting in a reduced inhibition potency. By conjugating MMP-14 and its native inhibitor TIMP-2 with different fluorescent dyes, we have demonstrated that dual color FACS can distinguish inhibitory clones from non-inhibitory clones[25]. This study further develops this method to improve the proteolytic stability of 3A2, while avoiding unwanted epitope drifts and retaining inhibition potency. We test the feasibility to govern a control over epitope by selection on MMP-14 under competition with nTIMP-2. In principle, only the 3A2 variants competing with TIMP-2 binding to inhibitory epitopes, and thus shown as MMP-14^{high} and TIMP-2^{low}, will be selected (). Furthermore, the *in vitro* and quantitative nature of FACS means that the incubation conditions and sorting windows can be adjusted in real-time to provide high stringency, especially by (1) extending incubation time with MMP-14 and (2) reducing MMP-14 concentration and increasing TIMP-2 concentration, to isolate highly potent inhibitory clones with improved proteolytic resistance.

3.2 Materials and Methods

3.2.1 Library construction

Genes of variable heavy (V_H) and variable light (V_L) domains of antibody 3A2[24] were amplified to assemble 3A2 scFv (V_H-SGGSGGGGSGSGS-V_L) by overlapping PCR. Error-prone PCR of 3A2 scFv gene was performed by using Taq DNA polymerase with 120 µM dATP, 100 µM dCTP, 360 µM dGTP, 2.5 mM dTTP, 5 µg/mL BSA, 3.28 mM $MgCl_2$ and 0.5 mM $MnCl_2$. The generated mutagenesis product was cloned into the yeast display plasmid pCTcon2[34] by transforming 5 µg

ligated DNA into *E. coli* competent cells. 100 µg library plasmid DNA was used to chemically transform *S. cerevisiae* EBY100 competent cells prepared by Frozen-EZ kit (Zymo). Transformants were selected on SD/-Trp/-Ura (Sunrise Science) agar plates, then collected and stored at -80^{o}C. Library quality and the mutation rate was analyzed by DNA sequencing of randomly picked clones. For surface display, 5×10^{9} library cells were cultured on SD/-Trp/-Ura/penicillin-streptomycin agar plates at 30^{o}C for 48 h. 30 OD_{600} of cultured cells were inoculated to 600 mL SD/-Trp/-Ura for incubation at 30^{o}C, 250 rpm for 12 h. Cells were collected by centrifugation at 6,000 × g for 2 min, and 8 OD_{600} cells were further cultured for scFv expression in 20 mL YNB (yeast nitrogen base)/-Trp/-Ura supplemented with 5 mL 20% galactose at room temperature 250 rpm for 48 h.

3.2.2 Fluorescent Labeling and FACS

Catalytic domain of MMP-14 was fused with superfolder GFP[37], expressed in periplasm of *E. coli*, and purified with Ni-NTA agarose (Qiagen). Enzymatic activity of produced cdMMP14-sfGFP was tested with FRET peptide substrate M2350 (Bachem). N-terminal domain of TIMP-2 (nTIMP-2) was prepared as previously described[38], and chemically conjugated with Alexa-647 (Invitrogen). Cells covering 10 × the library diversity were sequentially incubated with cdMMP14-sfGFP and nTIMP2-Alexa647 at concentrations adjusted during subsequent rounds of FACS. All of the incubation steps were performed at RT in dark for 1 h, and between incubations cells were washed with assay buffer (50 mM Tris-HCl pH 7.5, 150 mM NaCl, 5 mM $CaCl_2$, 0.1 mM $ZnCl_2$). Cells were sorted on

a Bio-Rad S3e flow cytometer equipped with 488/640 nm dual lasers. FL1 (526/48 nm) and FL3 (615/25 nm) were used for GFP and Alexa647 channels respectively. Forward and side scatter voltages were set at 317v and 341v with a threshold of 5. Both scanning and sorting were performed at a rate of 3,000 events/sec with a mild agitation to prevent cell settling. A triangle gate was designed to select cdMMP-14^{high} and nTIMP-2^{low} clones. Isolated cells were grown on SD/-Trp/-Ura/penicillin-streptomycin agar plates at 30 ^{o}C for 48 h, and collected in 20% glycerol SD/-Trp/-Ura for storage at -80 ^{o}C. In monoclonal FACS screening, cells were stained with 500 nM cdMMP14-sfGFP and 500 nM nTIMP2-Alexa647.

3.2.3 scfv Production and Stability Test

Antibody display plasmids were extracted from isolated yeast clones using Zymoprep plasmid kit (Zymo) and transformed into *E. coli* for DNA amplification and sequencing. Isolated scFv genes were then cloned into periplasmic expression vector pMopac16[39] for scFvs production. For *in vitro* stability tests, 1 µM purified scFvs were incubated with 1 µM cdMMP-14 in assay buffer at 37 ^{o}C for 1-10 h. Densitometric analysis of scFv bands on SDS-PAGE was performed using Image Lab (Bio-Rad). To reduce interference from variations in staining and destaining, gel background for each band was quantified and subtracted. Correlations of scFv amount over time were plotted for half-life determination. To produce IgG B3 for *in vivo* stability tests, its V_H and V_L genes were amplified by PCR, and separately cloned to pcDNA-intron-SPL-CH-WPRE and pcDNA-intron-SPL-CL-WPRE plasmids carrying human IgG1 constant heavy and kappa

constant light domains with associated signal peptides and Woodchuck hepatitis virus posttranscriptional regulatory elements to enhance the expression[40]. The two plasmids were co-transfected at a ratio of 1:1 into HEK293F cells (3.0×10^6 cells/mL with viability > 98%) with a DNA/PEI "Max" (MW 40,000, Polysciences) mixture at concentrations of 1 µg/mL DNA and 3 µg/mL PEI. The transfected cells were cultured in round bottles at 135 rpm 37°C 8% CO_2 for 7 days. Cultured media was clarified by centrifugation and 0.45 µM microfiltration, and B3 IgG was purified by protein A affinity chromatography (GenScript). Concentration of purified IgG was determined by UV spectrophotometer (BioTek) and its purity was analyzed by SDS-PAGE. To test *in vivo* stability, a single dosage of 100 µg IgG B3 was injected into three 8-week-old female BALB/c mice via tail vein and its clearance was examined by obtaining 50 µl plasma at various time points (2 h, 3, 6, 9, 12 and 15 days). The disappearance of IgG B3 was determined using a human IgG ELISA kit (Sigma). There was no cross-activity in the assay between mouse IgG, or other non-specific binding compounds of mouse serum. The animal procedures were conducted under UCR IACUC approved protocols.

3.2.4 Antibody characterizations

Binding kinetics of produced scFvs towards cdMMP-14 were analyzed by bio-layer interferometry BLItz (ForteBio). Purified cdMMP-14 was modified with EZ-link sulfo-NHS-LC-biotin (Thermo Scientific). Streptavidin biosensors were coated with biotinylated cdMMP-14 for 2 min and incubated in 50 mM HEPES (pH 6.8) to establish baselines. 40-800 nM scFvs were introduced and their

associations to immobilized cdMMP-14 were monitored for 2 min, then allowed to dissociate in 50 mM HEPES for 2 min. Determined k_{on} and k_{off} were used for K_D value calculation. For FRET inhibition assays, 1 μM purified scFv was serially diluted into assay buffer and incubated with 10 nM cdMMP-14 for 30 min at 4°C. The enzyme kinetic measurements were started with the addition of 1 μM M2350 and the fluorescence was monitored with excitation and emission wavelengths at 325 and 392 nm using Synergy2 microplate reader (BioTek) equipped with Gen5 software. Inhibition IC_{50} was determined by the change in V_{max} at different concentrations of scFv, and potency K_I was calculated using equation: $K_I = IC_{50}/(S/K_m+1)$[41]. Lineweaver-Burk plots were established to determine type of inhibition. Similarly, purified scFvs were tested against cdMMP-9 and cdMMP-14 single point mutants[24] to determine binding specificity and epitope.

3.3 Results

3.3.1 *In vitro* stability of scFv 3A2 wt and mutagenesis library construction

3A2 was converted to its scFv format (V_H-GS linker-V_L) for yeast surface display. The typical yield of purified scFv 3A2 was 2.5 mg per liter of *E. coli* culture. Toward catalytic domain of MMP-14 (cdMMP-14), scFv 3A2 showed a binding affinity K_D of 25 nM (k_{on} = 1.9 ×10^5 $M^{-1}s^{-1}$ and k_{off} = 4.9×10^{-3} s^{-1}) and an inhibition potency K_I of 39 nM. When 1 μM scFv 3A2 was incubated with 1 μM cdMMP-14 at 37 °C pH 7.5, scFv 3A2 was quickly degraded to generate fragments at 15 and 16 kDa as the cleavage products. SDS-PAGE analysis of remaining scFv 3A2 samples after incubation with cdMMP-14 for different times indicated a half-life of

1.0 hour (Figure 3.1). To improve proteolytic stability, scFv 3A2 wt gene was subjected to error-prone PCR, a well-documented and effective random mutagenesis method for antibody engineering[42,43]. The generated error-prone product was cloned to the yeast surface display vector carrying an A-agglutinin-binding subunit (aga2), and 4.5×10^8 *E. coli* colonies were obtained. DNA sequencing results of 20 randomly picked clones indicated that mutations occurred across the entire scFv genes with an average mutation rate of 2%, consistent with the experimental design. Transforming library plasmids into *S. cerevisiae* EBY100 resulted in 2×10^7 transformants, which were cultured and induced with 4% galactose for scFv expression. Labeling yeast cells expressing wt 3A2 scFv with cdMMP14-sfGFP demonstrated that 87% the population showed a positive signal, while only 0.1% of the non-expression cells were positive, indicating a successful surface display (Figure 3.4A).

3.3.2 Epitope specific FACS design and results

Crystal structure of cdMMP-14 complexed with its native inhibitor nTIMP-2 reveals that the reactive cleft of MMP-14 is directly occupied with a loop conformation of nTIMP-2, formed by its N-terminal residues (Cys1-Val4) and a surface loop (Ala68-Cys72) through a disulfide-bridge between Cys1 and Cys72[44]. Such substrate-like inhibition mechanism implies that an epitope-specific selection can be achieved by performing a competitive selection on cdMMP-14 in the presence of nTIMP-2. This allows the isolation of inhibitory scFv clones that compete with nTIMP-2 binding to cdMMP-14. In contrast, non-inhibitory scFv

clones that bind to epitopes other than the catalytic cleft do not compete with nTIMP-2. This results in double positive on both cdMMP-14 and nTIMP-2 signals, and is thus distinguishable from inhibitory clones (Figure 3.2).

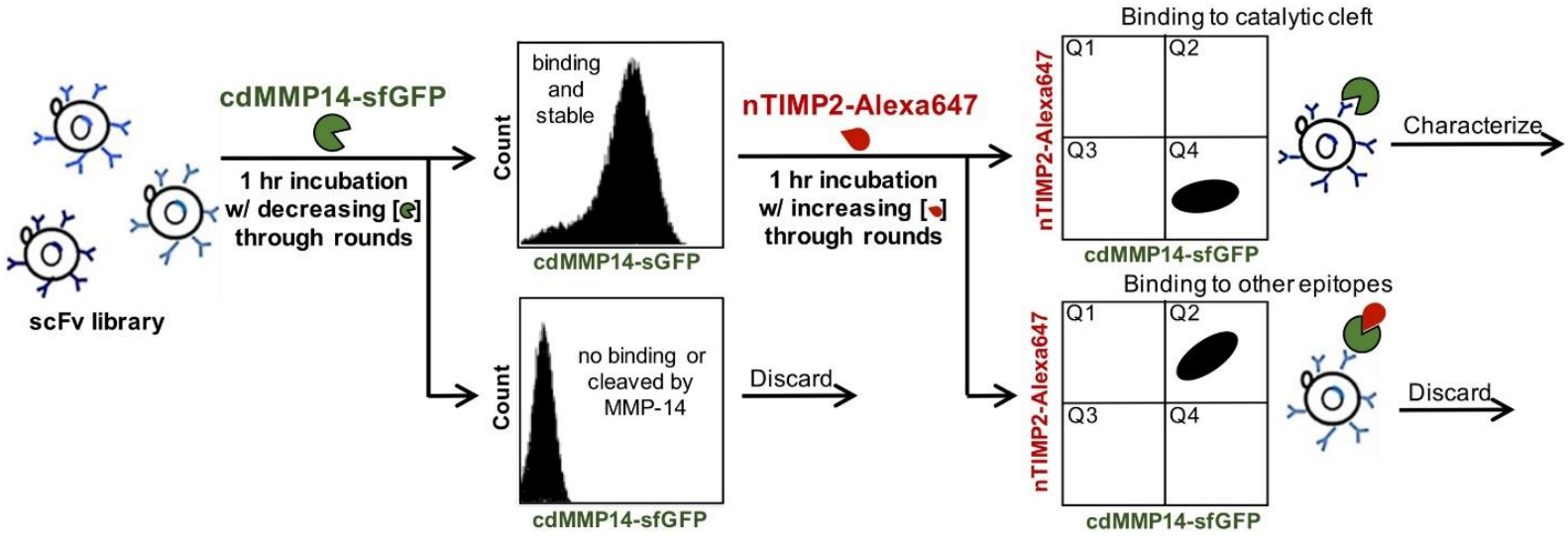

Figure 3.2: Scheme of dual color epitope specific FACS for inhibitory antibodies with improved stability and high potency.

To achieve the competitive selection, two fluorophores with different excitation/emission wavelengths were used: cdMMP-14 was fused with superfolder GFP[37] and nTIMP-2 was chemically conjugated with Alexa-647. After purification, their functions were confirmed by enzymatic assays using a FRET peptide substrate.

To improve the proteolytic stability, library cells displaying 3A2 mutants were reacted with cdMMP-14 for an extended period to remove the truncated and thus nonfunctional clones. In the first round of sorting, scFv library cells were incubated with 850 nM cdMMP14-sfGFP for one hour, washed, then followed by a competitive interaction with 450 nM nTIMP2-Alexa647. On FACS, 30 million library cells were sorted, and a triangle gate was designed to select the top 1.0 % (3×10^5 cells) of cdMMP14-sfGFP positive cells while excluding the cells with a high nTIMP2-Alexa647 signal (Figure 3.3).

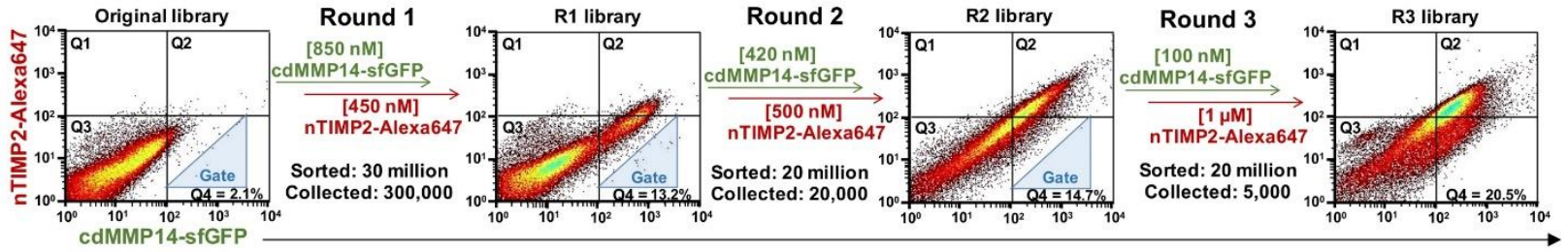

Figure 3.3: Progress of three rounds of epitope specific FACS sorting. Concentrations of cdMMP14-sfGFP and nTIMP2-ALEXA647 for each round are indicated. Triangle sorting gates are shown. And proportions of cells in Q4, representing MMP-14^{high} and nTIMP-2_{low} were also calculated.

To isolate scFv clones with improved binding affinity and/or inhibition potency, both selection stringency and competition pressure were intensified by decreasing cdMMP14-sfGFP concertation to 420 nM and 100 nM while increasing nTIMP2-Alexa647 concentration to 500 nM and 1 µM in the second and third rounds of sorting. Under these conditions, 20 million cells were sorted in R2/R3, and the selection gates were also tightened to top 0.1% and 0.025% of cdMMP14-sfGFP^{high} and nTIMP2-Alexa647^{low} population resulting in collection of 2×10^4 and 5×10^3 cells in R2 and R3. When stained with 500 nM cdMMP14-sfGFP and 500 nM nTIMP2-Alexa647, FACS data showed that the proportion of cells in quadrant Q4 (corresponding to MMP-14^{high} and nTIMP-2^{low} cells), was enriched from 2.1% in the original library, to 13.2% in R1, 14.7% in R2 and 20.5% in R3 (Figure 3.3).

3.3.3 Monoclonal screening and identifying affinity improved mutants

Thirty scFv clones randomly picked from R3 were analyzed by monoclonal FACS. Results indicated that majority (23/30) of isolated mutants had a significantly higher Q4 proportion than 3A2 wt. From this pool of candidates, DNA sequencing the top 10 clones with the highest Q4 % values identified 5 unique clones B1, B3 (6 repeats), T1, T3 and T4, with 4-7 mutations each scattered throughout their scFv genes in both framework regions and CDRs (Table 3.1).

Table 3.1: scFv clones obtained from monoclonal FACS studies

scFv	Q4 (%)	Mutations	
		Light Chain	Heavy Chain
3A2	10	-	-
B1	12	M4I; V19A; P94S	Y100nF; G104D; T107S
B3 (6 repeats)	15	A13T; S14T	P14L; V37A; G44D; Y58H; Y102H
T1	24	R18W; F62L; T69M	A40V
T3	23	M4K; C23S; E81K	M100rT
T4	30	D17G; V19S; K39E; T72S	-

Monoclonal FACS confirmed that Q4 proportions of these mutants were 12, 15, 24, 23 and 30% respectively, higher than that of 3A2 wt at 10% (Figure 3.4). Notably, considerable portions of sampled cells (7-15 %) were located at the Q2 quadrant (double positive on both cdMMP14-sfGFP and nTIMP2-Alexa647). FACS analysis of cells after single-labeled with 500 nM nTIMP2-Alexa647 revealed the relatively high backgrounds of non-specific binding of nTIMP2-Alexa647 to yeast cells (Figure 3.4A), explaining the disparity from conceptual populations located at the Q2 quadrant (Figure 4.1).

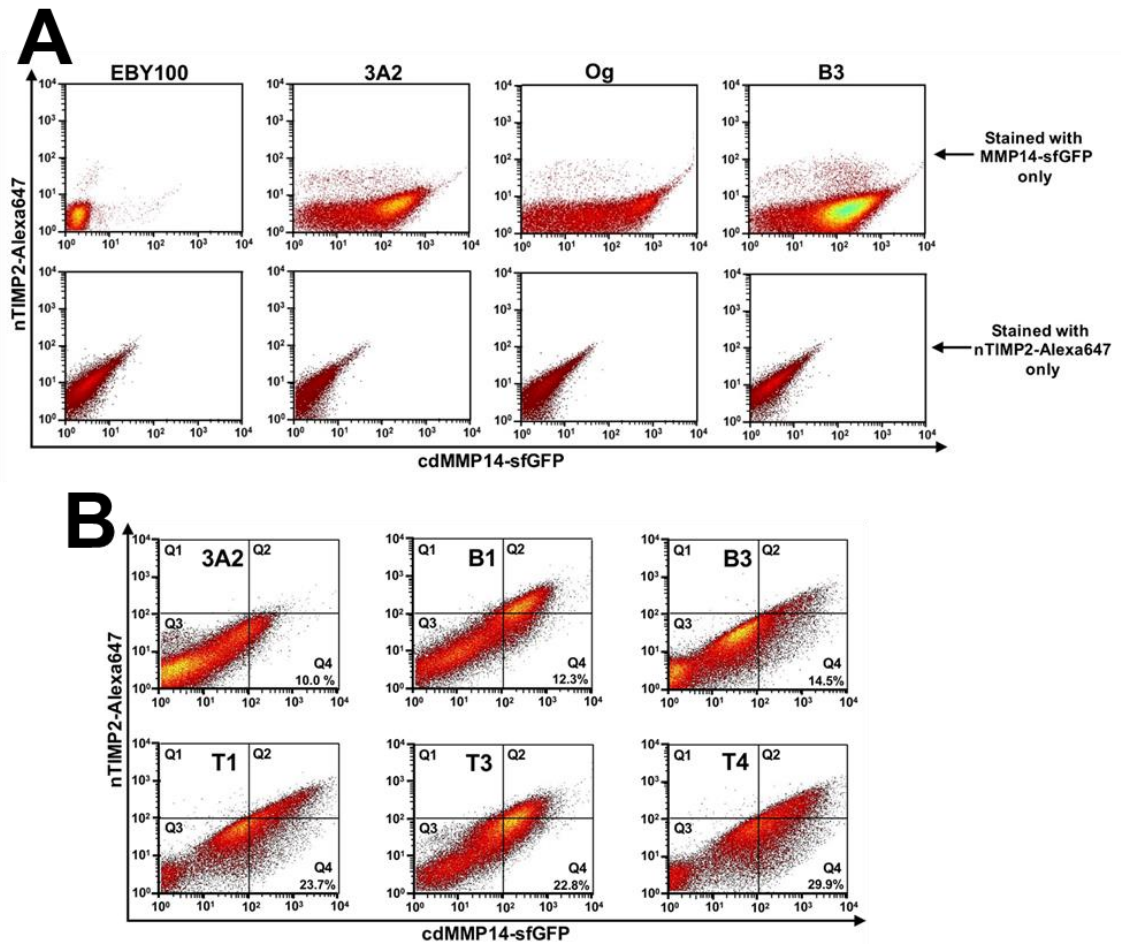

Figure 3.4: A: FACS scanning of cells stained with MMP14-sfGFP only and TIMP2-Alexa647 only. Host EBY100 and cells displaying 3A2, 3A2 error-prone library and isolated B3 scFvs were incubated with 500 nM cdMMP14-sfGFP or 500 nM nTIMP2-Alexa647 for 1 hour prior to FACS. B: Dual color monoclonal FACS of scFvs 3A2 wt and its isolated mutants. Cells displaying scFvs were stained with 500 nM cdMMP14-sfGFP and 500 nM nTIMP2-Alexa647 before FACS analysis.

The isolated scFv mutant genes were cloned downstream of a pLac promoter and a pelB leader peptide for periplasmic expression in *E. coli*[39]. Binding kinetics of purified 3A2 mutants on cdMMP-14 were measured by bio-layer interferometry, and results indicated that B1, B3 and T1 exhibited single-digit nanomolar affinities at 4.9, 6.3 and 2.5 nM respectively, significantly stronger than that of 3A2 wt at 25 nM. These improvements were mainly contributed by slower dissociation rates (Table 3.2), e.g. T1 had a k_{off} of 4.9×10^{-4} s^{-1}, 10-fold slower than that of 3A2 wt (k_{off} = 4.9×10^{-3} s^{-1}). Affinities of T3 and T4 at 39 and 75 nM were weaker than that of 3A2 wt, which were merely caused by their lower association rates k_{on}s. In fact, k_{off}s of T1 and T3 were improved compared to that of 3A2 wt. Collectively, these results suggested that random mutagenesis followed by dual color epitope-specific FACS generated 3A2 variants with improved affinities especially on disassociation rates k_{off}s, a phenomenon also found by other affinity maturation studies[45,46].

Table 3.2: Biochemical characterizations of scFv 3A2 wt and isolated variants.

scFv	k_{on} (1/Ms)	k_{off} (1/s)	K_D (nM)	Potency (nM)	Inhibition type	In vitro half-life (h)
3A2	1.9×10^{5}	4.9×10^{-3}	25 ± 2.1	39 ± 4.2	Competitive	1.0 ± 0.2
B1	7.9×10^{5}	3.9×10^{-3}	4.9 ± 1.7	150 ± 3.5	Competitive	9.0 ± 0.3
B3	3.5×10^{5}	2.2×10^{-3}	6.3 ± 2.4	41 ± 1.9	Competitive	7.5 ± 0.5
T1	2.0×10^{5}	4.9×10^{-4}	2.5 ± 1.3	79 ± 4.1	Competitive	6.8 ± 0.4
T3	6.2×10^{4}	2.4×10^{-3}	39 ± 4.6	572 ± 3.8	Competitive	11.0 ± 0.1
T4	5.3×10^{4}	4.0×10^{-3}	75 ± 3.8	1323 ± 5.3	Competitive	6.2 ± 0.6

3.3.4 Isolated 3A2 mutants were MMP-14 inhibitors with high selectivity and improved stability

Inhibition assays using a FRET peptide substrate indicated that all the five isolated 3A2 mutants inhibited cdMMP-14 activity, yet with various potencies ranging from 41 nM to 1.3 µM (Table 3.2). Particularly B3 and T1 showed their potencies less than 100 nM, marginally weaker than that of 3A2 wt (**Figure 3.5**A). To demonstrate the selectivity of isolated variants, 1 µM scFvs were incubated with either 10 nM cdMMP-14 or 10 nM highly homologous cdMMP-9 for FRET inhibition assays. At these conditions, B1, B3 and T1 completely (96-98%) inhibited MMP-14 (**Figure 3.5**B), while T4 displayed incomplete inhibition (34%) on MMP-14 due to its low potency (**Figure 3.5**A), but none of them showed cross reactivity on MMP-9 (0% inhibition). However, T3 gave incomplete inhibition on both MMP-14 (70%) and MMP-9 (30%). Therefore, except T3, other isolated 3A2 mutants exhibited excellent selectivity, similar as 3A2 wt (96% on MMP-14 and 0% on MMP-9).

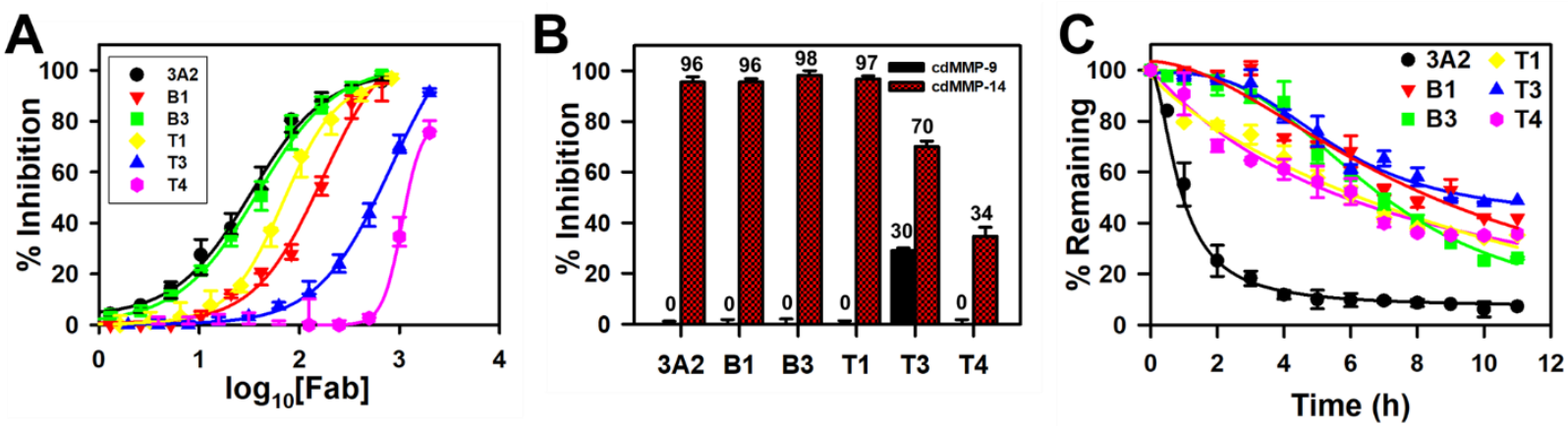

Figure 3.5: Characterization of isolated scFv clones. (A) Inhibition assays with 10 nM cdMMP-14, 0-2000 nM scFv and 1 µM FRET peptide substrate. (B) Selectivity on MMP-14 over MMP-9 demonstrated by relative inhibition. (C) *In vitro* stability results. Following 1 µM scFv incubation with 1 µM cdMMP-14 for indicated period time, SDS-PAGE bands associated with intact scFvs were quantitatively analyzed to calculate half-lives. See Figs S1&S3 for examples.

During *in vitro* stability tests, 1 µM purified scFvs were incubated with 1 µM cdMMP-14 at pH 7.5 37ºC, and samples collected at 1-10 h were densitometrically analyzed for quantification of intact scFvs. As the degradation progress of B3 was shown in **Figure 3.6**A, the relative quantities of remained scFv over time were plotted to determine that the half-life of B3 scFv is 7.5 hours (Figure 3.6B). Similarly, the half-lives of other isolated 3A2 scFv variants were measured to be 6.2-11.0 hours (Figure 3.5C, Figure 3.6B), significant longer than 3A2 wt scFv at 1.0 hour (Figure 3.5C). This dramatic improvement on stability was likely achieved by the extended incubation with cdMMP-14 prior and during FACS experiments, while the inhibition function and selectivity were well retained by controlling the epitope specificity via competition with nTIMP-2 during dual color sorting.

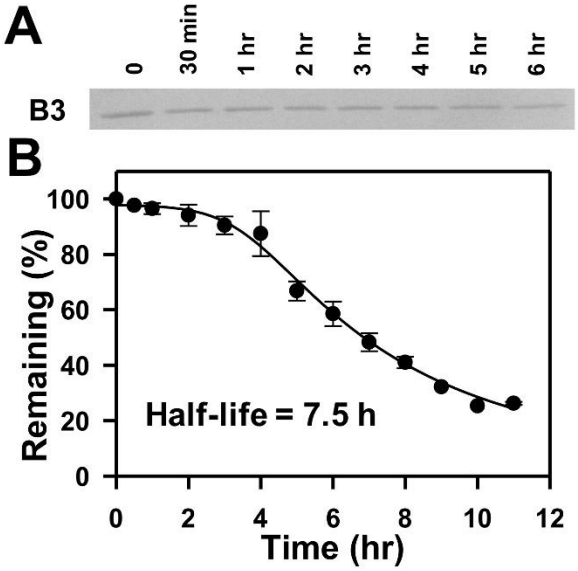

Figure 3.6: *In vitro* stability of scFv B3. (A) SDS-PAGE analysis of 1 µM scFv B3 after incubation with 1 µM cdMMP-14 at 37 oC for indicated time. (B) Quantification of scFv bands by densitometry was plotted over time to determine half-life.

3.3.5 Isolated 3A2 mutants were competitive inhibitors binding to the vicinity of reactive cleft

To understand the inhibition mechanism of isolated 3A2 mutants, their inhibitor type was determined by measuring the kinetics of 10 nM cdMMP-14 in the presence of 0, 250, 500, or 1000 nM scFvs. The generated Lineweaver-Burk plots indicated unchanged V_{max}s and increased K_ms with increasing concentration of scFv, suggesting that all isolated mutants had a competitive mode of inhibition (Figure 3.7).

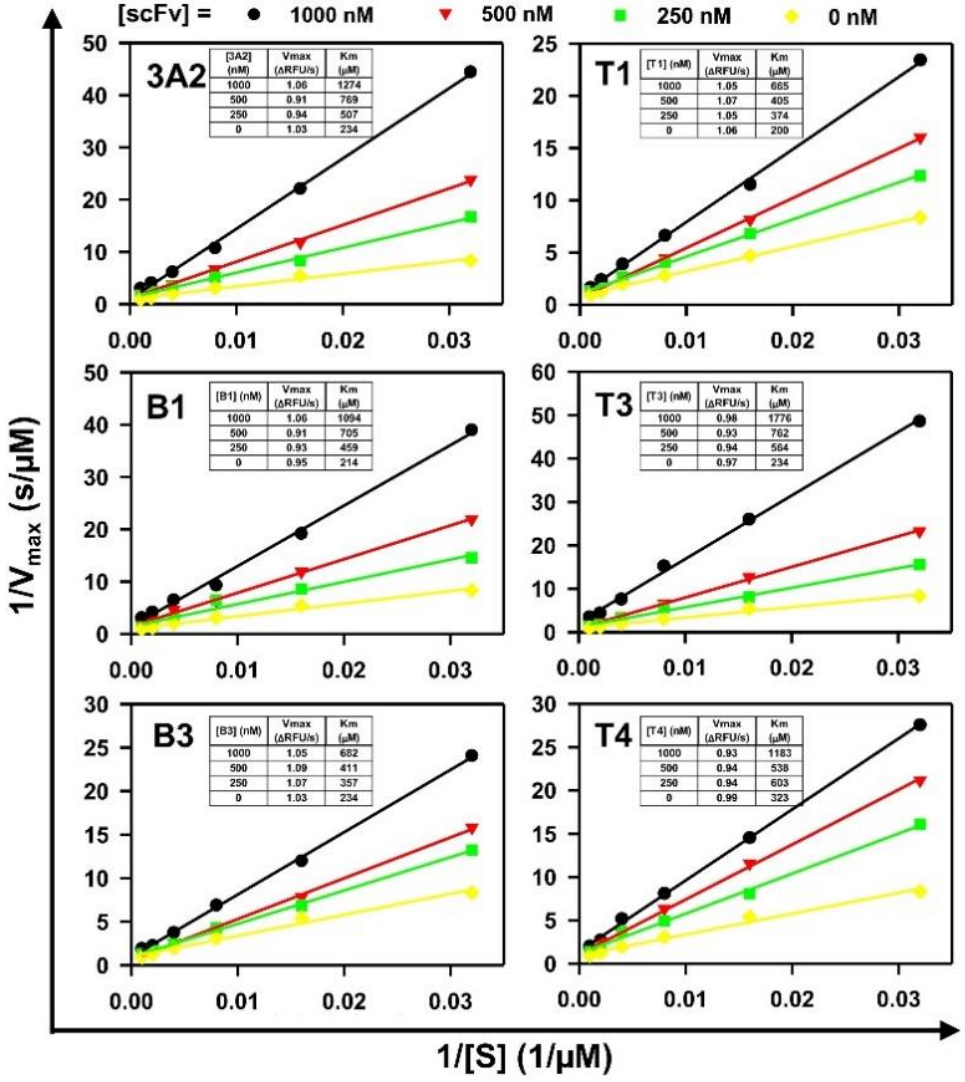

Figure 3.7: Determination of the type of inhibition. Enzymatic kinetics were measured in the presence of 0, 250, 500 and 1000 nM scFv. Lineweaver-Burk plots were generated to calculate V_{max} and K_m.

To further investigate whether these competitive inhibitions were governed by orthosteric or allosteric regulations, we performed alanine scanning on three phenylalanine residues F198, F204 and F260 of cdMMP-14 (Figure 3.8A). These positions were chosen because they are located around the catalytic cleft (yellow in Figure 3.8A) and among the binding epitope of nTIMP-2 (red in Figure 3.8A).

cdMMP-14 site-directed mutants F198A, F204A and F260A were produced and incubated with scFvs before their kinetic assays, to check whether these alanine mutations affected the inhibition functions of scFvs (Figure 3.8B).

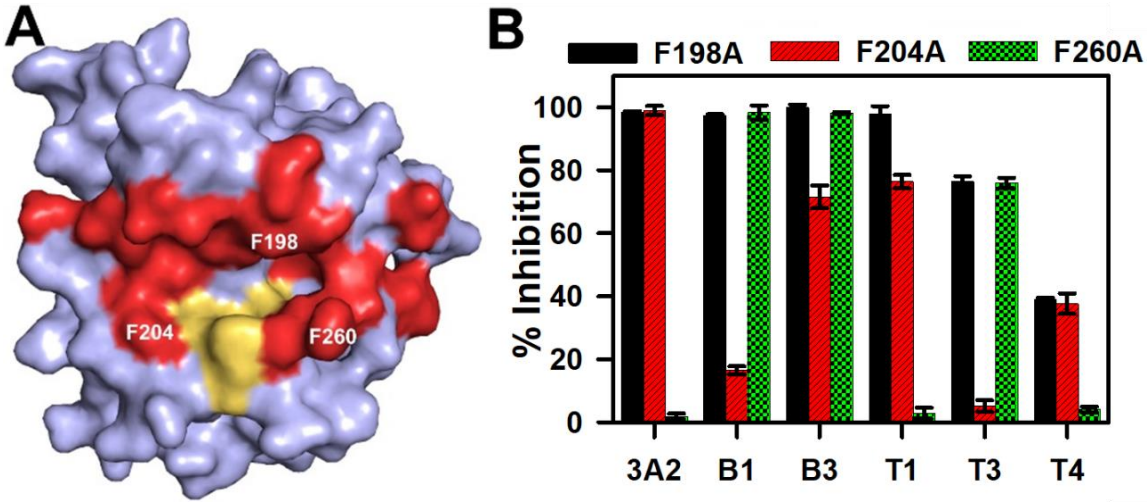

Figure 3.8: Epitope mapping of scFvs 3A2 wt and isolated variants. (A) Catalytic domain of MMP14 showing the reaction center (yellow) and binding region of TIMP-2 (red). The three phenylalanine residues selected for single site alanine mutations were labeled. (B) Relative inhibition of scFvs on cdMMP-14 mutants. 10 nM cdMMP-14, 1 µM scFv and 1 µM peptide substrate were used.

Toward MMP-14 mutant F260A, scFvs T1, T4 and 3A2 wt completely abolished their inhibition capability, suggesting that these scFvs interacted with cdMMP-14 strongly but not limited through F260. However, scFvs B1, B3 and T3 didn't change their inhibition capability toward F260A compared to cdMMP-14 wt (Figure 3.8B). In contrast, B1, B3 and T3 showed reduced inhibition to F204A at various degrees, implying that their epitopes at least partially shifted from F260 to F204. Interestingly, clone T1 also showed a reduction in inhibition for F204A, suggesting that it bound to both F204 and F260 which are located at the two sides

of the catalytic center. Towards F198A, none of tested scFv clones showed reduced inhibition, indicating tested scFvs did not directly interact with F198. Collectively, enzyme kinetics and alanine scanning results suggested that isolated 3A2 variants were competitive inhibitors directly binding to the vicinity of MMP-14 catalytic cleft. Therefore, dual color sorting with nTIMP-2 as the competitor is an effective method to control epitope specificity of isolated antibodies.

3.3.6 IgG B3 showed nanomolar affinity and potency with expected *in vivo* half-life in mice

The most promising varant B3 was converted to its human IgG1 format and produced in HEK293F cells with a typical yield of 35 mg purified IgG per liter of culture media. Binding kinetics of IgG B3 measured by bio-layer interferometry indicated k_{on} of 1.4×10^{5} $M^{-1}s^{-1}$ and k_{off} of 7.1×10^{-4} s^{-1} with K_D equal to 5.0 nM (Figure 3.9A). FRET assays suggested IgG B3 had a similar inhibition potency K_I equal to 6.5 nM (Figure 3.9B). The *in vivo* clearance rate of IgG B3 in three mice was examined following a bolus injection via tail vein. The amount of IgG B3 present in blood 2 hours after injection was considered the initial circulating concentration (100%). The relative amounts of IgG B3 dropped to 73.1%, 24.2%, 3.6%, 2% and 0.05% at days 3, 6, 9, 12 and 15, respectively (Figure 3.9C), giving a half-life of ~4.6 days, similar to that of serum immunoglobulins in adult mice[47].

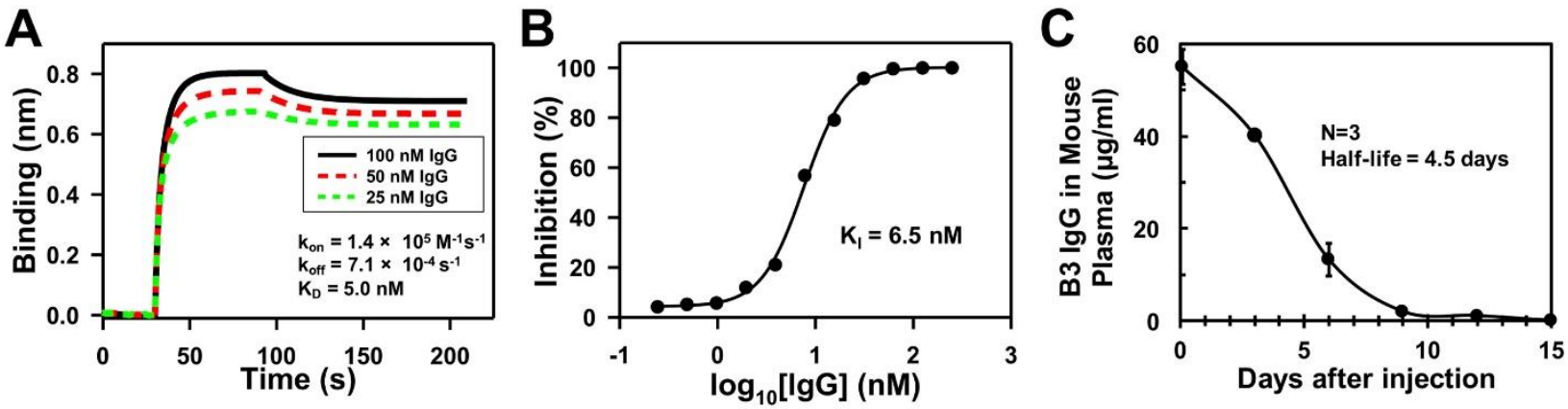

Figure 3.9: Characterization of IgG B3. (A) Binding kinetics. (B) Inhibition potency. (C) *In vivo* stability of IgG B3 antibody. N=3 for each time point and data are presented as the mean ± S.D.

3.4 Discussion and Conclusions

Studies of therapeutic mAbs have shown that targeting effectual epitopes is absolutely required to deliver the desired biological functions. For instance, HIV broadly neutralizing mAb b12 achieves its protective efficacy by recognizing a hidden but highly conserved epitope that overlaps with the CD4 binding site on gp120[7]. In the case of trastuzumab, it binds to domain IV of HER2 extracellular segment, which blocks its signal transduction and inhibits cancer cell growth. However, some HER2-specific mAbs targeting different epitopes exhibit adverse effects by stimulating tumor growth[4]. To achieve epitope-specific selection, competitive phage panning and FACS have been developed[11,12]. In the effort to isolate MMP-14 inhibitory mAbs, the use of nTIMP-2, a native inhibitor of MMP-14 as a competitive eluent led to the successful discovery a panel of inhibitory clones[28,24]. The current study developed a dual color FACS to perform selection on MMP-14 under competition with nTIMP-2 concurrently to govern a needed control over epitope. Furthermore, the quantitative nature of FACS allows the conditions and sorting windows to be readily adjusted, e.g. by reducing cMMP-14 concentration and increasing n-TIMP-2 concentration (Figure 3.3), that provides the desired stringency to generate highly potent inhibitory clones. Using these approaches, we isolated 3A2 variants that exhibited affinity improvement while maintaining high inhibition potency and high selectivity (**Figure 3.5**A & B). Our results indicate that even though epitope drift indeed happened for some of

isolated clones (e.g. F260 to F204 for scFvs B1 and B3, Figure 3.8B), dual color competitive FACS kept the effectual epitopes.

Standard mechanism protease inhibitors bind their targets in a substrate-like manner by inserting a reactive loop into the catalytic cleft[13,14]. Upon binding, the scissile bond of the inhibitor is slowly hydrolyzed by the targeted protease[31,32]. Improving proteolytic resistance of a protease inhibitor is essentially to bias the balance toward inhibition rather than substrate behavior. The challenge of such a task was well demonstrated by attempts to generate pepsin/chymotrypsin-resistant hirudin, a thrombin-specific inhibitor. The 5 N-terminal residues and the P1-P1' positons of major cleavage sites were subjected to mutagenesis. By phage panning, protease-resistant hirudin variants were isolated, however at the expense of ~100-fold reduction in the potency of thrombin inhibition[48]. To address this challenge, Cohen et al. developed an elegant yeast display and multi-modal library screening approach, and successfully engineered Kunitz protease inhibitor domain (APPI) with enhanced proteolytic stability and improved inhibition properties toward mesotrypsin[49]. In this study, we employed prolonged MMP-14 incubation and epitope-specific FACS, and isolated proteolytically resistant inhibitory antibodies with high potency and selection. Notably, the isolated beneficial variants had mutations located throughout the entire scFv gene (Table 3.1). This suggests that while binding specificity and affinity are largely given by CDRs, the proteolytic stability is strongly influenced by residues within the framework regions, in agreement with other studies[50].

Isolated mutant B1, B3 and T1 scFvs displayed higher binding affinity than 3A2 wt. However, only B3 exhibited similar inhibition potency compared to 3A2 (Table 2). Ideally, inhibitory mAbs should exhibit both high binding affinity and high inhibition potency at similar strength, which indicates the binding epitopes effectively contribute to inhibition. If affinity strength (K_D) is much higher than that of potency (K_I), e.g. B1 and T1, it is likely caused by less effective epitope that has little interferes on inhibition. Although B3 scFv showed 4-fold improvement on affinity (Table 3.2), when converted to IgG, B3 exhibiting a K_D of 5.0 nM and K_I of 6.5 nM, did not show improvements compared to 3A2 wt IgG (K_D = 3.8 nM, K_I = 3.0 nM). Such compromises introduced by format switch were not uncommon for antibody affinity maturation practices. Recent development on Fab yeast display holds great promise for more effective affinity maturation[51].

Protein-protein interactions (PPI) are essential for a wide variety of biological functions[52], and for any PPI, epitope specificity is critical. Targeting beneficial epitopes and avoiding ineffectual or adverse epitopes is also critical for the success development of biosimilars or biosuperiors. In addition to protease inhibitory antibodies, the competitive FACS described here can be applied for discovery and engineering biosimilars, and in general for other circumstances where epitope specific modulation is needed.

3.5 References

1. Buss, N.A., Henderson, S.J., McFarlane, M., Shenton, J.M., de Haan, L. Monoclonal antibody therapeutics: history and future. *Current Opinion Pharmacology*, **12**, 615–622. (2012).

2. Weiner, G.J. Building better monoclonal antibody-based therapeutics. *Nature Review Cancer*. **15**, 361–370. (2015).

3. Ecker, D.M., Jones, S.D., Levine, H.L. The therapeutic monoclonal antibody market. *MAbs*. **7**, 9-14. (2015).

4. Yip, Y.L., Smith, G., Koch, J., Dübel, S., Ward, R.L. Identification of epitope regions recognized by tumor inhibitory and stimulatory anti-ErbB-2 monoclonal antibodies: implications for vaccine design. *Journal of Immunology*. **166**, 5271–5278. (2001).

5. Teeling, J.L., et al. The biological activity of human CD20 monoclonal antibodies is linked to unique epitopes on CD20. *Journal of Immunology*, **177**, 362–371. (2006).

6. Wu, Y., et al. Structural insight into distinct mechanisms of protease inhibition by antibodies. *Proc Natl Acad Sci U S A*. **104**, 19784–19789. (2007).

7. Zhou, T., et al. Structural definition of a conserved neutralization epitope on HIV-1 gp120. *Nature*, **445**, 732–737. (2007).

8. He, W., et al. Epitope specificity plays a critical role in regulating antibody-dependent cell-mediated cytotoxicity against influenza A virus. *Proc Natl Acad Sci U S A*. **113**, 11931–11936. (2016).

9. Smith, A.J. New Horizons in Therapeutic Antibody Discovery: Opportunities and Challenges versus Small-Molecule Therapeutics. *Journal of Biomolecular Screening*. **20**, 437-453. (2015).

10. Chiu, M.L. & Gilliland, G.L. Engineering antibody therapeutics. *Current Opinion in Structural Biology*. **38**, 163–173. (2016).

11. Puri, V., Streaker, E., Prabakaran, P., Zhu, Z., Dimitrov, D.S. Highly efficient selection of epitope specific antibody through competitive yeast display library sorting. *mAbs,* **5**, 533–539. (2013).

12. Zhang, M.Y., et al. Selection of a novel gp41-specific HIV-1 neutralizing human antibody by competitive antigen panning. *Journal of Immunological Methods*. **317**, 21–30. (2006).

13. Laskowski, M. Jr., & Kato, I. Protein inhibitors of proteinases. *Annual Review of Biochemistry*. **49**, 593–626. (1980).

14. Farady, C.J., & Craik, C.S. Mechanisms of macromolecular protease inhibitors. *ChemBioChem*, **11**, 2341–2346. (2010).

15. Murphy, G. Tissue inhibitors of metalloproteinases. *Genome Biology*, **12**, 233. (2011)

16. Nagase, H., Visse, R., Murphy, G. Structure and function of matrix metalloproteinases and TIMPs. *Cardiovascular Research.* **69**, 562–573. (2006).

17. Zarrabi, K., et al. Inhibition of Matrix Metalloproteinase 14 (MMP-14)-mediated Cancer Cell Migration. *J. Biol. Chem*, **286**, 33167-33177. (2011).

18. Sela-Passwell, N. Antibodies targeting the catalytic zinc complex of activated matrix metalloproteinases show therapeutic potential. *Nat Med*. **18**, 143-147. (2011).

19. Ager, E.I. Blockade of MMP14 activity in murine breast carcinomas: implications for macrophages, vessels, and radiotherapy. *J Natl Cancer Inst*. **107**, djv017. (2015).

20. Remacle, A.G., et al. Selective function-blocking monoclonal human antibody highlights the important role of membrane type-1 matrix metalloproteinase (MT1-MMP) in metastasis. *Oncotarget*. **8**, 2781–2799. (2017).

21. Itoh, Y., et al. Homophilic complex formation of MT1-MMP facilitates proMMP-2 activation on the cell surface and promotes tumor cell invasion. *EMBO Journal,* **20**, 4782–4793. (2001).

22. Overall, C.M., Kleifeld, O. Validating matrix metalloproteinases as drug targets and anti-targets for cancer therapy. *Nat. Rev. Cancer*. **6**, 227-239. (2006).

23. Turk, B. Targeting proteases: successes, failures and future prospects. *Nature Reviews Drug Discovery* **5**, 785-799. (2006).

24. Nam, D.H., Rodriguez, C., Remacle, A.G., Strongin, A.Y., & Ge, X. Active-site MMP-selective antibody inhibitors discovered from convex paratope synthetic libraries. *Proc Natl Acad Sci U S A*. **113**, 14970–14975. (2016).

25. Nam, D.H., Fang, K., Rodriguez, C., Lopez, T., & Ge, X. Generation of inhibitory monoclonal antibodies targeting matrix metalloproteinase-14 by motif grafting and CDR optimization. *Protein Engineering, Design & Selection*. **30**, 113–118. (2017).

26. Lopez, T., Nam, D.H., Kaihara, E., Mustafa, Z., Ge, X. Identification of highly selective mmp-14 inhibitory fabs by deep sequencing. *Biotechnology and Bioengineering*, **114**, 1140–1150. (2017).

27. Udi, Y., et al. Inhibition Mechanism of Membrane Metalloprotease by an Exosite-Swiveling Conformational Antibody. *Structure*, **23**, 104–115. (2015).

28. Devy, L. Selective inhibition of matrix metalloproteinase-14 blocks tumor growth, invasion, and angiogenesis. *Cancer Res*. **69**, 1517-1526. (2009).

29. Appleby, T., et al. Biochemical characterization and structure determination of a potent, selective antibody inhibitor of human MMP9. *Journal of Biological Chemistry*, **292**, 6810–6820. (2017).

30. Ling, B., et al. A novel immunotherapy targeting MMP-14 limits hypoxia, immune suppression and metastasis in triple-negative breast cancer models. *Oncotarget.* **8**, 58372–58385. (2017).

31. Farady, C.J., Sun, J., Darragh, M.R., Miller, S.M., Craik, C.S. The mechanism of inhibition of antibody-based inhibitors of membrane-type serine protease 1 (MT-SP1). *J Mol Biol*. **369**, 1041-1051. (2007).

32. Zakharova, E., Horvath, M.P., Goldenberg, D.P. Structure of a serine protease poised to resynthesize a peptide bond. *Proc Natl Acad Sci U S A*. **106**, 11034–11039. (2009).

33. Boder, E. & Witrrup, K. D. Yeast surface display for directed evolution of protein expression, affinity, and stability. *Methods in Enzymology*. **328**, 430–444. (2000).

34. Feldhaus, M.J., et al. Flow-cytometric isolation of human antibodies from a nonimmune Saccharomyces cerevisiae surface display library. *Nature Biotechnology*. **21**, 163–170. (2003).

35. Colby, D., et al. Engineering antibody affinity by yeast surface display. *Methods in Enzymology.* **388**, 348–358. (2004).

36. Ohlin, M., Owman, H., Mach, M., Borrebaeck, C.A. Light chain shuffling of a high affinity antibody results in a drift in epitope recognition. *Mol Immunol*. **33**, 47-56. (1996).

37. Pédelacq, J.D., Cabantous, S., Tran, T., Terwilliger, T.C, Waldo, G.S. Engineering and characterization of a superfolder green fluorescent protein. *Nature Biotechnology*. **24**, 79–88. (2006).

38. Lee, K.B., et al. Direct expression of active human tissue inhibitors of metalloproteinases by periplasmic secretion in Escherichia coli. *Microbial Cell Factory*. **16**, 73. (2017).

39. Hayhurst, A., et al. Isolation and expression of recombinant antibody fragments to the biological warfare pathogen *Brucella melitensis*. *Journal of Immunological Methods*. **276**, 185–196. (2003).

40. Zufferey, R., Donello, J.E., Trono, D., & Hope, T.J. Woodchuck hepatitis virus posttranscriptional regulatory element enhances expression of transgenes delivered by retroviral vectors. *Journal of Virology*. **73**, 2886–2892. (1999).

41. Brandt, R.B., Laux, J.E., Yates, S.W. Calculation of inhibitor K_i and inhibitor type from the concentration of inhibitor for 50% inhibition for Michaelis–Menten enzymes. *Biochemical Medicine and Metabolic Biology*. **37**, 344–349. (1987).

42. Gram, H., et al. *In vitro* selection and affinity maturation of antibodies from a naive combinatorial immunoglobulin library. *Proc Natl Acad Sci U S A*. **89**, 3576–3580. (1992).

43. Daugherty, P.S., Chen, G., Iverson, B.L., Georgiou, G. Quantitative analysis of the effect of the mutation frequency on the affinity maturation of single chain Fv antibodies. *Proc Natl Acad Sci U S A*. **97**, 2029–2034. (2000).

44. Fernandez-Catalan, C. Crystal structure of the complex formed by the membrane type 1-matrix metalloproteinase with the tissue inhibitor of metalloproteinases-2, the soluble progelatinase A receptor. *EMBO J*. **17**, 5238-5248. (1998).

45. Yang, W.P., et al. CDR walking mutagenesis for the affinity maturation of a potent human anti-HIV-1 antibody into the picomolar range. *Journal of Molecular Biology*. **254**, 392–403. (1995).

46. Rajpal, A., et al. A general method for greatly improving the affinity of antibodies by using combinatorial libraries. *Proc Natl Acad Sci U S A*. **102**, 8466–8471. (2005).

47. Vieira, P., & Rajewsky, K. The half-lives of serum immunoglobulins in adult mice. *European Journal of Immunology*. **18**, 313–316. (1988).

48. Wirsching, F., Keller, M., Hildmann, C., Riester, D., & Schwienhorst, A. Directed evolution towards protease-resistant hirudin variants. *Molecular Genetics and Metabolism*. **80**, 451–462. (2003).

49. Cohen, I., et al. Combinatorial protein engineering of proteolytically resistant mesotrypsin inhibitors as candidates for cancer therapy. *Biochemical Journal*. **473**, 1329–1341. (2016).

50. Salameh, M.A., et al. Determinants of affinity and proteolytic stability in interactions of Kunitz family protease inhibitors with mesotrypsin. *Journal of Biological Chemistry*. **285**, 36884–36896. (2010).

51. Wang, B., et al. Functional interrogation and mining of natively paired human VH:VL antibody repertoires. *Nature Biotechnology*. **36**, 152–155. (2018).

52. Keskin, O., Tuncbag, N., Gursoy, A. Predicting protein-protein interactions from the molecular to the proteome level. *Chemical Review*, **116**, 4884–909. (2016).

Chapter 4: Conversion of Selectivity of Protease Inhibitory Antibodies

This chapter is based on: Lopez, T. et al. Selectivity Conversion of Protease Inhibitory Antibodies. *Antibody Therapeutics*. submitted (19 July 2018)

Abstract

Proteases are one of the largest pharmaceutical targets for drug developments. Their dysregulations result in a wide variety of diseases. Because proteolytic networks usually consist of protease family members that share high structural and catalytic homology, distinguishing them using compound inhibitors are often challenging. To achieve specific inhibition, this study developed a novel approach for the generation of protease inhibitory antibodies. Applying dual color competitive FACS, we converted a matrix metalloproteinase (MMP)-14 specific inhibitor to a panel of MMP-9 specific inhibitory antibodies with dramatic selectivity shifts of 690-4500 folds. Isolated scFvs inhibited MMP-9 at nM potency with high selectivity over MMP-2/-12/-14, and exhibited decent proteolytic stability. Enzyme kinetics, competitive ELISA and paratope mutagenesis studies revealed that these scFvs were competitive inhibitors binding to the MMP-9 reaction cleft vicinity via their CDR-H3s. The methodology demonstrated here can be readily applied to other MMPs and many proteases of biomedical importance.

4.1 Introduction

Accounting for roughly 2% of human genome, proteases are important signaling molecules precisely controlling a wide variety of physiological processes.

Consequently, many diseases are associated with altered protease expression or substrate proteolysis[1,2,3,4]. It has been estimated that 5-10% of all pharmaceutical targets for drug developments are proteases[5]. Some well characterized examples include: cathepsin B, which promotes tumor growth, metastasis and angiogenesis through its proteolytic cascades[6]; cysteine protease falcipain 1, which is required for malaria to invade host cells[7,8]; matrix metalloproteinases (MMPs), which cause wound healing delays due to excessive matrix degradation[9]; thrombin and factor XIa, whose dysregulated activities are responsible for blood coagulation[10]; and plasma kallikrein, whose upregulation due to genetic deficiency of serpin C1-inhibitor leads to hereditary angioedema[11]. One therapeutic strategy is to block these abnormal or pathogenic proteolysis by inhibiting their catalytic reactions.

Most therapeutic protease inhibitors currently in clinical use or under developments are chemical compounds or peptide mimics derived from their substrates[1,3]. Considering that at least 500-600 human proteases have been found[12], specificity is highly desired for any protease inhibition therapy[1,3]. However, achieving target specificity can be challenging because proteolytic pathways often consist of highly homologous family members that share the same domain folding and catalytic chemistry[13]. The crucial importance of specificity has been highlighted by the extensive studies on inhibition of MMPs using zinc-chelating compounds as a strategy for treating cancer[14]. Although pre-clinical results were promising, previous attempts focusing on development of broad-spectrum chemical compound inhibitors, e.g., hydroxamates, all failed in clinical trials due to

lack of efficacy and severe side effects caused by non-specific inhibition of other metalloproteinases[15].

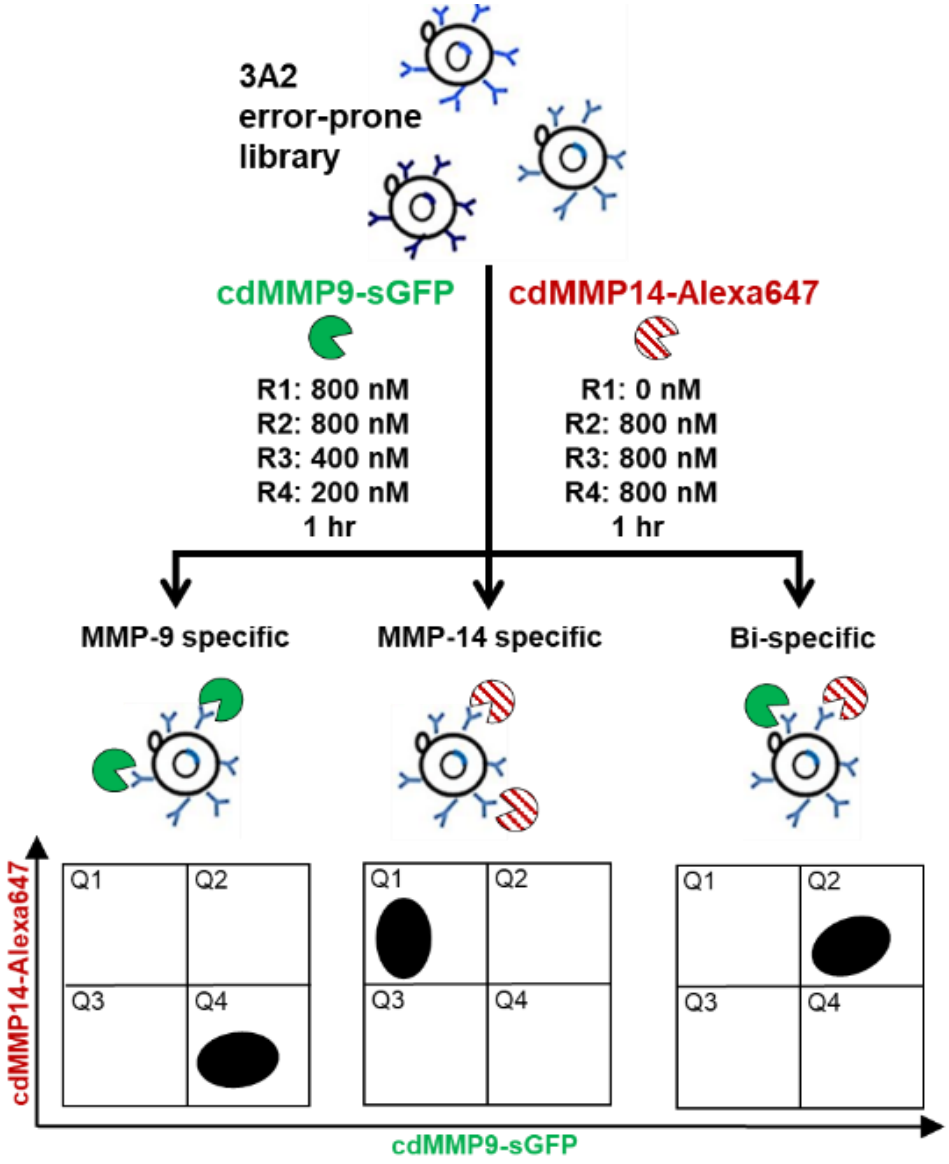

Figure 4.1: Scheme for specificity screening by competitive FACS. Random mutagenesis library of 3A2 scFv was displayed on yeast cell surface and co-incubated with cdMMP9-sfGFP and cdMMP14-Alexa647, allowing to isolate inhibitory antibodies either mono-specific on cdMMP-9 or cdMMP-14, or bi-specific on both.

Our studies[16,17,18], consistent with others[19,20,21,22,23,24,25,26,27], have demonstrated the feasibility of monoclonal antibodies (mAbs) to act as highly potent and highly selective inhibitors of secreted or cell surface proteases. However, even with recent technology advancements, such as epitope synthetic mimicry[21], competitive phage elution[19], convex paratope design[16], and epitope-specific FACS[17], the discovery of protease inhibitory mAbs still presents a challenge in general, because the isolated antibodies need to not only specifically bind but also efficiently inhibit the protease of interest. This study aims to develop a novel approach to facilitate the development of protease inhibitory antibodies, by engineering an active site inhibitor and switching its selectivity toward a new target. For proof-of-concept, we start with a MMP-14 specific inhibitor (scFv 3A2) and change its specificity toward MMP-9, an important collagenase associated with maladies such as neuropathic pain[28].

We hypothesize that affinity maturation using yeast surface display and competitive FACS can achieve this selectivity conversion. Our underlying rationale is that antibody affinity and its selectivity are correlated[29,30,31,32], i.e. a perfect shape complementarity and strong interaction are the factors leading to both high-affinity binding and high-selectivity inhibition. By incubating 3A2 random mutagenesis library cells with MMP-9 and MMP-14 conjugated/fused with different fluorophores simultaneously, dual color competitive FACS can in principle isolate antibodies either mono-specific on MMP-14 or MMP-9, or bi-specific on both (Figure 4.1). This study mainly focuses on mono-specific MMP inhibitors, especially on converting

3A2's specificity from MMP-14 to MMP-9. The beneficial effects on proteolytic stability improvement will also be studied.

4.2 Materials and Methods

4.2.1 3A2 Error-Prone scFv Yeast Display

V_H and V_L genes of Fab 3A2 were amplified and its scFv gene was assembled by overlapping PCR. Error-prone mutagenesis of 3A2 scFv was generated using Taq DNA polymerase with 120 µM dATP, 100 µM dCTP, 360 µM dGTP, 2.5 mM dTTP, 5 µg/mL BSA, 3.28 mM $MgCl_2$ and 0.5 mM $MnCl_2$. Mutation product was cloned into yeast display plasmid pCTCon2 and transformed to *Saccharomyces cerevisiae* competent cells. Library size was determined by serial dilution. Mutation was measured by Sanger sequencing of randomly picked clones. 5×10^9 cells of constructed library were cultured on SD/-Trp/-Ura/penicillin-streptomycin agar plates at 30°C for 48 hours. 30 OD_{600} cultured cells were inoculated to 600 mL SD/-Trp/-Ura at 30°C 250 rpm for incubation 12 hours. Cells were collected by centrifugation at 6,000 × g for 2 min, and 8 OD_{600} cells were further cultured for scFv expression in 20 mL YNB (yeast nitrogen base)-Trp/-Ura drop-out medium supplemented with 5 mL 20% galactose at room temperature 250 rpm for 48 hours.

4.2.2 FACS

For fluorescence labeling, superfolder GFP (sfGFP) was cloned to C-terminal of catalytic domain (cd) of MMP-9. cdMMP9-sfGFP was periplasmically

expressed in *E. coli*, purified with Ni-NTA column (Qiagen). cdMMP-14 was produced as previously described[33], and chemically conjugated with Alexa-647 (Invitrogen). Both enzymatic activities were tested. In the first round of sorting (R1), 4 OD_{600} cultured library cells were incubated with 600 µL 800 nM cdMMP9-sfGFP at dark for 1 hour. After three washes with assay buffer (50 mM Tris-HCl pH 7.5, 150 mM NaCl, 5 mM $CaCl_2$, 2.0 mM $ZnCl_2$), cells were suspended in 4 mL assay buffer for FACS. EBY100 host was labeled the same way as the negative control. Cells were sorted on a BioRad Se3 flow cytometer equipped with 488/640 nm lasers. Filters FL1 (526/48 nm) and FL3 (615/25 nm) were used for cdMMP9-sfGFP and cdMMP14-Alexa647 respectively. The forward and side scatter voltages were set at 317v and 341v with a threshold of 5. A triangle gate was used to select the top portion of GFP positive cells while excluding the clones showing high Alexa-647 signals. Isolated cells were plated on a SD/-Trp/-Ura/penicillin-streptomycin agar plates for growth at 30^{o}C for 48 hours, and collected in 20% glycerol SD/-Trp/-Ura media and stored at -80^{o}C. In R2-R4, cells covering 10× the library diversity of previous round were cultured and labeled with preset concentrations of cdMMP9-sfGFP and cdMMP14-Alexa647. Colonies were randomly picked after R4 for monoclonal FACS screening, in which cells were labeled with 400 nM cdMMP9-sfGFP and 400 nM cdMMP14-Alexa647. Both scanning and sorting were performed at a rate of 2,000 events/sec with a mild agitation to prevent cell settling.

4.2.3 Biochemical Characterizations

Plasmids of isolated clones were extracted using Zymoprep yeast plasmid kit (Zymo). scFv fragments of isolated clones and their site-directed mutants were cloned into pMoPac for *E. coli* periplasmic expression[34], and purified by Ni-NTA column. Binding kinetics were measured by biolayer interferometry using BLItz (ForteBio) on streptavidin biosensors coated with cdMMP-9, which were biotinylated using EZ-Link Sulfo-NHS-LC biotinylation kit (Thermo Fisher). Determined k_{on} and k_{off} parameters were used to calculate the K_D values. Inhibition assays were performed by reacting serially diluted scFvs with 10 nM cdMMP-9 for 30 min, and the remaining activity of cdMMP-9 was measured with 1 μM M2350 peptide substrate (Bachem). The fluorescence was monitored with excitation and emission wavelengths at 325 and 392 nm using a spectrophotometer (BioTek). Inhibition potency K_i was calculated using equation $K_I = IC_{50}/(S/K_m+1)$[35]. Inhibition mode was determined by establishing Lineweaver-Burk plots at different scFv concentrations. cdMMP-12 mutation was designed using PROSS algorithm[36] and produced in the periplasmic space of *E. coli* for inhibition specificity tests. Recombinant human MMP-2 was obtained from Anaspec. Their enzymatic activities were tested. In completive ELISA, Maxisorp microplates (Thermo Scientific) were coated with 4 μg/mL cdMMP-9 and blocked with skim milk. After washing, plates were incubated with scFv at its EC_{50} concentrations for 1 hour and washed again. 4 μM to 3 nM N-terminal domain of TIMP-2 (nTIMP-2), prepared as previously described[37], was then added and incubated for 1 hour to compete with

scFv for binding on immobilized cdMMP-9. Anti-cMyc-HRP was added to detect captured scFvs and the signals were developed using TMB substrate (Thermo Fisher). For *in vitro* stability tests, 1 μM purified scFvs were incubated with 1 μM cdMMP-9 in assay buffer at 37^{o}C for 3 or 12 h. Densitometric analysis of scFv bands (30 kDa) on SDS-PAGE was performed using Image Lab (Bio-Rad). To reduce errors from variations in staining and destaining, gel background for each band was quantified and subtracted.

4.3 Results

4.3.1 MMP homology analysis

The objective of this study is to test the feasibility of Discovering MMP-9 inhibitory antibodies from an error prone library based on an MMP-14 inhbitory antibody. As a proof of concept, we aimed to generate MMP-9 specific inhibitory antibodies by engineering a MMP-14 inhibitor. As zinc-dependent endopeptidases, catalytic domains (cd) of human MMPs possess a homologous protein folding with highly conserved secondary structures (Figure 4.2A).

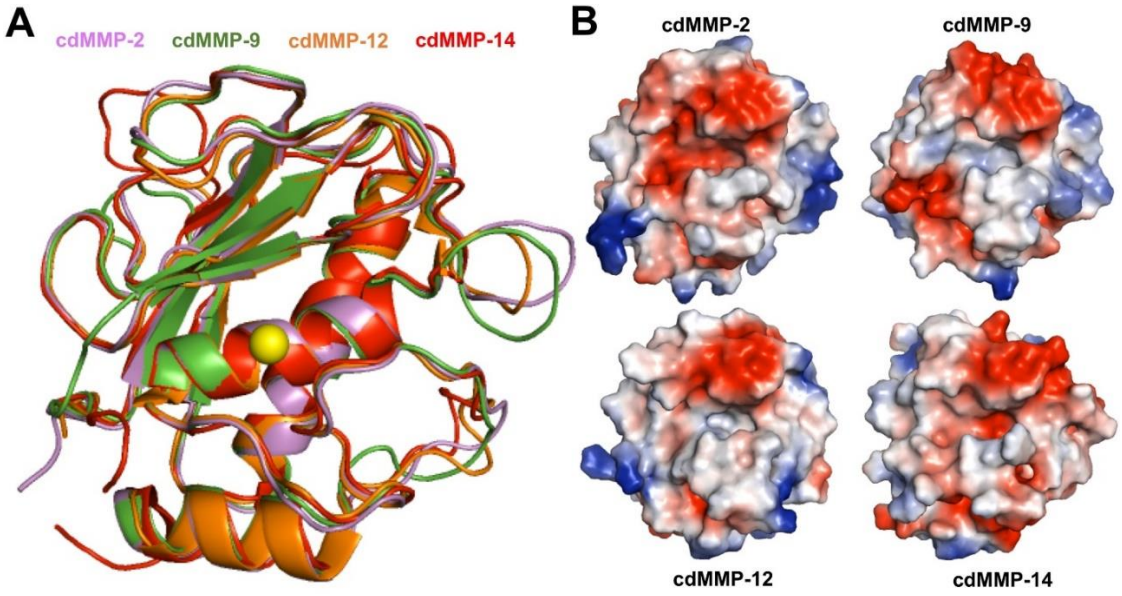

Figure 4.2: Superimpose of catalytic domains of MMP-2 (purple), -9 (green), -12 (orange), and -14 (red) shown as (A) cartoon and (B) surface charge. cdMMPs share highly conserved overall protein folding, secondary structure backbones and catalytic zinc (yellow sphere). The catalytic clefts are well pronounced with subtle differences on surface topology and charges.

Amino acid sequence comparison of cdMMP-2/-9/-12/-14 reveals that they share 47-60% identity and 56-67% similarity (Table 4.1). Major structural differences occur in the loop regions while the variations of surface topology and surface charge around their well pronounced catalytic clefts are relatively subtle (Figure 4.2B). Encouraged by the exclusive specificity usually offered by monoclonal antibodies, we hypothesized that mAb inhibitors can distinguish among closely related MMP family members with high selectivity.

Table 4.1: Amino acid sequence similarity and identity (%).

		Similarity			
		cdMMP-2	cdMMP-9	cdMMP-12	cdMMP-14
Identity	cdMMP-2	-	67	66	59
	cdMMP-9	60	-	61	57
	cdMMP-12	57	49	-	56
	cdMMP-14	47	48	50	-

Catalytic domains without propeptide or fibronectin domains were used for sequence comparison: cdMMP-2 (Y83-D251), cdMMP-9 (F110-G215; Q391-Y443), cdMMP-12 (G106-G263) and cdMMP-14 (I91-S264). Amino acid sequence analysis was done using MUSCLE (v3.8).

4.3.2 3A2 scFv surface display and mutagenesis library construction

MMP-14 specific inhibitory Fabs were previously isolated from synthetic antibody libraries[16]. Particularly, Fab 3A2 exhibited single digit nM affinity / potency toward cdMMP-14 without significant inhibitory functions on other MMPs at µM concentrations. To achieve surface display, gene of scFv 3A2 (V_H-GS linker-V_L) was assembled and fused to the C-terminus of the a-agglutinin mating protein Aga2p subunit, and the fusion protein was expressed in *Saccharomyces cerevisiae* EBY 100. Surface display of scFv 3A2 wt was examined by FACS after cells were concurrently incubated with 400 nM cdMMP9-sfGFP (superfolder GFP[38]) fusion protein and 400 nM cdMMP14 conjugated with Alexa-647. FACS results indicated that the cells expressing Aga2p-3A2 showed a mean fluorescence signal of 97 on cdMMP14-Alexa647, significantly higher that of host cells EBY 100 without scFv expression at a mean of 4.2 (Figure 4.3), suggesting successful

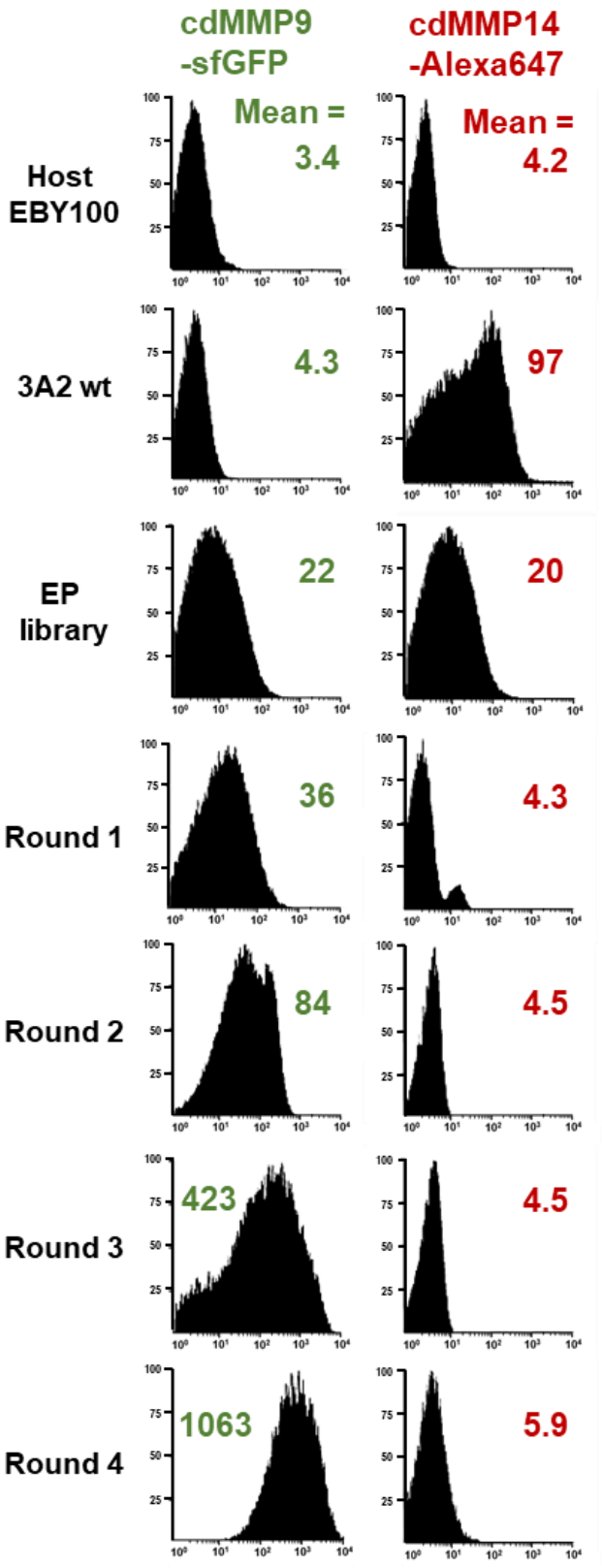

Figure 4.3: FACS analysis of cell populations before and after each round of sorting. For each sample, cells were stained with 400 nM cdMMP9-sfGFP and 400 nM cdMMP14-Alexa647. Cells displaying scFv 3A2 wt and host cells without scFv display were included as controls.

display of scFv 3A2 on yeast cell surface. In addition, the fluorescence signals on cdMMP9-sfGFP showed no difference between 3A2 or the host, indicating that 3A2 was selective without cross reaction with cdMMP-9, consistent with our previous observations[16].

Cloning error-prone mutagenesis product of scFv 3A2 gene into the yeast surface display vector obtained 4.5×10^8 *E. coli* colonies. DNA sequencing 20 randomly picked clones indicated a 2% mutation rate in average. Transforming EBY100 competent cells with scFv 3A2 mutagenesis plasmids generated a library with size of 2×10^7. Library cells were cultured and induced with 4% galactose for scFv expression, and staining with 400 nM cdMMP9-sfGFP and 400 nM cdMMP14-Alexa647. FACS analysis revealed that the histogram of fluorescence signal associated with MMP-9 was widened with a mean of 22 (Figure 4.3). This value was higher than that of host cells or the cells displaying scFv 3A2 (stained in the same manner), implying that the constructed library had the potential to isolate clones with affinities to cdMMP-9.

4.3.3 Competitive FACS for cdMMP-9 positive clones

To isolate scFvs specific to cdMMP-9 without cross reaction with cdMMP-14, library cells were stained with various concentrations of cdMMP9-sfGFP and cdMMP14-Alexa647, and sorted for cdMMP-9^{high} and cdMMP-14^{low} clones by four rounds of FACS. More specifically, in the first round of sorting, 30 million scFv library cells were incubated with 800 nM cdMMP9-sfGFP for 1 hour and the top 5 % (1.5×10^6 cells) of GFP positive cells were selected to enrich for any cdMMP-9

binders. In R2, to achieve selectivity, competitive incubation was introduced by staining library cells with 800 nM cdMMP9-sfGFP and 800 nM cdMMP14-Alexa647 simultaneously. 20 million cells were sorted, and on FACS 2-D histogram, a triangle gate was set to select the top 1% (2×10^5 cells) of cdMMP9-sfGFP positive cells while excluding the ones with a high cdMMP14-Alexa647 signal. To isolate scFv clones with improved binding affinity and selectivity, in R3 and R4, the concentration of cdMMP9-sfGFP was decreased to 400 nM and 200 nM respectively, while keeping cdMMP14-Alexa647 at 800 nM. 20 and 10 million cells were sorted in R3 and R4 with the selection gates tightened to be 1% and 0.5% of cdMMP9-sfGFP^{high} and cdMMP9-Alexa647^{low} population, resulting in collection of 2×10^5 and 5×10^4 cells in R3 and R4. FACS analysis on the post-sort populations for each round (stained with 400 nM cdMMP9-sfGFP and 400 nM cdMMP14-Alexa647) revealed that the fluorescence signals associated with cdMMP-9 were gradually and significantly shifted from a mean of 22 in the error-prone library to 36 after R1, 84 after R2, 423 after R3, and finally reaching 1063 after R4 (Figure 4.3). The cdMMP-9 signal of R4 was dramatically higher than that of 3A2 wt or the library, suggesting FACS indeed enriched MMP-9 binders. Furthermore, the mean fluorescence on cdMMP14-Alexa647 decreased from 20 in the error-prone library to a background level of ~5 in R2-R4. These values were significantly less than the one associated with 3A2 (mean = 97), indicating that the competitive FACS successfully removed MMP-14 binders.

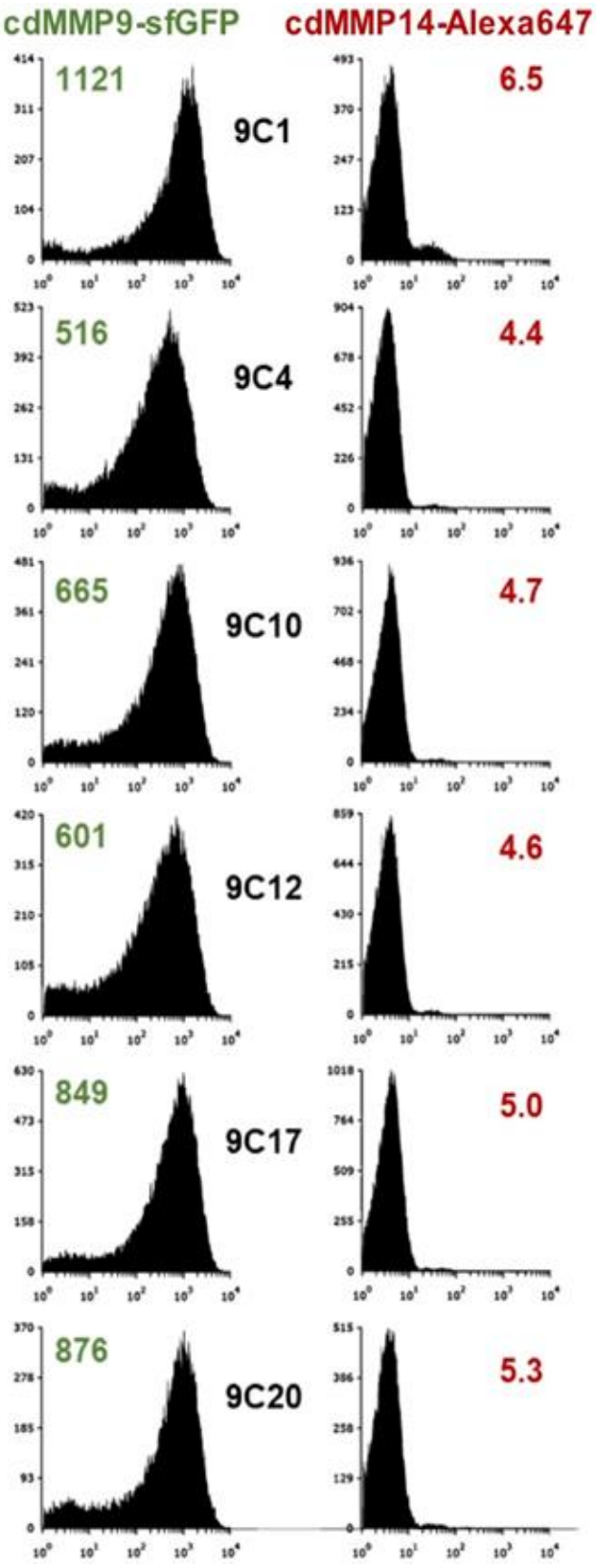

Figure 4.4: Monoclonal FACS analysis. Yeast cells displaying isolated scFv 3A2 mutants were incubated with 400 nM cdMMP9-sfGFP and 400 nM cdMMP14-Alexa647 concurrently and analyzed by FACS. The mean fluorescent signals of MMP9-sfGFP (left) and cdMMP14-Alexa647 (right) were shown for each scFv clone. Host cells without scFv display and cells displaying scFv 3A2 wt were labeled and scanned the same way, and their results are shown in **Figure 4.2**.

4.3.4 Monoclonal screening and identifying MMP-9 specific scFvs

After 4 rounds of screening, 20 randomly picked scFv clones were analyzed by monoclonal FACS. Their Q4 percentages, corresponding to cdMMP9-sfGFP positive cdMMP14-Alexa647 negative, were used to select the clones for further characterizations. Out of this pool of 20 candidates, 6 scFvs had a Q4 percentage greater than 90%, 13 were between 80% and 90%, and the last clone had a Q4 percentage of 72%. As comparison, 3A2 and the error-prone library had Q4 percentages of 0.6 % and 2.7%. More specifically, scFv clone 9C1 showed the highest cdMMP9-sfGFP fluorescence signal mean at 1121, with other 5 clones (9C4, 9C10, 9C12, 9C17 and 9C20) showing signal means in the range of 500-900 (Figure 4.4). These values were dramatically greater than that of 3A2 at 4.3. Furthermore, all the 6 selected clones had their fluorescence signal means on cdMMP14-Alexa647 reduced from 97 of 3A2 to a background level of 4.4 - 6.5. Collectively, monoclonal FACS analysis indicated a clear shift of binding specificity from cdMMP-14 to cdMMP-9 for the isolated clones.

Genes of these 6 scFv clones were recovered for DNA sequencing. Results revealed that all of them were unique with most mutations scatted throughout scFv genes. As their specific mutations shown in Table 4.2, 9C1, 9C10, 9C12, 9C17 and 9C20 scFvs each had 2-4 amino acid mutations on their V_H and V_L. 9C4 as an exception, had 12 mutations, with 5 single-site mutations and a continual mutation at CDR-H3 from $L_{100i}VATPYGR_{100p}$ to RSRPRTGG. DNA sequence analysis revealed this octapeptide mutation was caused by a frameshift given by

a single nucleotide deletion in the middle of CDR-H3. A single nucleotide addition was found close to the C-terminal of the CDR-H3, to bring the open reading frame back.

Table 4.2: Identifying MMP-9 specific scFvs and their binding affinity and inhibition selectivity.

scFv	Mutations		Affinity K_D (nM)	Inhibition potency K_I (nM)				
	VH	VL	cdMMP-9	cdMMP-2	cdMMP-9	cdMMP-12	cdMMP-14	Ratio -2 : -9 : -12 : -14
3A2	-	-	>5000	2600	4600	2100	**40**	65 : 115 : 53 : 1
9C1	A100kV	M4V	29	1600	**120**	1300	2600	13 : 1 : 11 : 22
9C4	W36R/I69K/N76D/L97P/ L_{100i}VATPYGR->RSRPRTGGG	I21N	54	1200	**170**	1600	2000	7 : 1 : 9 : 12
9C10	V37M/I51F/S70G	F83S	34	3700	**100**	1300	1600	37 : 1 : 13 : 16
9C12	M100sI	I75F/P94L	78	1500	**91**	94	1500	16 : 1 : 1 : 16
9C17	V63D	A51T	24	3300	**150**	3400	870	22 : 1 : 23 : 6
9C20	F27I/Y56H/W100eR	-	126	4400	**220**	4400	8500	20 : 1 : 20 : 39

4.3.5 MMP-9 inhibitory scFvs with high selectivity and stability

Isolated scFvs were sub-cloned to *E. coli* periplasmic expression vectors for production. Purified scFvs were tested for their binding affinities on cdMMP-9. As data shown in Table 4.2, 9C1 exhibited a K_D value of 29 nM (k_{on} = 1.3×10^5 M^{-1}s^{-1}, k_{off} = 3.9×10^{-2} s^{-1}), 9C10 had a K_D of 34 nM (k_{on} = 1.5×10^5 M^{-1}s^{-1}, k_{off} = 4.8×10^{-2} s^{-1}) and 9C17 had a K_D of 24 nM (k_{on} = 4.2×10^5 M^{-1}s^{-1}, k_{off} = 1.0×10^{-2} s^{-1}), with the other three scFvs showing K_D between 54 and 130 nM. As expected, 3A2 scFv bound to cdMMP-9 very weakly with a K_D estimated larger than 5 µM. Next, the selectivity of isolated scFvs on cdMMP-9 over a panel of cdMMPs (-2/-12/-14) was tested by FRET inhibition assays using a general MMP substrate. In contrast to 3A2 showing its inhibition selectivity toward cdMMP-14, five isolated scFv mutants (9C1, 9C4, 9C10, 9C17 and 9C20) strongly preferred cdMMP-9 over cdMMP-2/-12/-14 (Figure 4.5). The only exception was 9C12, which bi-specifically inhibited both cdMMP-9 and -12 with a similar strength.

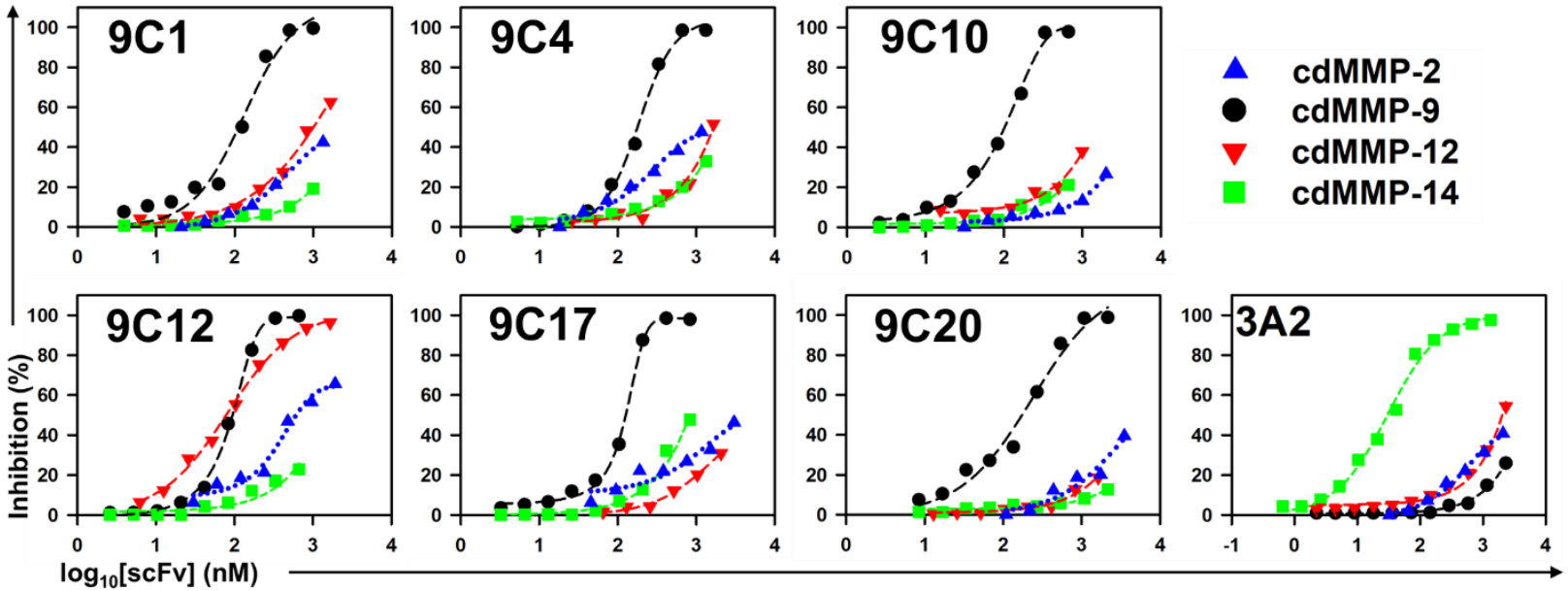

Figure 4.5: Inhibition of isolated scFvs on cdMMP-2/-9/-12/-14. The scFvs were serially diluted and reacted with 10 nM individual cdMMP and 1 µM M2350, a MMP general FRET peptide substrate. 3A2 scFv was tested as control.

Inhibition potency K_Is were further calculated for quantitative comparisons (Table 4.2). For example, 9C1 inhibited cdMMP-9 with a K_I of 120 nM which was 22-fold stronger than its K_I on cdMMP-14 (2.6 µM). Taking K_Is of 3A2 on cdMMP-9/-14 (4.6 µM vs 40 nM) into account, our study converted the inhibition selectivity of cdMMP-9 over -14 from 3A2's 1:155 to 9C1's 22:1, equivalent to a selectivity change of 3400-folds. Furthermore, although only cdMMP-14 was used for the counter selection during our FACS, isolated scFvs also exhibited strong selectivity over other cdMMPs in general which were not used during screening. Taking cdMMP-2, a gelatinase sharing a high degree of homology with cdMMP-9 (Table 4.1) as an example, isolated scFvs showed K_Is of 1.2-4.4 µM, which were in average 19-folds weaker than their K_Is on cdMMP-9. The bi-specificity of 9C12 on cdMMP-9 and -12 was confirmed by quantitative analysis with K_Is of 91 and 94 nM respectively. Notably, 9C12 still retains its selectivity on cdMMP-9 over cdMMP-14 at a ratio of 23:1.

During FACS preparation and sorting, library cells were incubated with cdMMP9-sfGFP. This treatment should bias the selection of proteolytic resistant clones, as the vulnerable scFvs were cleaved by cdMMP-9 and the generated scFv truncations likely lost their binding affinities which could be efficiently removed by FACS. To validate the stability of isolated clones, 1 µM purified scFvs were incubated with 1 µM cdMMP-9 at pH7.5 37^{o}C. After 3 and 12 hours, samples were subjected to SDS-PAGE (Figure 4.6). As densitometric analysis results shown in

Figure 4.6, in average 98% intact scFvs remained after incubation for 3 hours. And after 12 hour incubation, 70% 9C1, 79% 9C4, and 92-99% other four scFvs were remained, indicating a decent proteolytic stability.

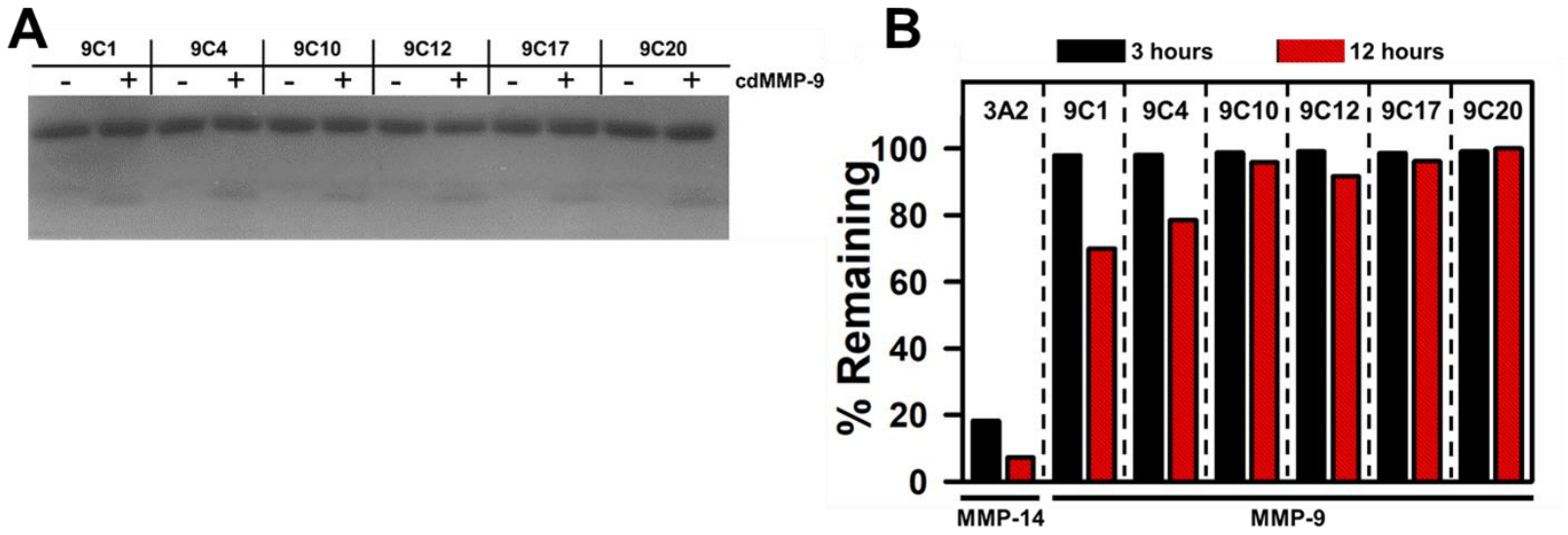

Figure 4.6: **Stability of isolated cdMMP-9 specific scFvs.** (A) 1 µM scFv was reacted with 1 µM cdMMP-9 at 37ºC pH 7.5 for 12 hours. Samples were separated by 12% SDS-PAGE and densiometrically analyzed. (B) The results in the presence or absence of cdMMP-9 were compared to determine % remaining.

4.3.6 Inhibition mechanism of MMP-9 specific scFv inhibitors

To understand their inhibition mechanism, kinetics of cdMMP-9 were measured in the presence of purified scFvs at different concentrations. As the Lineweaver-Burke plots with scFv 9C1 shown in Figure 4.7A, when 9C1 increased its concentration from 125 nM to 500 nM, K_m significantly increased from 1.8 µM to 7.7 µM, while V_{max} remained unchanged (inset table of Figure 4.7A), suggesting that 9C1 behaved as a classical competitive inhibitor. Similar assays were applied to the other 5 scFvs, and their results of unaltered V_{max} with increased K_m at increasing scFv concentrations indicated a competitive inhibition mode for all scFvs (Figure 4.8A).

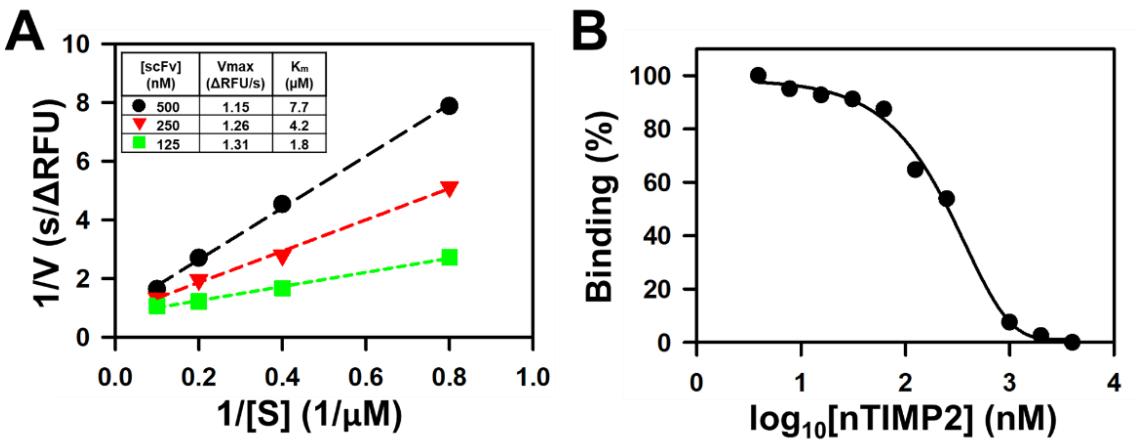

Figure 4.7: Inhibition mechanism of 9C1. (A) The method inhibition of 9C1 was checked by developing Lineweaver-Burke plots of cdMMP-9 in the presence of 3 different concentrations of scFv. Unaltered V_{max} and increased K_m. (B) Competitive ELISA was performed between the scFv and nTIMP-2. The dose dependent response shows that the scFvs are directly competing with the binding site of nTIMP-2 on the catalytic cleft of cdMMP-9.

To distinguish whether these scFv competitive inhibitors targeted at cdMMP-9 substrate-binding cleft or allosterically acted on cdMMP-9, we further performed competitive ELISA with N-terminal domain of TIMP-2. As the native inhibitor of MMP and ADAM family metalloproteinases, nTIMP-2 achieves its inhibitory function by directly binding to the active-site cleft in a manner similar to that of substrate. In the competitive ELISA, mixtures of a fixed amount of scFv with various concentrations of nTIMP2 were incubated on cdMMP-9 surface, then the scFvs captured by the immobilized cdMMP-9 were detected for signal generation. As the sigmoidal curve shows in Figure 4.7B, high concentrations of nTIMP-2 displaced scFv 9C1 on its binding to cdMMP-9, suggesting that the epitope of 9C1 at least partially overlapped with that of nTIMP-2. Analysis of the other 5 scFvs indicated a similar competitive nature with nTIMP-2 on binding to cdMMP-9 (Figure 4.8B). These behaviors of competitive inhibition and an overlapped epitope with nTIMP-2 were also the characteristics of 3A2 wt[16], implying that switching the inhibition selectivity among protease family members by antibody engineering retained the action mode of inhibition.

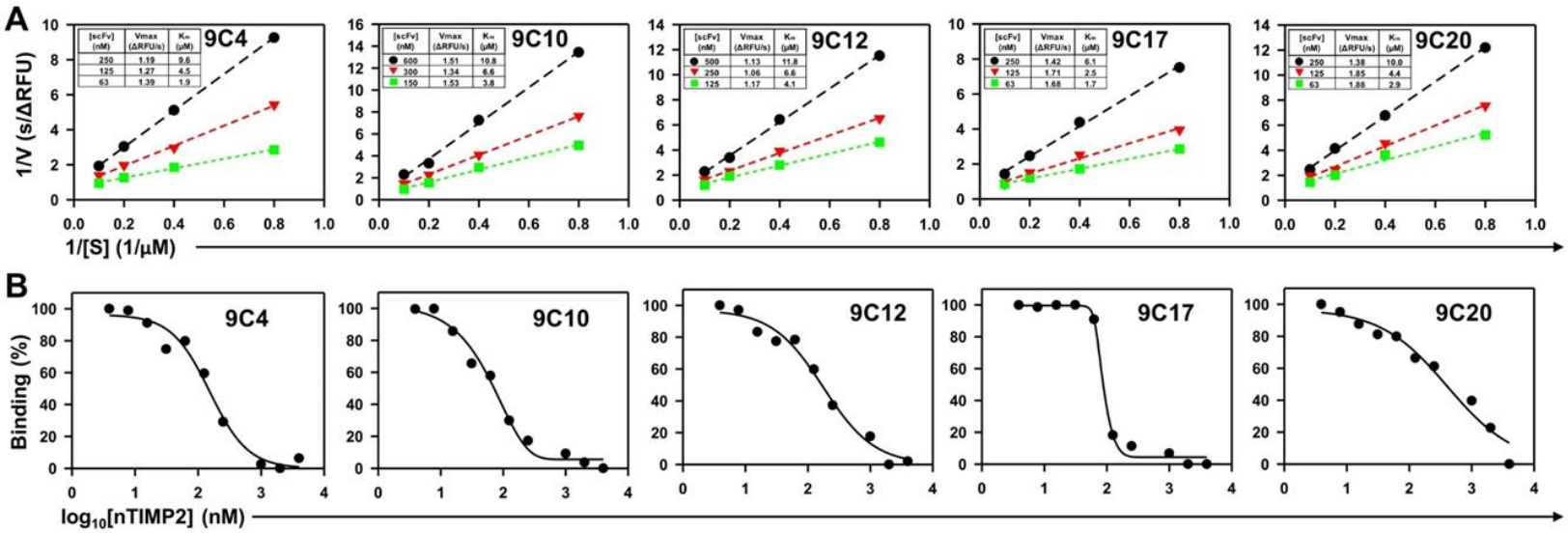

Figure 4.8: Inhibition mechanism of 9C4, 9C10, 9C12, 9C17 and 9C20. (A) Lineweaver-Burke plots of cdMMP-9 in the presence of 125, 250 and 500 nM scFv were developed to determine kcat and Km. (B). Competitive ELISA with nTIMP-2.

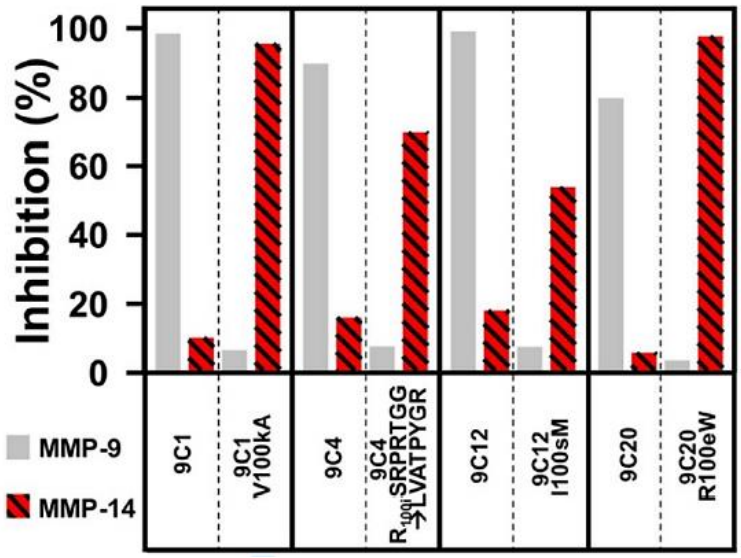

Figure 4.9: Paratope mutation studies of 9C1, 9C4, 9C12, and 9C20. The mutations in CDRH3s were changed back to the amino acids of 3A2, and their inhibitory activities were tested. 500 nM scFvs and 10 nM cdMMP-9/-14 were used. Results were compared with inhibitory activities of 9C1, 9C4, 9C12, and 9C20 under the same assay conditions.

Out of the six isolated MMP-9 specific scFvs, 9C1, 9C4, 9C12 and 9C20 had mutations within their CDR-H3s. We hypothesized that these CDR-H3 mutations provided the key interactions responsible for their inhibition selectivity on MMP-9 over MMP-14. To test this hypothesis, we performed site-directed mutagenesis on paratopes of these four scFvs, by changing these CDR-H3 mutants back to the residues of 3A2 wt, and compared their inhibition activities on 10 nM cdMMP-9 or cdMMP-14. Unlike 9C1 scFv which showed selective inhibition toward cdMMP-9 (98% inhibition) over cdMMP-14 (10% inhibition), 9C1-V_{100k}A scFv reduced its inhibitory activity on cdMMP-9 to 8% while regaining its inhibition of cdMMP-14 to 95%. 9C4, 9C12 and 9C20 paratope mutants showed similar inhibition reduction towards cdMMP-9 with restoration of their activity on

cdMMP-14 (Figure 4.9), however to different degrees. For example, 9C12 $I_{100s}M$ only restored 50% inhibition on cdMMP-14, suggesting that other residues on 9C12 also contributed to the selectivity switch. Collectively, enzyme kinetics, competitive ELISA and paratope mutagenesis studies suggested that isolated MMP-9 specific scFvs were competitive inhibitors having epitope overlapped with TIMP-2 and their key residues in the CDR-H3 region significantly contributed to their inhibition selectivity.

4.3.7 Affinity and selectivity matured cdMMP-14 specific scFvs

After three rounds of FACS with selection on cdMMP14-Alexa647 and counter selection on cdMMP9-sfGFP, three unique scFv clones with MMP-14 specificity were identified (Table 4.3). On monoclonal FACS, clones 14C4, 14C5 and 14C10 showed 5.3-6.6 fold increases of fluorescence signals on cdMMP14-Alexa647 compared to that of 3A2, while retaining low signals on cdMMP9-sfGFP at the background level. Blitz analysis on cdMMP-14 revealed enhanced affinity (K_D) compared to 3A2 scFv's at 25 nM: 14C4 at 5.9 nM ($k_{on} = 4.4\times10^6$ $M^{-1}s^{-1}$, $k_{off} = 2.6\times10^{-2}$ s^{-1}), 14C5 at 1.9 nM ($k_{on} = 2.2\times10^7$ $M^{-1}s^{-1}$, $k_{off} = 4.2\times10^{-2}$ s^{-1}), and 14C10 at 2.2 nM ($k_{on} = 9.8\times10^6$ $M^{-1}s^{-1}$, $k_{off} = 2.2\times10^{-2}$ s^{-1}). Inhibition potency on cdMMP-14 were also improved to 6.1-23 nM from 39 nM of 3A2. Similarly to 3A2, isolated scFvs exhibited weak inhibition on cdMMP-9 even at 1 μM scFv concentration. *In vitro* stability tests by incubating 1 μM scFv and 1 μM cdMMP-14 at 37°C pH 7.5 for 12 hours indicated that isolated mutants had 82-95% intact scFv remaining, in

contrast with 3A2 wt which showed 96% degradation, suggesting significant improvements on proteolytic stability (Figure 4.10).

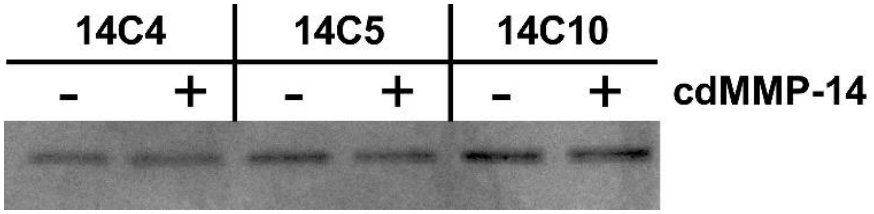

Figure 4.10: Stability of isolated cdMMP-14 specific scFvs. 1 µM scFv was reacted with 1 µM cdMMP-14 at 37ºC pH 7.5 for 12 hours. Samples were separated by 12% SDS-PAGE and densiometrically analyzed. The results in the presence or absence of cdMMP-14 were compared to determine % remaining.

Table 4.3: Biochemical characterizations of scFv 3A2 wt and isolated variants.

scFv	Mutations		Fluorescence signal		Affinity K_D w/ cdMMP-14 (nM)	Inhibition K_I w/ cdMMP-14 (nM)	Inhibition (%) on cdMMP9, [scFv] = 1 µM	Stability – % remaining at 12 h
	VH	VL	cdMMP9-sfGFP	cdMMP14-Alexa647				
3A2	-	-	4.3	97	25	39	12	4
14C4	Y52H/V100jA	-	5.8	520	5.9	23	5.6	88
14C5	T77A	-	5.0	640	1.9	6.1	12	82
14C10	A60V	-	4.3	630	2.2	14	9.3	95

4.4 Discussion and Conclusions

At least 23 MMP family members have been identified in human genome. Although different in their domain arrangements and substrate preferences, the catalytic subunits of all MMPs share high degrees of sequence similarity and protein folding. Many MMPs play important, albeit frequently paradoxical, roles in multiple pathologies including cancer[39], neuropathic pain[28], chronic wounds[40], hypertension[41], and infectious diseases[42]. MMPs together with their native regulatory inhibitors (TIMP1-4) and associated substrates form a complicated proteolytic network. It is an urgent need to develop selective and efficient inhibitors of individual MMPs for both disease therapies and biomedical research. In fact, the lack of highly specific inhibitors is a major hurdle for understanding proteolytic degradome. For instance, during tumor progression, it remains rather elusive when, where, and how much certain MMPs exhibit their proteolytic activities. Using MMP specific mAbs and their dye/radioisotope conjugations as imaging probes will enable us to narrow down the location and the time frame of particular proteolytic action. Specifically blocking individual MMP by inhibitory mAbs will further advance our understandings on the molecular mechanisms by which diseases develop, e.g. how cancer cells migrate through extracellular matrix. One application is to identify the dominate proteases present in tumor microenvironments for the development of prodrug therapeutics, which are activated by the proteolytic cleavage of certain protease(s).

Current methods for protease inhibitory mAb discovery usually start with the isolation of target specific binders, followed by functional screening to identify inhibitors. However, isolated mAbs which specifically bind do not necessarily function as inhibitors. Recent developments on antigen mimicry design[21], antibody library customization[16], and functional selections[17] have greatly advanced the field. This study developed a novel and complementary approach able to switch the inhibition selectivity among closely related protease family members. More specifically, such selectivity change was achieved by performing FACS selection and counterselection simultaneously, a similar method has been recently applied for engineering MMP specific TIMPs[43]. As proof-of-concept, we converted a MMP-14 inhibitor to a panel of MMP-9 inhibitors with 690-4500 fold selectivity shift. Notably, sorting without depletion of MMP-14 positive cells, generated two cell populations on cdMMP14-Alexa647 spectrum: a major peak at 4.2 and a minor peak at 18 (Figure 4.3), suggesting there could be a small fraction of cells binding both MMP-14 and MMP-9. Therefore, this method can be applied to generate not only monospecific inhibitors to single MMPs, but also inhibitors with bi- or oligo-specificity. During FACS, antibody library cells were incubated with MMP(s) for extensive periods of time. As a result, all the isolated antibody mutants exhibited excellent proteolytic stability (Figure 4.6, Figure 4.10). In addition, mAbs inhibiting numerous biomedically important proteases, such as MT-SP1 (membrane type serine protease)[20], plasma kallikrein[26], factor Xa[27], BACE-1 (beta-secretase 1)[44] etc, have been identified. Because most of these proteases are present in families,

the method described here can be applied to convert these isolated inhibitory mAbs to inhibit other members of the associated families.

In summary, the advantages of this study over current methods of protease inhibitory antibody include (1) its straightforwardness without immunization or phage panning; (2) high proteolytic stability of isolated clones; (3) potential to generate mono-, bi-, and oligo-specific inhibitors; (4) its quantitative and high-throughput nature; and (5) other than applications for mAb inhibitors targeting MMPs, we believe the methodology demonstrated here can be particularly useful for many other proteases of biomedical importance.

4.5 References

1. Lopez-Otín, C. & Bond, J.S. Proteases: Multifunctional Enzymes in Life and Disease. *JBC*. **283**, 30433–30437. (2008).

2. Docherty, A.J., Crabbe, T., O'Connell, J.P., Groom, C.R. Proteases as drug targets. *Biochemical Society Symposia.* **70**, 147-161. (2003).

3. Turk, B. Targeting proteases: successes, failures and future prospects. *Nature Reviews Drug Discovery* **5**, 785-799. (2006).

4. Cudic, M., & Fields, G.B. Extracellular Proteases as Targets for Drug Development. *Current Protein & Peptide Science.* **10**: 297-307. (2009).

5. Drag, M. & Salvesen G.S. Emerging principles in protease-based drug discovery. *Nat Rev Drug Discov*. **9**, 690–701. (2010).

6. Koblinski, J.E., Ahram, M., Sloane, B.F. Unraveling the role of proteases in cancer. *Clin Chim Acta*. **291,** 113-35. (2000).

7. Greenbaum, D.C., et al. A role for the protease falcipain 1 in host cell invasion by the human malaria parasite. *Science.* **298**, 2002-2006. (2002).

8. Hopp, C.S., et al. Deletion of the rodent malaria ortholog for falcipain-1 highlights differences between hepatic and blood stage merozoites. *PLoS Pathog*. **1,** e1006586. (2017).

9. McCarty, S., & Percival, S. Proteases and Delayed Wound Healing. *Adv Wound Care*. **2**, 438–447. (2013).

10. Walker, C.P., & Royston, D. Thrombin generation and its inhibition: a review of the scientific basis and mechanism of action of anticoagulant therapies. *Br J Anaesth*. **88,** 848-863. (2002).

11. Kaplan, A.P. Enzymatic pathways in the pathogenesis of hereditary angioedema: The role of C1 inhibitor therapy. *J Allergy Clin Immunol*. **126**, 918-925. (2010).

12. Puente, X.S., Sánchez, L.M., Overall, C.M., López-Otín, C. Human and mouse proteases: a comparative genomic approach. *Nat Rev Genet*. **4**, 544-558. (2003).

13. Tallant, C., Marrero, A., Gomis-Rüth, F.X. Matrix metalloproteinases: fold and function of their catalytic domains. *Biochim Biophys Acta*. **1803**, 20-28. (2010).

14. Lee, M., Fridman, R., Mobashery, S. Extracellular proteases as targets for treatment of cancer metastases. *Chemical Society Reviews* **33**: 401-409. (2004).

15. Overall, C.M., & Kleifeld, O. Towards third generation matrix metalloproteinase inhibitors for cancer therapy. *British Journal of Cancer.* **94**, 941-946. (2006).

16. Nam, D.H., Rodriguez, C., Remacle, A.G., Strongin, A.Y., & Ge, X. Active-site MMP-selective antibody inhibitors discovered from convex paratope synthetic libraries. *Proc Natl Acad Sci U S A*. **113**, 14970–14975. (2016).

17. Nam, D.H., Fang, K., Rodriguez, C., Lopez, T., & Ge, X. Generation of inhibitory monoclonal antibodies targeting matrix metalloproteinase-14 by motif grafting and CDR optimization. *Protein Engineering, Design & Selection*. **30**, 113–118. (2017).

18. Lopez, T., Nam, D.H., Kaihara, E., Mustafa, Z., Ge, X. Identification of highly selective mmp-14 inhibitory fabs by deep sequencing. *Biotechnology and Bioengineering*, **114**, 1140–1150. (2017).

19. Devy, L. Selective inhibition of matrix metalloproteinase-14 blocks tumor growth, invasion, and angiogenesis. *Cancer Res*. **69**, 1517-1526. (2009).

20. Schneider, E.L. A reverse binding motif that contributes to specific protease inhibition by antibodies. *J Mol Biol*. **415**, 699-715. (2012).

21. Sela-Passwell, N. Antibodies targeting the catalytic zinc complex of activated matrix metalloproteinases show therapeutic potential. *Nat Med*. **18**, 143-147. (2011).

22. Genst, E., at el. Molecular basis for the preferential cleft recognition by dromedary heavy-chain antibodies. *Proc Natl Acad Sci U S A*. **103**, 4586-4591. (2006).

23. Farady, C.J., Sun, J., Darragh, M.R., Miller, S.M., Craik, C.S. The mechanism of inhibition of antibody-based inhibitors of membrane-type serine protease 1 (MT-SP1). *J Mol Biol*. **369**, 1041-1051. (2007).

24. Wu, Y., et al. Structural insight into distinct mechanisms of protease inhibition by antibodies. *Proc Natl Acad Sci U S A*. **104**, 19784–19789. (2007).

25. Ling, B., et al. A novel immunotherapy targeting MMP-14 limits hypoxia, immune suppression and metastasis in triple-negative breast cancer models. *Oncotarget.* **8**, 58372–58385. (2017).

26. Kenniston, J.A., et al. Inhibition of Plasma Kallikrein by a Highly Specific Active Site Blocking Antibody. *J Biol Chem*. **289**, 23596-23608. (2014).

27. David, T., et al. Factor XIa–specific IgG and a reversal agent to probe factor XI function in thrombosis and hemostasis. *Sci Transl Med*. **8**, 353ra112. (2016).

28. Ji, R.R., Xu, Z.Z., Gao, Y.J. Emerging targets in neuroinflammation-driven chronic pain. *Nat Rev Drug Discov*. **13**, 533-48. (2014).

29. Panda, S., Zhang, J., Yang, L., Anand, G., Ding, J. Molecular interaction between natural IgG and ficolin – mechanistic insights on adaptive-innate immune crosstalk. *Scientific Reports*. **4,** 10.1038/srep03675. (2014).

30. Levina, M., Weiss, G.A. Optimizing the affinity and specificity of proteins with molecular display. *Mol. BioSyst*. **2**: 49-57. (2016).

31. Eaton, B., Gold, L., Zichi, D. Let's get specific: the relationship between specificity and affinity. *Chemistry & Biology*. **2**, 633-638. (1995).

32. Yin, J., Beuscher, A., Andryski, S., Stevens, R., Schultz, P. Structural Plasticity and the Evolution of Antibody Affinity and Specificity. *J. Mol. Biol*. **330**, 651–656. (2003).

33. Nam, D., Ge, X. Direct production of functional matrix metalloproteinase -14 without refolding or activation and its application for *in vitro* inhibition assays. *Biotechnol. Bioeng*. **113**, 717-723. (2015).

34. Hayhurst, A., et al. Isolation and expression of recombinant antibody fragments to the biological warfare pathogen *Brucella melitensis*. *Journal of Immunological Methods*. **276**, 185–196. (2003).

35. Brandt, R.B., Laux, J.E., Yates, S.W. Calculation of inhibitor K_i and inhibitor type from the concentration of inhibitor for 50% inhibition for Michaelis–Menten enzymes. *Biochemical Medicine and Metabolic Biology*. **37**, 344–349. (1987).

36. Goldenzweig, A., et al. Automated Structure- and Sequence-Based Design of Proteins for High Bacterial Expression and Stability. *Mol Cell*. **63**, 337–346. (2016).

37. Lee, K.B., et al. Direct expression of active human tissue inhibitors of metalloproteinases by periplasmic secretion in Escherichia coli. *Microbial Cell Factory*. **16**, 73. (2017).

38. Pédelacq, J.D., Cabantous, S., Tran, T., Terwilliger, T.C, Waldo, G.S. Engineering and characterization of a superfolder green fluorescent protein. *Nature Biotechnology*. **24**, 79–88. (2006).

39. Gialeli, C., Theocharis, A.D., Karamanos, N.K. Roles of matrix metalloproteinases in cancer progression and their pharmacological targeting. *FEBS Journal*. **278**, 16-27. (2011).

40. Cook, H., Stephens, P., Davies, K.J., Harding, K.G., Thomas, D.W. Defective extracellular matrix reorganization by chronic wound fibroblasts is associated with alterations in TIMP-1, TIMP-2, and MMP-2 activity. *Journal of Investigative Dermatology*. **11,** 225-233. (2000).

41. Castro, M.M., & Tanus-Santos, J.E. Inhibition of Matrix Metalloproteinases (MMPs) as a Potential Strategy to Ameliorate Hypertension-Induced Cardiovascular Alterations. *Current Drug Targets*. **14**, 335-343. (2013).

42. Elkington, P.T.G., O'Kane, C.M., Friedland, J.S. The paradox of matrix metalloproteinases in infectious disease. *Clinical and Experimental Immunology*. **142**, 12-20. (2005).

43. Shirian, J., et al. Converting a broad matrix metalloproteinase family inhibitor into a specific inhibitor of MMP-9 and MMP-14. *FEBS Lett*. **592**, 1122-1134. (2018).

44. Atwal, J.K., et al. A therapeutic antibody targeting BACE1 inhibits amyloid-β production *in vivo*. *Science Translational Medicine*. **3**, 84ra43. (2011).

Chapter 5: Discovery of Protease Inhibitory Antibodies by Genetic Selection

Abstract:

In recent years monoclonal antibodies have risen in popularity as therapeutic treatments. The inherent specificity of antibodies results in a reduction of cross reactivity, and subsequently, side effects. One of the major bottlenecks in the development of a therapeutic antibody is discovery. Often large synthetic libraries undergo several rounds of binding based selection, ie phage panning, to enrich clones targeting a specific protease of interest, however, the resulting antibodies still need to be screened for function. In this study we develop a method of genetic selection based solely on inhibitory function by utilizing the interactions of a Fab, a protease of interest, and a modified β-lactamase in the periplasmic space of E. coli. Inhibitory antibodies will prevent the protease from cleaving the modified β-lactamase thereby allowing the cell to survive in the presence of ampicillin. Using this technique we were able to screen large synthetic antibody libraries against four classes of proteases: catalytic domain of matrix-metalloprotease – 9 (cdMMP-9), cdMMP-14, aspartic acid protease β-secretase (BACE1), autophagic serine protease (Alp2), and cysteine protease cathepsin B (CTSB). A panel of inhibitory antibodies against all five targets was discovered and the top candidates were selected for in depth analysis. Specifically, antibodies L13, 2B4, B1A4, r4A1, and CTSBA3 were shown to be potent inhibitors of MMP-9, MMP-14, BACE1, Alp2, and CTSB respectively. Additionally, all of the antibodies tested for their ability to inhibit a protease from cleaving its natural substrate were successful to some

degree. L13 was further proven to be effective in mouse models of neuropathic pain, and r4A1 was used to target lung tissues infected with fungus expressing Alp2. This comprehensive analysis shows the viability of this technique for the discovery of protease inhibitory antibodies with therapeutic potential.

5.1 Introduction

In the early stages of protease discovery it was believed that proteases were simple proteins responsible for protein catabolism and the generation of amino acids[1]. In more recent years it has been discovered that proteases are in fact a large family of enzymes responsible for influencing a huge number of biological processes. Proteases exist in a delicate balance to maintain homeostasis and their dysregulation is implicated in several diseases such as cancer, inflammation, osteoporosis, neuropathic pain, and neurodegenerative diseases[2,3,4,5,6,7,8,9]. There are five main classes of proteases: serine, cysteine, threonine, aspartyl, and metalloproteases (Figure 1.1).

Currently, there are many small molecules capable of effectively inhibiting a variety of therapeutically relevant proteases. However, in clinical trial many of these protease inhibiting small molecules have displayed severe side effects due to lack of specificity[10,11]. Conversely, monoclonal antibodies have high inherent specificity making them an attractive alternative to small molecule inhibition[12,13]. Currently, some of the most popular methods of antibody discovery are phage display[14,15,16], yeast display[17], and hybridoma technologies[18]. However, these techniques are largely limited to binding and not inhibitory antibodies.

Previously, in order to recover more potential inhibitors we used next generation sequencing to obtain data on competitively eluted phage panned libraries[19]. This enabled us to isolate several more inhibitory antibodies from a phage derived library, however, enrichment does not necessarily correlate with inhibitory function and several of the most enriched clones were not inhibitory[19]. Screening and function testing is the most labor intensive portion of the entire antibody discovery process[18], and the lack of a high-throughput function based screening method is one of the biggest challenges to overcome when developing new antibodies against proteases for therapeutic use.

In order to address this difficulty we developed a rapid selection system based on the interactions of an antibody, modified β-Lactamase, and an active protease of interest (Figure 5.1). In order to use this technique all three components must be present in the same location. β-Lactamase is naturally expressed in the periplasmic space of E. coli in order to process the β-Lactam ring in the penicillin class of antibiotics resulting in antibiotic resistance[20]. Antibody Fabs are also routinely expressed in the periplasmic space of E. coli using the sec secretion system. Finally, in addition to active expression of Fabs in the periplasmic space, many proteases have been recently discovered to be actively expressed in the periplasmic space of E. coli[21]. The ability for all three components for selection to be present and active make the periplasmic space of E. coli the perfect locale for developing a genetic selection screening technique.

The ability to rapidly screen an entire population makes genetic selection one of the most powerful tools for the selection of desirable traits and has been used in a variety of different applications[22,23,24,25]. In particular, genetic selection has the ability to reduce a population to only individuals that contain a select trait necessary for survival. In this study we discuss the introduction of protease cleavable peptide linkers (CPLs) into β-Lactamase for the selection of inhibitory antibodies against (1) the catalytic domain of matrix-metalloprotease – 14 (cdMMP-14) for cancer treatment, (2) cdMMP-9 for neuropathic pain, (3) autophagic serine protease (Alp2) for aspergillosis infections, (4) aspartic acid protease β-secretase (BACE1) for Alzheimer's disease, and (5) cysteine protease cathepsin B (CTSB) for neurodegenerative disorders[1,6], cancer[26], and Chagas' disease[7] (Figure 1.2). These proteases were chosen to cover four of the major classes of proteases.

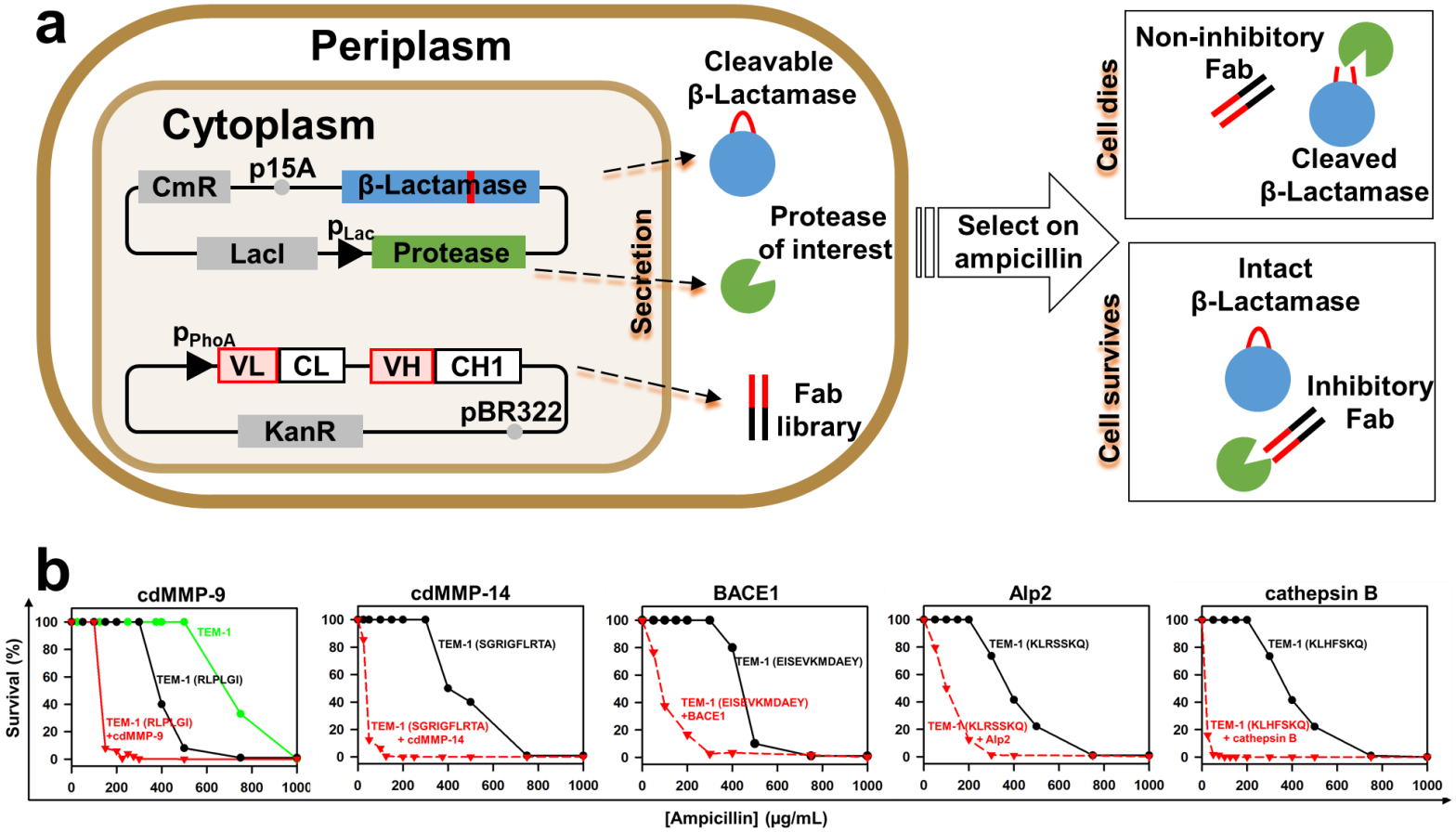

Figure 5.1: a) **Cartoon depicting the scheme of the genetic selection** technique based on the co-expression of an Fab (black and red), a protease of interest (green), and a modified β-lactamase (blue with cleavable peptide linker shown in red). b) Introduction of the modification to the wt β-lactamase (green) resulted in a decrease in a functionality of the β-lactamase even in the absence of protease (solid black). The introduction of the protease resulted in a dramatic decrease in survival (dashed red). This allows the identification of ampicillin selection windows.

5.2 Materials and Methods

5.2.1 Development of protease cleavage reporters

Plasmid pHP153 carrying β-lactamase TEM-1 gene was PCR amplified to introduce unique *Xba*I and *Nco*I sites between G196 and E197 of TEM-1. The PCR product was ligated with 5' phosphorylated oligonucleotide assembled adapters encoding protease specific cleavable peptide sequences flanked with serine-glycine linkers (GSG[peptide]SGG) to obtain modified TEM-1s. Genes encoding catalytic domain of human MMP-9 (cdMMP-9), human cdMMP-14, human β-secretase 1 extracellular domain (BACE1), *Aspergillus fumigatus* autophagic serine protease 2 (Alp2) and human cathepsin B catalytic domain (CTSB) were PCR assembled and cloned into *Sfi*I sites on pMopac16 carrying a p15A origin[27] and a pelB leader peptide to obtain periplasmic expression plasmids. Modified TEM-1 genes were then sub-cloned into these protease expression plasmids using *Nsi*I and *Nhe*I sites to generate associated reporter plasmids. All cloned plasmids were confirmed by DNA sequencing. β-lactam ring hydrolysis activities of modified TEM-1s in the absence or presence of associated proteases were assayed by culturing transformed *E. coli* BL21 cells at serial dilutions on 2×YT agar plates containing 34 μg/mL chloramphenicol, 50 μg/mL kanamycin, 0-0.1 mM IPTG, 0-2% glucose and 0-1000 μg/mL ampicillin at 30 ^{o}C for 16 hours. The ratios of colony numbers on ampicillin plates over on ampicillin-free plates were used to determine survival rates and the optimal conditions for selecting inhibitors for each protease target.

5.2.2 Selection of protease inhibitory antibodies

Fab fragments of antibody libraries were PCR amplified from previously designed libraries containing either regular length[28] or ultra-long CDR-H3s[29] with a hexahistidine tag at C-terminal of VH and cloned into pHPK (kanR, ColE1 origin, phoA promoter and STII leader peptide). *E. coli* Jude-I electrocompetent cells were transformed for pHPK-Fab library plasmid production. 20 randomly picked colonies from both libraries were sequenced for quality and diversity tests. Electrocompetent cells of BL21 carrying the reporter plasmid for each protease were transformed with 100 μg pHPK-Fab. Transformed cells were cultured on 2×YT agar plates of the pre-determined selection conditions optimal for each protease at 30 ^{o}C for 12 hours followed by 37 ^{o}C for 5 hours. Small aliquots of transformed cells were also serially diluted and cultured on 2×YT agar plates supplemented with 50 μg/mL kanamycin and 34 μg/mL chloramphenicol for library size determination. Colonies surviving the initial selection were individually inoculated in the 2×YT selection media with a higher ampicillin concentration for secondary screening. Well-grown clones were selected for Fab plasmid extraction and V_H and V_L DNA sequencing.

5.2.3 Production of isolated antibodies and targeted proteases

Fab expression plasmids of isolated antibodies were transformed into BL21 cells for periplasmic production by culturing in 2×YT media at 30^{o}C for 12 hours. Fabs were purified using Ni-NTA agarose (Qiagen) from periplasmic fractions

prepared by lysozyme and osmotic shock[27]. IgGs were produced using HEK293F (ThermoFisher Scientific) as previously described[30]. Purified Fabs and IgGs were dialyzed at 4°C against the following assay buffers: 50 mM Tris-HCl pH 7.5, 150 mM NaCl, 5 mM $CaCl_2$, 0.4 mM $ZnCl_2$ for cdMMP-9; 50 mM Tris-HCl pH 7.5, 150 mM NaCl, 5 mM $CaCl_2$, 0.1 mM $ZnCl_2$ for cdMMP-14; PBS pH 7.5 for Alp2 and for cathepsin B; and 20 mM HEPES, 125 mM NaCl pH 5.0 for BACE1. Dialyzed antibody samples were concentrated by 10 kDa MWCO ultrafiltration (Amicon), and their purity and concentration were determined by SDS-PAGE and UV spectrophotometer (BioTek).

cdMMP-14 and cdMMP-9 were produced in their active format in the periplasmic space of *E. coli* without refolding or activation as previously described[27]. Similarly, Alp2 and CTSB were periplasmically produced and purified using Ni-NTA agarose (Qiagen). BACE1-CH1-Fc fusion was produced by HEK293F using pcDNA-intron-SPL-BACE1-CH1-Fc-WPRE containing human IgG_1 Fc domain with associated signal peptides and Woodchuck hepatitis virus posttranscriptional regulatory elements to enhance the expression[31]. Cultured media was clarified by centrifugation and 0.45 µm filtration, and BACE1-Fc was purified by protein A affinity chromatography (GenScript).

5.2.4 Biochemical characterizations of isolated antibodies

Binding kinetics of produced antibodies towards associated protease targets were analyzed by biolayer interferometry BLItz (ForteBio). Biotinylated

protease was loaded onto a streptavidin biosensor and incubated in its respective assay buffer for 30 sec to establish baselines. Purified Fabs in their antigen's respective assay buffer were then introduced at a variety of concentrations and their association to immobilized Ag was monitored for 1 min then allowed to dissociate in protease specific assay buffer for 2 min. Determined k_{on} and k_{off} were used to calculate K_D values. Fabs binding to the sensor in absence of protease was monitored as negative controls. For IgGs, protein A sensors were used and protease bindings without IgG were checked as negative controls. Binding affinities of Fabs were also determined with direct ELISA using biotinylated proteases on streptavidin coated plate (Thermo Scientific) blocked with biotin-BSA. Competitive ELISA on immobilized cdMMP-9/-14 in the presence of 0.5 nM - 1 µM nTIMP-2 was used to determine the binding epitopes. *In vitro* stability of Fabs in complex with their respective protease was tested by incubating 1 µM Fab with 1 µM protease in the protease's specific reaction buffer for 12 hours and the samples were analyzed by SDS-PAGE.

For inhibition tests, 1 µM Fabs were 2-fold serially diluted into protease specific assay buffer and incubated with 1-10 nM proteases for 30 min at room temperature. The kinetic measurements were started with the addition of 1 µM FRET peptide substrate (M-2350, Bachem, for MMP-9/14; M-2420, Bachem, for BACE1; MCA-KLRSSKQ-LYS(DNP), Biomatik, for Alp2; and M-2595, Bachem, for CTSB) and the fluorescence was monitored with excitation and emission wavelengths at 325 and 392 nm (except M-2595 monitored at 320 and 420 nm)

using a fluorescence plate reader (BioTek). Inhibition percentages at given concentrations were calculated by comparing the initial slopes in the presence or absence of inhibitor. IC_{50} was determined as the concentration that achieved 50% inhibition. V_{max} and K_m at various concentrations of Fabs were measured to determine inhibition type. FRET inhibition assays were also used for selectivity tests of isolated Fabs with relevant proteases.

For amyloid precursor protein (APP) degradation studies, the Swedish mutation of APP was cloned to the C-terminal of MBP for *E. coli* expression and purification. 5 μM purified MBP-APP was incubated with 1 μM BACE1 in the absence or presence of 1 μM IgG B1A4 in BACE1 assay buffer at 37 ^{o}C for 24 h. Samples were taken hourly and analyzed by SDS-PAGE under non-reducing conditions. Similarly, 1 μM cdMMP-9 was incubated with 300 μg/mL rat collagen I (Corning) in the absence or presence of 1 μM Fabs in MMP-9 assay buffer at 37 ^{o}C for 24 h for hydrolysis analysis.

FITC-conjugated collagen type I at 10 μg/mL with 2 μM Alp 2 in PBS was incubated incubated at room temperature overnight in the presence or absence of 10 μM r4A1. The reaction solution was centrifuged at 3,000 g for 10 min and the fluorescence of the supernatant was measured at Ex/Em=490/520 nm.

5.2.5 Animal test, fungal imaging, APP cell assays

5.2.5.1 Animals

Wild-type CD1 (male and female, 8-10 weeks old) were purchased from Charles River Laboratories and housed at the vivarium animal facility of Duke University Medical Center. The protocol of animal experiments was approved by the Animal Care Committee of Duke University Medical Center.

5.2.5.2 Drugs and Administration

Intrathecal injection was performed as described previously[32], mice were anesthetized with isoflurane and a spinal cord puncture was performed between the L5 and L6 level to deliver drugs (10 μL) using a 30G needle.

5.2.5.3 Animal Model

Chronic constriction injury (CCI) was performed as described previously[32,33,34]. Briefly, the left sciatic nerve was exposed at mid-thigh level under isoflurane anesthesia, and three loose silk ligatures (6-0 suture) approximately 1 mm apart were made around the sciatic nerve and the incision was closed with non-absorbable silk suture (5-0). To produce chemotherapy-associated neuropathic pain, paclitaxel (PAX, 2 mg/kg, i.p.) was injected at day 0, 2, 4, and 6[35,34].

5.2.5.4 Behavioral Analysis

All behavioral tests were performed in boxes on an elevated metal mesh floor under stable room temperature and humidity. Mice were habituated to the environment for at least 2 days before the experiments. To assess mechanical allodynia, the plantar surface of left hind-paw was stimulated using a series of von Frey fibers with logarithmically increasing stiffness (0.02-2.56 gram, Stoelting), presented perpendicularly to the central plantar surface. 50% paw withdrawal threshold was determined following Dixon's up-down method. The frequency response was measured by stimulating the hind-paw with a 0.4 gram von Frey hair for ten times and the percentage withdrawal response was calculated as frequency. To assess cold allodynia, two acetone applications (20 µl each) were gently applied to the hindpaw bottom using a pipette and the responses to acetone were scored: 0, no response; 1, quick withdrawal, paw stamping or flicking; 2, prolonged withdrawal or repeated flicking of the paw; 3, repeated paw flicking and licking[36,37]. All the behavioral tests were performed in a blinded manner.

5.3 Results

All five of the proteases were able to be actively expressed in the periplasmic space of E. coli making them ideal candidates for genetic selection. cdMMP-9, cdMMP-14, Alp2, and CTSB were able to be actively expressed in mg / L concentrations from the periplasmic space of E. coli. BACE1 was able to be actively expressed in µg / L concentrations, however, in order to obtain enough protein for multiple studies and to improve the activity via glycosylation, BACE1

was produced and purified using HEK 293F mammalian cells. Fabs were highly expressed in the periplasmic space of E. coli and purified in mg / L concentrations for further studies against their respective antigen.

Following confirmation of the target protease, a reporter plasmid unique to each protease had to be cloned. This reporter plasmid contained the antigen of interest with a pelB leader peptide for expression in the periplasmic space of E. coli as well as a modified TEM-1 gene containing a protease specific CPL between G196 and E197 of the native TEM-1 gene. This location lies between the two functional domains of β-Lactamase and disruption to this area of the protein will result in loss of functionality. Additionally, the CPL is located on a surface loop which is easily accessible to periplasmic proteins. As such, care also must be taken to avoid peptides that are cleaved by endogenous proteases in the periplasmic space of E. coli. The CPL in the flexible loop must be short enough to remain in the loop conformation and avoid secondary structure such as helices and sheets which will often prevent the protease from properly cleaving the linker.

The use of β-Lactamase in genetic selection is a new technique that has recently been used to isolate aggregating proteins, however, it is difficult to incorporate a selection marker into an existing protein while maintaining the protein's native function[25,38,39]. Engineering β-Lactamase is difficult in particular because if modifications interfere with the native function then the cell will die when exposed to antibiotics (Figure 5.1a). This delicate balance between cell death in the presence and absence of protease generates survival windows that allow for

determination of optimal ampicillin concentration for selection (Figure 5.1b). cdMMP-9, cdMMP-14, BACE1, Alp2, and CTSB CPLs: RLPLGI, SGRIGFLRTA, EISEVKMDAEY, KLRSSKQ, and KLHFSKQ respectively were able to be engineered into β-Lactamase without much loss of function (Figure 5.1b). SGRIGFLRTA is a broad substrate for MMPs and was therefore used for selection of antibodies against both cdMMP-9 and cdMMP-14. 300 µg/mL ampicillin with 0.1 mM IPTG yielded a high survival of cells in the absence of protease while resulting in nearly complete death in the presence of protease; therefore, these concentrations were chosen for the initial selection conditions with the exception of cdMMP-14 (Table 5.4).

Selection using a synthetic antibody library containing a long CDR-H3 against cdMMP-9 under these conditions resulted in 37 candidates from the SGRIGFLRTA CPL and 22 from the RLPLGI CPL from a potential of 6.7×10^8 or 6.2×10^8 transformants respectively (Table 5.4). To narrow down the candidates, individual clones were re-selected in 400 µg/mL ampicillin with 0.1 mM IPTG which resulted in 5 unique clones from the SGRIGFLRTA CPL and 8 from the RLPLGI CPL. These clones were expressed and 11 out of the 13 clones were found to be inhibitory with potencies ranging from >1 µM to 100 nM and the 2 clones not showing inhibition in the FRET assay came from the selection with SGRIGFLRTA. The top 3 clones: H3, H4 (RLPLGI) and L13 (SGRIGFLRTA) had potencies of 97 nM, 103 nM and 247 nM respectively and were chosen for further characterization (Figure 5.2, Figure 5.6).

Protease	MMP-9	MMP-14	BACE1		Alp2	cathepsin B
Library						
CDR-H3 length (aa)	23-27	23-27	23-27	5-21	5-21	5-21
Size	6.2×10^8	8.6×10^8	7.1×10^8	1.8×10^8	2.9×10^8	1.5×10^8
Initial selection						
[Amp] (µg/mL)	300	200	300	300	300	300
[IPTG] (mM)	0.1	-	0.1	0.1	0.1	0.1
[glucose] (%)	-	2	-	-	-	-
Temp (°C)	30	30	30	30	30	30
# of clones selected	59	190	24	87	43	122
Second selection						
[Amp] (µg/mL)	400	300	400	400	500	400
[IPTG] (mM)	0.1	-	0.1	0.1	0.1	0.1
[glucose] (%)	-	-	-	-	-	-
Temp (°C)	30	30	30	30	30	30
# of clones selected	15	161	21	52	29	6 [note]
Sequenced	15	40	10	8	10	6
Correct sequences	13	39	5	6	8	3
Fabs produced	13	6	5	6	8	3
Binders	13	6	5	6	8	3
Inhibitors	11	6	5	6	6	3

Table 5.4: Genetic selection statistics. Initial kanamycin library was developed to have a diversity of 1.1×10^9, during selection however the library size screened was on the order of 10^8. The initial selection conditions were chosen to dramatically decrease the diversity of the selected library and result in a number of clones manageable for monoclonal second round screening. Because the conditions were more stringent in the second round only several clones were able to survive. Of these clones a portion were selected for sequencing and expression. Finally, the purified antibodies were tested for binding and inhibitory activity, of which, the vast majority showed both.

Protease Type	Target (indication)	Cleavable Peptide on Bla	Fab †	CDR-H3 (length)	Binding Affinity K_D (nM)	Inhibition Potency K_I (nM)
Metallo-	MMP-9 (neuropathic pain)	RLPLGI	H3	RFEPGLLKRNKRWISYTLCEAGYGMDY (27)	82 (71) ‡	97 (100) ‡
			H4	SSLAWAQDRVYKPVEAMTWAYGMDY (25)	6.9	100
			L13	KYMVFGTRMGWVEHTDFAGQGYYAMDY (27)	120 (53) ‡	250 (220) ‡
			H25	CKLYTSYMIPVGSDSVNRCMSSYGMDY (27)	430	510
	MMP-14 (cancer)	SGRIGFLRTA	2B4	SDSAVYSVRRMGSSGLAAYAMDY (23)	62	110
			2B12	DCCSCVFSQSAGITLACVYVMDY (23)	76	130
			1A5	LDFLMRDIYYDLGGGALGWLIKYAMDY (27)	57	170
			2B10	QLFACWRQSILTPPLLSAMMMGYAMDY (27)	46	250
			2D9	GVTRFTNDASVGQVWAGAYGMDY (23)	260	260
			2A6	VVRMLPVRCIPRCIKTTLPLYGMDY (25)	130	480
Aspartic	BACE-1 (Alzheimer's)	EISEVKMDAEY	B3B12	YICGHRWRDFDMWRARTGVNYAMDY (25)	15 (10) ‡	27 (20) ‡
			B1A4	HYYVSVGSGIDY (12)	37 (21) ‡	55 (45) ‡
			B2B5	WHGYPPGYSYYSSFSSSGFDY (21)	130	97
			B2B2	YWGYYAWFGSXPWAYGAFDY (20)	52	110
			B2B3	SASGIDY (7)	100	130
			B2B9	SSSSYYYGMDY (11)	110	150
			B2B6	DNSICVLTQKEVDTKFLVGQHSYVMDY (27)	54	160
			B1B3	ERSSCPVGWRDSRFGADGYGLEY (23)	31	260
Serine	Alp2 (aspergillosis)	KLRSSKQ	A4A1	FGSWSYAIDY (10)	11	15
			A4A2	KTSDQYLLVGGSFFKLRDCCYVMDY (25)	110	240
			A4A7	GRSPGPYAVCGNLFRSVSYGMDY (23)	420	360
Cysteine	Cathepsin B (cacner)	KLHFSKQ	CBA3	GFAWSPGLDY (10)	120	140
			CBA2	YGYPGGYHFWGWWSSPYAFDY (21)	190	190
			CBA1	GGGSWSAMDY (10)	290	250

Note: † Only Fabs with inhibition potency at 500 nM or greater are shown. For each protease target, Fabs are ranked by potency.
‡ Affinity and potency values of associated IgGs are shown in parentheses.

Table 5.5: **For all four classes of proteases many inhibitory antibodies were able to be discovered** with binding affinities and potencies ranging from 15 nM – 500 nM.

L13 and H3 were further investigated to determine their binding affinity using both ELISA and Blitz. Both methods of characterization were in excellent agreement and showed an affinity of 120 nM for L13 and 82 nM for H3. Using the ForteBio Blitz we obtained k_{on} values for L13 and H3 of 8.30 x 10^4 (1/Ms) and 6.17 x 10^4 (1/Ms) respectively and k_{off} values of 1.00 x 10^{-2} (1/s) and 4.98 x 10^{-3} (1/s) respectively (Figure 5.4). To investigate the method of inhibition by the cdMMP-9 antibodies Lineweaver-Burke plots were developed for Fabs H3, L13 (Figure 5.2a),

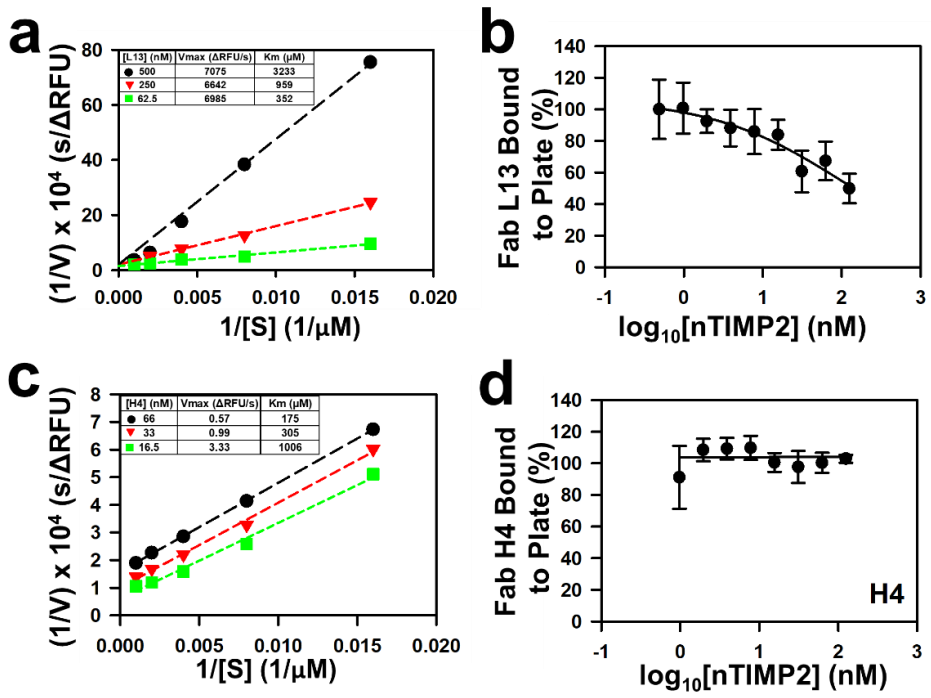

Figure 5.2: **Determination of mechanism of inhibition** a) Lineweaver–Burke plots of cdMMP-9 at the presence of 62.5, 250, 500 nM Fab L13. Unaltered V_{max} and increased K_m with increasing Fab concentrations indicate a competitive inhibition mode. b) Competitive ELISA testing L13's method of inhibition. MMP-9 was bound to an ELISA plate, Fab L13 was then bound to the MMP-9, and finally, nTIMP-2 was added at gradient dilutions to compete off the Fab. L13 showed competition with nTIMP-2. c) Lineweaver–Burke plots of cdMMP-9 at the presence of 16.5, 33, 66 nM Fab H3. Increasing V_{max} and increased K_m with increasing Fab concentrations indicate an uncompetitive inhibition mode. d) Competitive ELISA testing H3's method of inhibition. H3 was not competitive with nTIMP-2.

and H4 (Figure 5.2c). H3 and L13 both had competitive inhibition while H4 was non-competitive with the FRET substrate.

In order to check the binding epitope, a competitive ELISA with TIMP2 was performed on L13, H4 (Figure 5.2b/d). This ELISA indicated that TIMP2 was able to compete off L13 while H4 remained bound to the immobilized MMP-9. L13 was then tested for its specificity towards cdMMP-9 by FRET assays using cdMMP-2, 12, and 14, no cross reactivity was observed (Figure 5.5). Additionally, L13 was tested for its stability in complex with the antigen. One of the beneficial aspects of having a survival based selection is that the inhibitory function must be maintained over the entire course of the growth phase, after 12 hours L13 93% remained intact demonstrating excellent proteolytic stability (Figure 5.3).

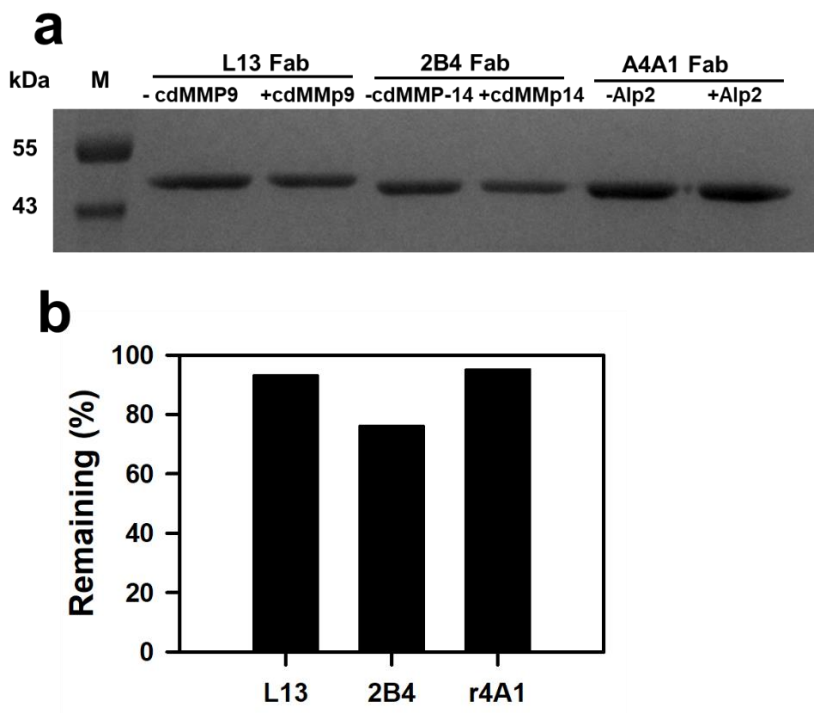

Figure 5.3: **Stability of selected antibodies**, 1 µM Fab was reacted with 1 µM of its respective antigen for 12 hours and the samples were separated by 12% SDS-PAGE (a) and densiometrically analyzed to determine the % remaining (b).

Fab L13 was then successfully cloned into IgG format for expression in HEK 293F mammalian cells and purified with a yield of 40 mg/L. Inhibition and affinity were retested to ensure switching format did not affect the functionality of the antibodies. L13 IgG had a potency of 224 nM with an affinity of 52.9 nM (Figure 5.6a). Following potency and affinity assays IgG L13 was tested for its ability to inhibit MMP-9 from degrading collagen type 1. L13 was able to reduce the MMP-9 hydrolytic activity by 94 % (Figure 5.6b). Finally, L13 was selected for testing *in vitro* using paclitaxel-induced neuropathic pain in mice. In the mouse study the L13 IgG antibody resulted in an improvement in paw withdrawal threshold and frequency compared to control IgGs (Figure 5.6c).

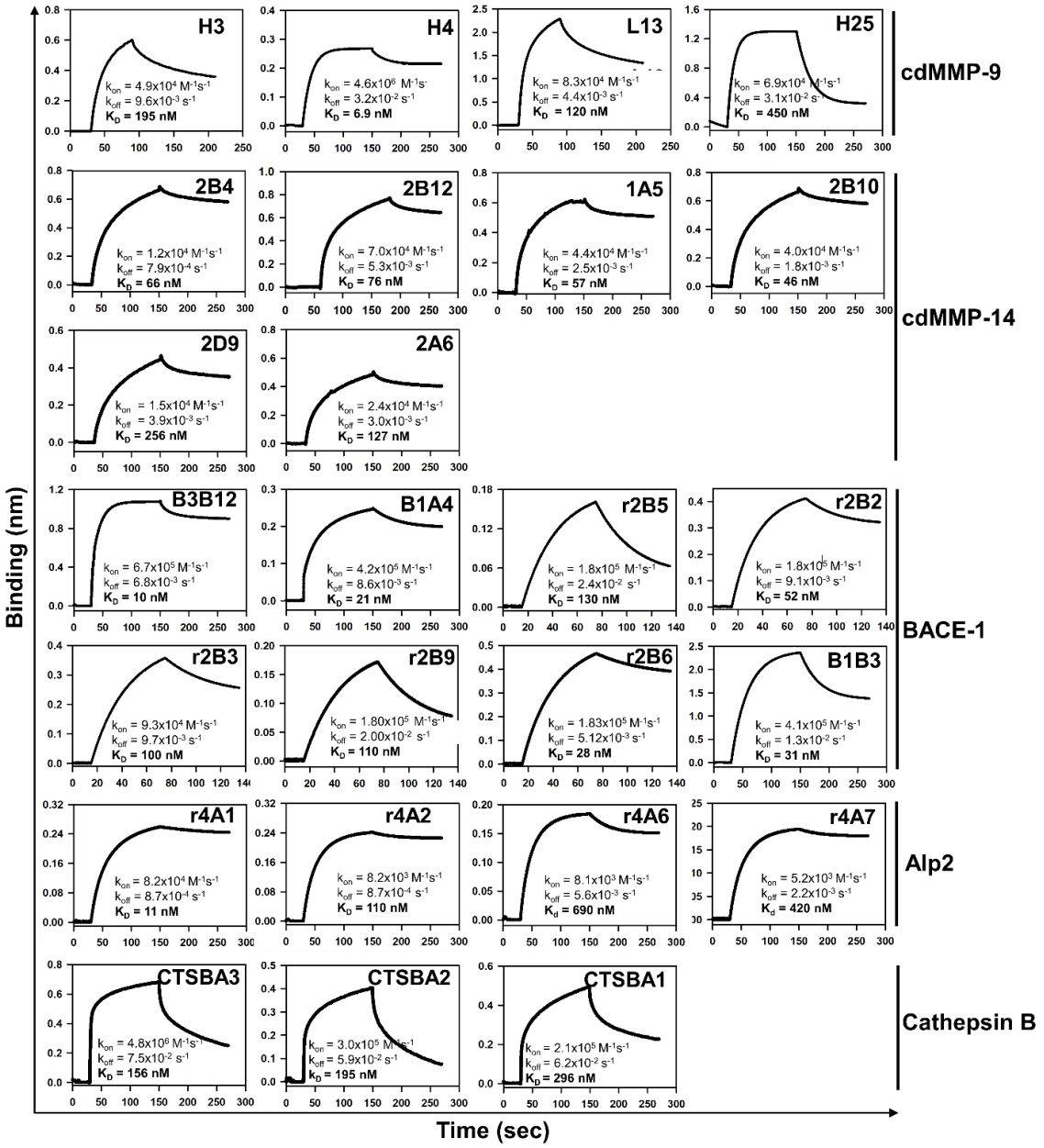

Figure 5.4: **Binding kinetics measurements of Fabs** by bio-layer interferometry using ForteBio BLItz system. Determined k_{on} and k_{off} parameters were used to calculate KD values.

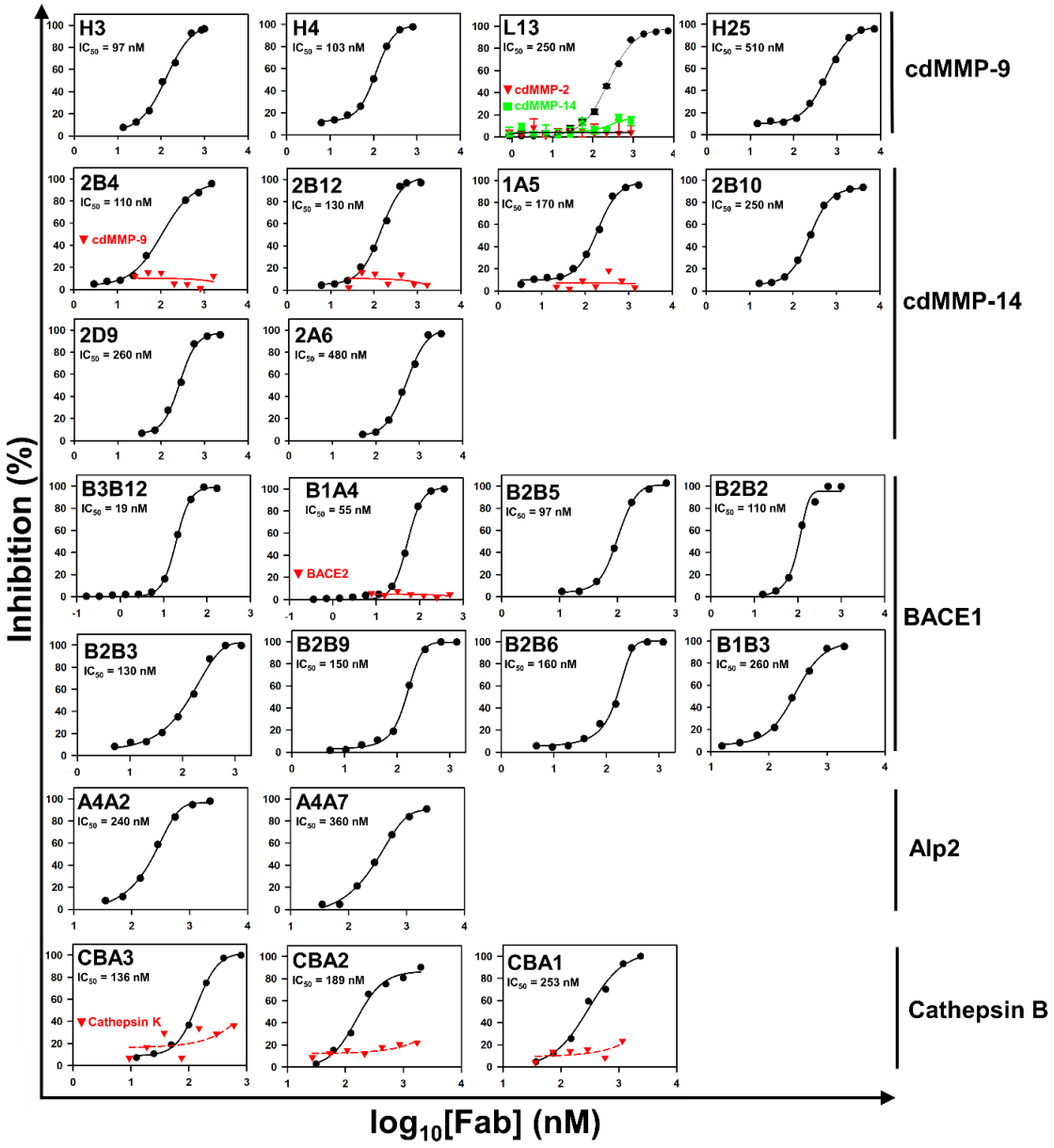

Figure 5.5: **Potencies of inhibitory Fabs** by FRET assays. FRET assays were performed by reacting the purified Fabs with antigen for 30 min then adding the corresponding FRET peptide substrate. The increase in fluorescence was monitored for 1 h to determine inhibitory function. A variety of inhibitory clones with potencies ranging from 15 nM to 510 nM were found. Additionally, selected Fabs were checked for their specificity by inhibition assays against additional protease(s). The off target protease is shown in red or green.

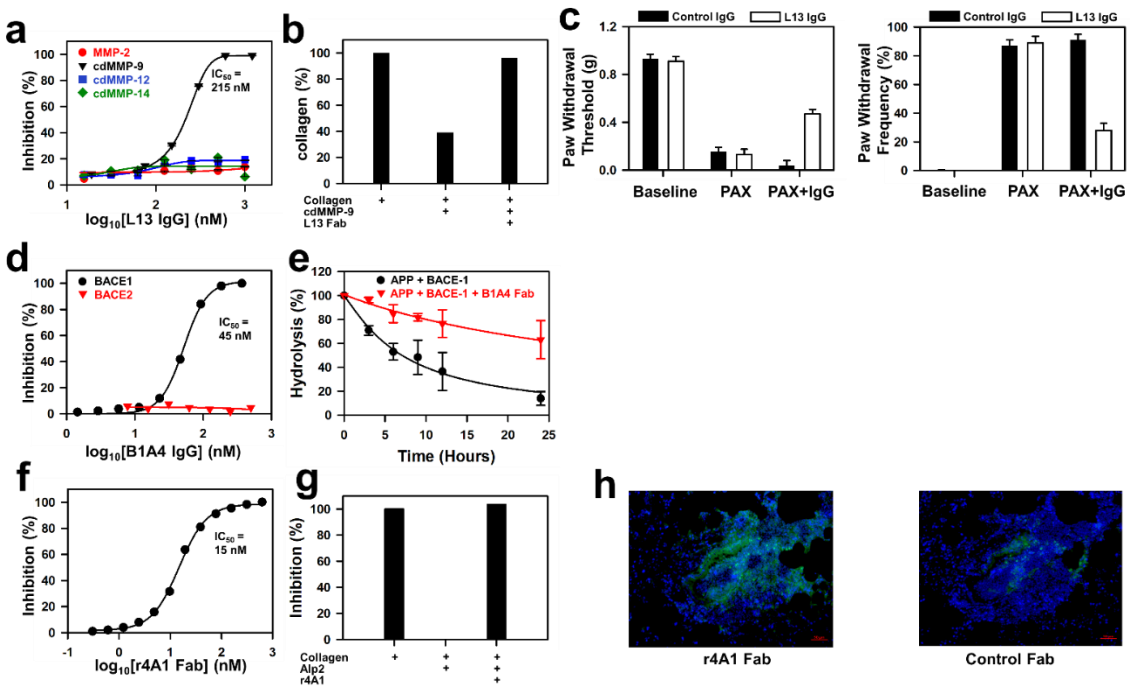

Figure 5.6: **In depth studies of selected antibodies**. a) Inhibition potency of IgG L13 against its target cdMMP-9 (black) and highly homologous MMP-2 (red), cdMMP-12 (blue), and cdMMP-14 (green) showing excellent specificity towards cdMMP-9. b) L13 Fab collagen degradation studies showed that L13 Fab was able to inhibit cdMMP-9 from degrading collagen over a 24 hour period at 37 ^{o}C. c) IgG L13 was I.V. injected (200 ug, 100 ul) on day 15 after PAX injection. Behavior test was performed in a double-blind way. L13 was able to improve paw withdrawal threshold while decreasing the paw withdrawal frequency showing L13's ability to reduce neuropathic pain. d) IgG B1A4 showed excellent specificity between BACE1 and BACE2 by FRET assay. e) APP and BACE1 were incubated at low pH at 37^{o}C for 24 hours in the presence (red) or absence (black) of B1A4 IgG showing that B1A4 was able to inhibit BACE1 from cleaving APP. f) Fab r4A1 showed excellent inhibition potency at 15 nM against Alp2 by FRET assay. g) FITC-collagen was incubated with Alp2 in the presence or absence of r4A1. r4A1 was able to effectively inhibit the Alp2. h) Immunostaining on Aspergillus fumigatus-infected mouse lung tissue indicated r4A1 was able to specifically target Alp2. Green indicates r4A1 binding to fungus.

The genetic selection technique was also used to select inhibitory antibodies with extended CDR-H3s against MMP-14. MMP-14 is highly expressed and very active in the periplasmic space of E. coli, therefore, a unique selection condition of 200 μg/mL ampicillin with 2% glucose was used for initial selection (Table 5.4). This resulted in a very large pool of candidates that was narrowed down by not only increasing the concentration of ampicillin as in other selections, but also removing the glucose to recover the MMP-14 expression. After both rounds of selection, 39 viable clones were discovered, 6 of which were randomly chosen for function testing. All 6 showed inhibition function with ranges from 110 nM – 480 nM. Clones 2B4, 2B12, and 1A5 showed excellent specificity to cdMMP-14 by FRET inhibition assays over cdMMP-9 (Figure 5.5). 2B4 also showed decent proteolytic stability and only 24% was hydrolyzed when exposed to MMP-14 for 12 hours (Figure 5.3).

Following the selection of cdMMP-9/14 antibodies both libraries were used for selection against BACE1 using the EISEVKMDAEY CPL. Selection using 300 μg/mL ampicillin with 0.1 mM IPTG then 400 μg/mL ampicillin with 0.1 mM IPTG resulted in 5 BACE1 antibodies from the long CDR-H3 and 6 from the regular Fab library (Table 5.4). All 11 of the selected BACE1 antibodies showed binding affinities using the ForteBio Blitz ranging from 10 nM to > 3 μM (Figure 5.4) The 5 long CDR Abs had potencies of 19 nM, 55 nM, 258 nM, 1.58 μM, and > 3 μM for clones B3B12, B1A4, B1B3, B1A1, and B1A9 respectively (Figure 5.5). The 6

regular Fabs had potencies of 97, 110, 130, 150, 160 and 190 nM for Abs r2B5, r2B2, r2B3, r2B9, r2B6, r2B10 respectively (Figure 5.5).

B1A4 and B3B12 Fab were chosen for format switching from Fab into IgG. The inhibition and affinity were retested to ensure switching format did not affect the functionality of the antibodies. B3B12 IgG was discovered to have a potency of 18.9 nM with an affinity of 10 nM while B1A4 had a potency of 55.3 nM and an affinity of 21 nM. IgG B1A4 was also shown to be specific to BACE1 over BACE2 by FRET assay (Figure 5.6d). IgG B1A4 was then test for its ability to inhibit BACE1 from cleaving its native substrate APP. The smAPP was cloned on the C-terminal of MBP for expression in E. coli and purification on a xylose resin affinity column. The purified B1A4 was reacted with BACE1 for 5 min to give the complex time to form before the MBP-smAPP was added. Aliquots were taken every 3 hours for 24 hours and the samples run on SDS revealed moderate inhibition of BACE1 (Figure 5.6e). Specifically, after 24 hours only 14% of the full length APP remained without an inhibitor while the reaction with the B1A4 had 63% remaining (Figure 5.6e).

Alp2 selection with the CPL KLRSSKQ was performed using a combination of the regular length CDR-H3 library and the extended CDR-H3 library. Selection using 300 µg/mL ampicillin with 0.1 mM IPTG then 400 µg/mL ampicillin with 0.1 mM IPTG resulted in 8 Alp2 Abs. Although all 8 of the antibodies were binding to Alp2, the remaining 2 non-inhibitory Alp2 antibodies actually increased the activity of Alp2. The top candidate, r4A1, showed an excellent inhibition potency of 15 nM with 11 nM binding affinity (Figure 5.4, Figure 5.5, Figure 5.6f). After 12 hours at

37ºC in the presence of Alp2 only 5% of the Fab was hydrolyzed showing the highest stability of the tested antibodies (Figure 5.3). The r4A1 also able to inhibit Alp2 from cleaving its native substrate collagen type 1 (Figure 5.6g). As such, the r4A1 was used to target Alp2 expressing fungus in aspergillosis infected lung cells (Figure 5.6h). Alp2 was able to specifically target the Alp2 and has the therapeutic benefit of inhibition in addition to identification.

Cathepsin B selection was only performed with the regular CDR-H3 library resulting in 122 clones after a single round of selection. 10 colonies were randomly picked for a second round of selection, 3 survived and were found to have proper sequences. The 3 proper clones were tested for inhibition function and all 3 were found to be inhibitory with potencies ranging from 140 nM - 250 nM and binding affinities from 156 – 296 nM (Figure 5.4, Figure 5.5).

5.4 Discussion and Conclusions

In recent years the ability to create large diverse synthetic antibody libraries has greatly advanced the field of antibody therapeutics[19,29,40,41,42,43,44,] . One of the biggest difficulties in antibody discovery is utilizing these large libraries for the discovery of functional antibodies for therapeutic purposes. Currently phage panning is used to develop libraries enriched in antibodies binding to a specific target[14,15,16]. This has been widely used and has resulted in several antibodies for therapeutic and diagnostic application[45]. However, using phage panning requires several rounds of enrichment followed by functional screening[19,13,29]. Additionally, phage panning is highly dependent on the purity of the antigen and assumes that

there is limited conformational change due to immobilization. These limitations highlight the need for a high throughput function based screening technique.

In this study we developed a genetic selection technique using the coexpression of a modified β-lactamase containing a protease specific CPL, a corresponding protease, and a Fab library. A single Fab clone per cell can be either inhibitory or non-inhibitory to the protease of interest. In the case that the Fab is inhibitory the protease is unable to cleave the linker, the β-lactamase will remain functional, and the cell will survive in the presence of ampicillin. Conversely, if the Fab is unable to inhibit the protease, the cell will not survive when exposed to ampicillin. There exists a balance between expressions of the protease, Fab, and β-lactamase. Ideally, an optimum condition will be discovered in which only strongly inhibiting Fabs will be selected. By increasing or decreasing the concentration of ampicillin we can adjust the selection window to exclude weak inhibitors and recover only the most potent antibodies from a given library.

One of the main difficulties in developing this window is the effect of the CPL on the native function of the β-lactamase. In this study, simply by adding the CPL the functionality of the β-lactamase is reduced by about 40% (Figure 5.1b). This result highlights the importance of selecting a CPL that does not disrupt β-lactamase and is not cleaved by endogenous proteases within the cell. While this reduction in native function narrows the usable window it does not impede the selection process because in all tested cases the complete die off point was at or before 400 μg/mL of ampicillin in the presence of protease. The ideal selection

condition is a concentration of ampicillin in which 100% of negative (non-Fab containing) cells die and 100% of the cells without protease survive. It becomes more difficult to choose a selection condition with proteases that exhibit die off curves similar to Alp2 and BACE1 (Figure 5.1b). With difficult to express proteases such as these there is a relatively high survival rate even in the absence of inhibitor. One method of improving the expression and activity of proteases in the periplasmic space of E. coli is by the use of chaperone proteins such as DSBA/C[46]. With these types of proteases it is especially important to further diminish false positives and weak inhibitors by performing a second round of selection on individual clones using increased stringency. On the other end of the spectrum are proteases that are expressed too well. In this situation to much protease is expressed for the Fabs to inhibit effectively. These proteases can be suppressed with the addition of glucose as displayed by the selection with cdMMP-14. The variety of controls over the expression and activity of proteases allows for fine tuning of the selection windows to achieve selection of the strongest antibodies.

Another level of control comes from purpose oriented libraries focusing specifically on diverse CDR-H3s enriched in clones with specific characteristics. These types of libraries have been used to successfully identify antibodies towards difficult to inhibit antigens[42]. The genetic selection technique described here complements the success of these tailored libraries, such as the long CDR-H3 library for MMPs, by allowing easy screening of different libraries focused on different CDR characteristics. Beyond the manipulation of CDR-H3 length, libraries

have also been developed which are enriched in positive amino acids for stronger interactions with negatively charged catalytic domains[42].Also libraries enriched in histidines have been shown to impart pH dependence to the antibody antigen interaction resulting in interesting clinical applications[47].

Recently, it has been found that tissue inhibitors of metalloproteases (TIMPs) can be actively expressed in the periplasmic space of E. coli[21]. TIMPs have the benefit of binding very strongly to MMPs, however they lack specificity. To this end TIMP libraries have been developed to push the specificity of a TIMP towards a specific antigen[44,40]. Because TIMPs can be actively expressed in the periplasmic space of E. coli, it is possible to use libraries derived from native TIMPs in this genetic selection technique to discover specific potent inhibitors.

In addition to engineering the library, the protease substrate being used for selection may be engineered to select for antibodies inhibiting a protease from cleaving a specific substrate. This is particularly important when the protease of interest has both beneficial and harmful effects depending on which substrate is being cleaved. For example, while many facets of MMP proteolytic action are pro-tumorigenic, some MMP family members exhibit tumor-suppressing effects in certain circumstances[48,49,50], and in certain microenvironments even MMP-9 produces endogenous angiogenesis inhibitors, promotes inflammatory anti-tumour activity, and induces apoptosis[51,52]. For these reasons, selectively blocking disease-promoting activity while retaining beneficial functions is highly desired for a successful therapy.

In conclusion, the genetic selection technique for the discovery of protease inhibiting antibodies described in this study is a unique and powerful tool for screening large libraries. 5 antigens representing 4 different classes of protease were targeted using large Fab libraries. All of the 41 unique antibodies discovered showed binding to the target antigen and 37 were inhibitory. The best candidates L13, B1A4, and r4A1 were also proven to be effective in inhibiting MMP-9, BACE1, and Alp2 from cleaving their native substrate. L13 in particular conveyed a resistance to neuropathic pain in mice. The success of the antibodies described in this study shows that this technique can be readily adopted for the discovery of antibodies against a wide variety of therapeutically relevant proteases.

5.5 References

1. Yamashima, T., et al. Inhibition of ischaemic hippocampal neuronal death inprimates with cathepsin B inhibitor CA-074: a novelstrategy for neuroprotection based on ‘calpain–cathepsinhypothesis. *European Journal of Neuroscience*. **10**, 1723–1733. (1998).

2. Kwan, J., Eksioglu, E., Liu, C., Paul, V., Luesch, H. Grassystatins A-C from Marine Cyanobacteria, Potent Cathepsin E Inhibitors That Reduce Antigen Presentation. *J. Med. Chem*, **52**, 5732–5747. (2009).

3. Nagase, H.. Matrix Metalloproteinase Inhibitors in Cancer Therapy. *Springer*. 39-66. (2001).

4. Flexner, C. HIV Protease Inhibitors. *N Engl J Med*. **338**, 1281-1293. (1998).

5. Lu, Q., et al. L655,240, acting as a competitive BACE1 inhibitor, efficiently decreases β-amyloid peptide production in HEK293-APPswe cells. *Acta Pharmacologica Sinica.* **33**, 1459–1468. (2012).

6. Hook, G., Jacobsen, J.S., Grabstein, K., Kindy, M., Hook, V. Cathepsin B is a New Drug Target for Traumatic Brain injury Therapeutics: evidence for e64d as a Promising Lead Drug Candidate. *Frontiers in Neurology*, **6**, 10.3389/fneur.2015.00178. (2015).

7. Doyle, P.S., Zhou, Y.M., Engel, J.C., Mckerrow, J.H. A cysteine protease inhibitor cures Chagas’ disease in an immunodeficient-mouse model of infection. *Antimicrob Agents Chemother.* **51**, 3932–3939. (2007).

8. Alkhouri, N., Carter-Kent, C., Feldstein, A.E. Apoptosis in nonalcoholic fatty liver disease: diagnostic and therapeutic implications. *Expert Rev Gastroenterol Hepatol*. **5**, 201–212. (2011).

9. Drag, M. & Salvesen G.S. Emerging principles in protease-based drug discovery. *Nat Rev Drug Discov*. **9**, 690–701. (2010).

10. Puri, V., Streaker, E., Prabakaran, P., Zhu, Z., Dimitrov, D.S. Highly efficient selection of epitope specific antibody through competitive yeast display library sorting. *mAbs,* **5**, 533–539. (2013).

11. Marshall, D.C., et al. Selective Allosteric Inhibition of MMP9 Is Efficacious in Preclinical Models of Ulcerative Colitis and Colorectal Cancer. *PLoS One*. **10**, e0127063. (2015).

12. He, W., et al. Epitope specificity plays a critical role in regulating antibody-dependent cell-mediated cytotoxicity against influenza A virus. *Proc Natl Acad Sci U S A*. **113**, 11931–11936. (2016).

13. Nam, D.H., Fang, K., Rodriguez, C., Lopez, T., & Ge, X. Generation of inhibitory monoclonal antibodies targeting matrix metalloproteinase-14 by motif grafting and CDR optimization. *Protein Engineering, Design & Selection*. **30**, 113–118. (2017).

14. Jones, M.L., et al. Targeting membrane proteins for antibody discovery using phage display. *Scientific Reports*. **6**, 26240. (2016).

15. Zhao, A., Tohidkia, M.R., Siegel, D.L., Coukos, G., & Omidi Y. Phage antibody display libraries: a powerful antibody discovery platform for immunotherapy. *Critical Reviews in Biotechnology*. **36**, 276–289. (2016).

16. Bazan, J., Całkosiński, I., Gamian A. Phage display—A powerful technique for immunotherapy. *Human Vaccines & Immunotherapeutics*. **8**, 1817–1828. (2012).

17. Levina, M., Weiss, G.A. Optimizing the affinity and specificity of proteins with molecular display. *Mol. BioSyst*. **2**: 49-57. (2016).

18. Greenfield, E.A. Generating Monoclonal Antibodies. *Antibodies: A Laboratory Manual*. **2**, 201–221 (2014).

19. Lopez, T., Nam, D.H., Kaihara, E., Mustafa, Z., Ge, X. Identification of highly selective mmp-14 inhibitory fabs by deep sequencing. *Biotechnology and Bioengineering*, **114**, 1140–1150. (2017).

20. Knowles, J.R. Penicillin Resistance: The Chemistry of β-Lactamase Inhibition. *Acc. Chem. Res*. **18**, 97–104. (1985).

21. Lee, K.B., et al. Direct expression of active human tissue inhibitors of metalloproteinases by periplasmic secretion in Escherichia coli. *Microbial Cell Factory*. **16**, 73. (2017).

22. Massey-Gendel, E., et al. Genetic selection system for improving recombinant membrane protein expression in E. coli. *Protein Science.* **18**, 372–383. (2009).

23. McDonough, E.K., Lazinski, D.W., Camilli, A. Identification of *in vivo* regulators of the Vibrio cholerae xds gene using a high-throughput genetic selection. *Molecular Microbiology*. **92**, 302–315. (2014).

24. Muranaka, N., Sharma, V., Nomura, Y., Yokobayashi, Y. An efficient platform for genetic selection and screening of gene switches in Escherichia coli. *Nucleic Acids Res*. **37**, e39. (2009).

25. Saunders, J., et al. An *in vivo* platform for identifying inhibitors of protein aggregation. *Nature Chemical Biology*. **12**, 94–101. (2016).

26. Olson, O., & Joyce, J. Cysteine cathepsin proteases: regulators of cancer progression and therapeutic response. *Nature Reviews*. **15**, 712-729. (2015).

27. Nam, D., Ge, X. Direct production of functional matrix metalloproteinase -14 without refolding or activation and its application for *in vitro* inhibition assays. *Biotechnol. Bioeng*. **113**, 717-723. (2015).

28. Persson, H., et al. CDR-H3 diversity is not required for antigen recognition by synthetic antibodies. *J Mol Biol*. **425**,803-811. (2013).

29. Nam, D.H. & Ge, X. Generation of Highly Selective MMP Antibody Inhibitors. *Proteases and Cancer*. **1731**, 307-324. (2018).

30. Lopez, T., et al. Epitope-specific affinity maturation improved stability of potent protease inhibitory antibodies. DOI: 10.1002/bit.26814. (2018).

31. Zufferey, R., Donello, J.E., Trono, D., Hope, T.J. Woodchuck hepatitis virus posttranscriptional regulatory element enhances expression of transgenes delivered by retroviral vectors. *J Virol*. **73**, 2886-2892. (1999).

32. Taves, S., et al. Spinal inhibition of p38 MAP kinase reduces inflammatory and neuropathic pain in male but not female mice: Sex-dependent microglial signaling in the spinal cord. *Brain, Behavior, and Immunity*. **55**, 70-81. (2016).

33. Chen, G., Park, C.K., Xie, R.G., Ji, R.R. Intrathecal bone marrow stromal cells inhibit neuropathic pain via TGF-β secretion. *J Clin Invest*. **125**, 3226-3240. (2015).

34. Luo, X., et al. Intrathecal administration of antisense oligonucleotide against p38α but not p38β MAP kinase isoform reduces neuropathic and postoperative pain and TLR4-induced pain in male mice. *Brain Behav Immun*. **72**, 34-44. (2018).

35. Xu, Z.Z., et al. Inhibition of mechanical allodynia in neuropathic pain by TLR5-mediated A-fiber blockade. *Nat Med*. **21**, 1326-1331. (2015).

36. Chen, G., et al. β-arrestin-2 regulates NMDA receptor function in spinal lamina II neurons and duration of persistent pain. *Nat Commun*. **7**, 12531. (2016).

37. Han, Q., et al. SHANK3 deficiency impairs heat hyperalgesia and TRPV1 signaling in primary sensory neurons. *Neuron*. **92**, 1279–1293. (2016).

38. Choi, J.H., Laurent A.H., Hilser, V.J., & Ostermeier, M. Design of protein switches based on an ensemble model of allostery. *Nature Communications*. **6**, 6968. (2015).

39. Ke, W., et al. Structure of an Engineered β-Lactamase Maltose Binding Protein Fusion Protein: Insights into Heterotropic Allosteric Regulation. *PLoS ONE*. **7**, e39168 (2012).

40. Shirian, J., et al. Converting a broad matrix metalloproteinase family inhibitor into a specific inhibitor of MMP-9 and MMP-14. *FEBS Lett*. **592**, 1122-1134. (2018).

41. Sela-Passwell, N. Antibodies targeting the catalytic zinc complex of activated matrix metalloproteinases show therapeutic potential. *Nat Med*. **18**, 143-147. (2011).

42. Bonvin, P., Venet, S., Kosco-Vilbois, M., Fischer, N. Purpose-Oriented Antibody Libraries Incorporating Tailored CDR3 Sequences. *Antibodies*. **4**, 103-122. (2015).

43. Smith, A.J. New Horizons in Therapeutic Antibody Discovery: Opportunities and Challenges versus Small-Molecule Therapeutics. *Journal of Biomolecular Screening*. **20**, 437-453. (2015).

44. Arkadash, V., et al. Development of high-affinity and high-specificity inhibitors of matrix metalloproteinase 14 through computational design and directed evolution. *J. Biol. Chem.* **292**, 3481–3495. (2017).

45. Dimitrov, D.S. & Marks J.D. Therapeutic Antibodies: Current State and Future Trends – Is a Paradigm Change Coming Soon? *Methods Mol Biol*. **525**, 1–xiii. (2009).

46. Chen, J., et al. Chaperone Activity of DsbC. *JBC*. **274**, 19601-19605. (1999).

47. Bonvin, P. De novo isolation of antibodies with pH-dependent binding properties. *mAbs.* **7**, 294-302. (2015).

48. Overall, C.M., Kleifeld, O. Validating matrix metalloproteinases as drug targets and anti-targets for cancer therapy. *Nat. Rev. Cancer*. **6**, 227-239. (2006).

49. Kessenbrock, K., Plaks, V., Werb, Z. Matrix metalloproteinases: regulators of the tumor microenvironment. *Cell*. **141**, 52-67. (2010).

50. Decock, J., Thirkettle, S., Wagstaff, L., Edwards, D.R. Matrix metalloproteinases: protective roles in cancer. *J Cell Mol Med*. **15**, 1254. (2011).

51. Egeblad, M., Werb, Z. New functions for the matrix metalloproteinases in cancer progression. *Nat. Rev. Cancer*, **2,** 161. (2002).

52. Farina, A.R. & Mackay A.R. Gelatinase B/MMP-9 in Tumour Pathogenesis and Progression. *Cancers*. **6**, 240–296. (2014).

Chapter 6: Conclusions and Future Directions

6.1 Conclusions

In this study, four discovery methods for protease inhibitory antibodies were developed: (1) fast identification of all inhibitory Fabs by deep sequencing, (2) epitope specific affinity maturation for proteolytic stability improvement, (3) selectivity conversion of protease inhibitory antibodies, and (4) discovery of protease inhibitory antibodies by genetic selection. Each method has unique properties.

(1) In Chapter 2, deep DNA sequencing on phage panned libraries discovered new antibodies that would otherwise be lost during standard ELISA screening, especially for the antibodies that failed to enrich continuously due to expression and toxicity issues. In addition, deep sequencing allowed mapping library enrichment progress at a digital resolution that led to insights on the properties necessary for inhibition, e.g. an enrichment in positive amino acids in MMP-14 inhibitors. Such insights can provide guidance for novel function-based library designs.

(2) Maintaining the specific epitope of a given mAb during its affinity maturation is essential to achieve the desired therapeutic efficacy. However, during standard affinity maturation, which is usually based on binding exclusively, epitope can possibly migrate, a phenomenon known as epitope drift. In the case of protease inhibitory antibodies, epitope drift results in reduced inhibition potency. In Chapter 3, we developed an epitope specific dual color FACS to maintain the

inhibitory epitope during affinity maturation. The antibody mutants generated by this method exhibited improved affinity and high potency with unchanged epitopes. In addition, isolated mutants improved in vitro stability 6-10 folds with desired in vivo half-lives in mice. This technique can be employed for the improvement of antibodies or biologics while keeping their desired epitopes.

(3) One major challenge for developing a successful protease inhibiting therapeutic is the requirement for high specificity among proteases of the same family, which often share a high structural homology. Ironically, such high homology also provides the benefit of allowing us to shift the inhibition selectivity by only mutating a few key residues on the inhibitor. By employing dual color FACS using two proteases of the same family labeled with different fluorophores, in Chapter 4, we effectively converted the selectivity of an MMP-14 inhibitory antibody to become an MMP-9 inhibitor with a selectivity shift of 4,500 folds. Furthermore, isolated antibody mutants showed decent selectivity against MMP-2 and MMP-12, which were not included in the counter-selection. This technique can be expanded to discover antibodies inhibiting a wide variety of proteases which are present as family members.

(4) The final technique developed in this dissertation (Chapter 5) is discovering protease inhibiting antibodies using genetic selection. Theoretically this rapid method can select inhibitors for any protease, when three conditions are met: (a) actively expressing the protease of interest in the periplasmic space of *E. coli*; (b) developing a sensor responding to protease activity by designing and

grafting a specific cleavable peptide sequence into a surface loop of β-lactamase; (c) expressing a large Fab library in the periplasm. Using this method, we selected monoclonal antibodies inhibiting MMP-9, MMP-14, BACE1, Alp2, and cathepsin B with nM potency and high selectivity. This technique can be readily expanded for a wide variety of protease targets with biomedical significance. In addition, the involved cleavable peptide sequences can be optimized for inhibition potency improvement and for the selection of substrate specific inhibitors, i.e. blocking the protease from cleaving pathogenic substrates while sparing beneficial substrates.

6.2 Future Directions

(1) One benefit of using antibodies as protease inhibitors is the myriad of ways to improve particular attributes through affinity, potency, and stability enrichment. Recently, methods of expressing Fabs on the surface of yeast have been developed. This technique can be coupled with the techniques described in Chapters 3 and 4 for evolving protease inhibitory antibodies. Specifically, by using Fab format during enrichment the beneficial mutations should translate more closely to benefits in IgG characteristics. In addition to yeast display, Fab display on the surface of mammalian cells can also be used to achieve a similar goal.

(2) Numerous inhibitory mAbs with decent potency and selectivity were successfully isolated / engineered in this study. To fully understand their inhibition mechanisms and to guide rational design on future generations of inhibitors, determining their crystal structures in the complex of associated proteases is the

logical and necessary next step. Because substrate-like inhibitors have a tendency to be cleaved by their targets over time, it becomes an issue for crystallization. Fortunately, with the proteolytic stability improved mAbs developed in Chapters 3&4, we are confident we can solve antibody-protease complex structures in our future study.

(3) Once potent, stable, and specific antibodies have been discovered / engineered mouse studies are required to test their in vivo efficacy. One example of this is the PAX induced neuropathic pain study described in Chapter 5. In addition to this study we would also like to test our inhibitory mAbs for their therapeutic functions on inhibiting the spread of cancer and slowing the progression of Alzheimer's disease in mice. Fortunately, there are several established animal models for these diseases[1,2].

(4) Testing the inhibition of BACE1 for the treatment of AZ in mice needs to overcome an additional difficulty: crossing the blood brain barrier (BBB). One unique technique for crossing the BBB is to use low affinity antibodies of transferrin receptor (TfR)[3,4,5,6]. Developing bispecific TfR/BACE1 antibodies holds a great promise to inhibit BACE1 in brain.

(5) The overall objective of this study is to develop functional selection/screening methods to facilitate the discovery and engineering of protease inhibitory antibodies. In addition to the targets demonstrated in this study (MMP-9/-14, BACE1, Alp2, and cathepsin B), these new techniques developed can be used for many other proteases of biomedical importance. For example:

MMP-12 is implicated in the degradation of the ECM resulting in cancer and plaque progression[7,8]; cathepsin K inhibition is a promising treatment for osteoporosis and breast cancer[9,10,11,12]; ADAM17 is a promising target for the treatment on cancer and inflammation[13,14]; neuraminidase is a key protease responsible for influenza viral invasion and progression[15]. Notably, these proteases only represent a small percentage of the potential protease therapeutic targets available. We believe the ease and flexibility of the technique described in Chapter 5 can be readily adapted to many proteases for achieving specific inhibition and desired therapeutic efficacy.

6.3 References

1. Hall, A. & Roberson, E. Mouse models of Alzheimer's disease. *Brain Research Bulletin*. **88,** 3-12. (2012).

2. Cheon, D. & Orsulic, S. Mouse Models of Cancer. *Annual Review of Pathology: Mechanisms of Disease.* **6**, 95-119. (2011).

3. Bien-Ly, N., et al. Transferrin receptor (Tf R) trafficking determines brain uptake of TfR antibody affinity variants. *J. Exp. Med*. **211**, 233-244. (2014).

4. Couch, J. et al. Addressing Safety Liabilities of TfR Bispecific Antibodies That Cross the Blood-Brain Barrier. *Sci Transl Med*. **5**, 183ra57. (2013).

5. Yu, Y., et al. Boosting Brain Uptake of a Therapeutic Antibody by Reducing Its Affinity for a Transcytosis Target. *Sci Transl Med*. **25**, 84ra44. (2011).

6. Chen, Y. & Liu L. Modern methods for delivery of drugs across the blood–brain barrier. *Advanced Drug Delivery Reviews*. **64**, 640–665. (2012).

7. Johnson, J., et al. A Selective Matrix Metalloproteinase-12 Inhibitor Retards Atherosclerotic Plaque Development in Apolipoprotein E–Knockout Mice. *Arterioscler Thromb Vasc Biol*. **31**, 528-535. (2011).

8. Pavlaki, M., & Zucker, S. Matrix metalloproteinase inhibitors (MMPIs): The beginning of phase I or the termination of phase III clinical trials. *Cancer and Metastasis Reviews.* **22**, 177–203. (2003).

9. Herroon, M.K., et al. Macrophage cathepsin K promotes prostate tumor progression in bone. *Oncogene*. **32**, 1580–1593. (2013).

10. Costa, A. et al. Cathepsin K: its skeletal actions and role as a therapeutic target in osteoporosis. *Nat Rev Rheumatol*. **14**, 447-456. (2011).

11. Olson, O. & Joyce, J. Cysteine cathepsin proteases: regulators of cancer progression and therapeutic response. *Nat Rev Cancer*. **15**, 712-729. (2015).

12. Duong, L., Leung, A., Langdahl, B. Cathepsin K Inhibition: A New Mechanism for the Treatment of Osteoporosis. *Calcif Tissue Int.* **98**, 381–397. (2016).

13. Minond, D., et al. Discovery of Novel Inhibitors of A Disintegrin And Metalloprotease 17 (ADAM17) Using Glycosylated and Non-Glycosylated Substrates. *JBC*. **287**, 36473-36487. (2012).

14. Gooz, M. ADAM-17: The Enzyme That Does It All. *Crit Rev Biochem Mol Biol*. **45**, 146–169. (2010).

15. Moscona, A. Neuraminidase Inhibitors for Influenza. *N Engl J Med*. **353**, 1363-1373. (2005).